Effect of Martensite Morphology on the Tensile Deformation Behavior of a DP590 Steel

A Dissertation Submitted
In Partial Fulfilment of the Requirements
for the Degree of

Master of Engineering

in

Production Engineering

by

Vishal Singh
Regd. No. 801382030

Under the guidance of

Dr. Tarun Nanda
Assistant Professor
MED, TU, Patiala

Dr. B. Ravi Kumar
Scientist (E2)
NML, Jamshedpur

to the

MECHANICAL ENGINEERING DEPARTMENT

THAPAR UNIVERSITY, PATIALA

JULY, 2015

CERTIFICATE

I hereby declare that the thesis entitled "**Effect of Martensite Morphology on the Tensile Deformation Behavior of a DP590 Steel**" is an authentic record of my study carried out as requirements for the award of the degree of **Master of Engineering** in **Production Engineering** at **Thapar University, Patiala** under the supervision of **Dr. Tarun Nanda,** Assistant Professor, Mechanical Engineering Department, Thapar University, Patiala and **Dr. B. Ravi Kumar**, Scientist (E2), National Metallurgical Laboratory (NML), Jamshedpur during July, 2013 to July, 2015. The matter embodied in this report has not been submitted in partial or full to any other university or institute for the award of any degree.

Vishal Singh

Vishal Singh

Date:

It is certified that the above statement made by the student is correct to the best of my/our knowledge and belief.

Dr. Tarun Nanda
Assistant Professor
MED, TU, Patiala

Dr. B. Ravi Kumar
Scientist (E2)
NML, Jamshedpur

Countersigned by

Dr. S.K. Mohapatra
Sr. Professor and Head
MED, TU, Patiala

Dr. S.S. Bhatia
Dean of Academic Affairs
TU, Patiala

Acknowledgement

I express my deep sense of gratitude and a very sincere thanks to my guides **Dr. Tarun Nanda** Assistant Professor, Mechanical engineering department, Thapar University, Patiala and **Dr. B Ravi Kumar**, Scientist (E2), National Metallurgical Laboratory (NML), Jamshedpur for their indefatigable guidance and full support which helped me in the accomplishment of my thesis work. I am highly indebted to them for their painstaking efforts and valuable suggestions during the period of work.

The greatest thanks go to my **Parents** for their infinite support. Above all, I express my indebtedness to the 'ALMIGHTY' for all his blessing and kindness.

Vishal Singh

VISHAL SINGH

Abstract

The automotive industry aims at the production of vehicles with low weight, fulfilling high requirements concerning safety improvements and reduced fuel consumption. Reduction of vehicle weight is believed to be the most promising factor responsible for significant improvement in fuel economy in the future. Dual phase (DP) steels of AHSS category are considered to be the most promising in achieving high strength with low weight. These steels derive their excellent combination of mechanical properties by second phase martensite and/or bainite in a ferrite matrix. Research conducted so far in dual phase steels provides the information about the effect of phase fraction of martensite on tensile properties of dual phase steels but lags to provide the effect of the morphology and distribution of the martensite islands on the tensile deformation behavior in dual phase steels. Thus, the present work is an attempt to look into effect of the morphology and distribution of the martensite islands on the tensile deformation behavior of dual phase steels. Additionally, an attempt is made to refine the martensite phase fraction and improve the mechanical properties without compromising on ductility. Martensite of fine size and that too mainly embedded within the ferrite grains has been found effective to retain high ductility at high ultimate tensile strength.

Contents

List of Figures

List of Tables

List of Acronyms

Acronym	Full Name
AHSS	Advanced High Strength Steels
ASS	Austenitic Stainless Steels
ASTM	American Society for Testing and Materials
BH	Bake hardening
CA	Continuous Annealed
CG	Coarse Grained
CP	Complex Phase
DIC	Digital Image Correlation
DIFT	Deformation Induced Ferrite Transformation
DP	Dual Phase
DSC	Differential Scanning Calorimetry
EBSD	Electron Backscatter Diffraction
F	Ferrite
FG	Fine Grained
FH	Fast Heated
FQ	Fast Quenched
HSLA	High strength low alloy
IF	Interstitial Free
IQ	Image Quality
L-IP	Light Weight with Induced Plasticity
LNQ	Liquid Nitrogen Quenched
M-A	Martensite- Austenite
MART	Martensitic
M-TRIP	Martensite based TRIP

MVF	Martensite Volume Fraction
OM	Optical Microscopy
Q&P	Quenching and Partitioning
QT	Quenching Temperature
RVE	Representative Volume Element
SB-TRIP	Super Bainite TRIP
SEM	Scanning Electron Microscope
SFE	Stacking Fault Energy
SIP	Shear band formation Induced Plasticity
TC	Thermal Cycling
TEM	Transmission Electron Microscope
TMP	Thermo Mechanical Processing
TRIP	Transformation Induced Plasticity
TS-EI	Tensile Strength-Elongation
TWIP	Twinning Induced Plasticity
UFG	Ultra-Fine Grained
UTS	Ultimate Tensile Strength
VHN	Vickers Hardness Number
X-AHSS	Extra Advanced High Strength Steels
XRD	X-Ray Diffraction
YS	Yield Strength

Symbols

Symbol	Full Name
γ	Gamma
α	Alpha
θ	Theta
n	Strain hardening constant

λ	Lambda
M_s	Martensite start temperature
M_f	Martensite finish temperature
Ac_1	Lower critical temperature
Ac_3	Upper critical temperature
s	Seconds
℃	Degree Celsius

Chapter 1

Introduction

1.1 General

The automobiles with light weight and enhanced safety are key issue in the automobile industry. A strong competition between steel and low density metal industries has been observed due to increase in requirements of passenger safety, vehicle performance and fuel economy. The steel industry has responded to these new challenges by development of high strength steels, named Advanced High Strength Steels (AHSS) with improved formability and crash worthiness compared to conventional steel grades [Kuziak et al., 2008]. There are three generations of AHSS; the first generation AHSS is called ferrite based steels. This generation includes dual-phase (DP) steels, martensitic (MART/ MS) steels, complex-phase (CP) steels and transformation-induced plasticity (TRIP) steels. Although the strength level of 1st generation of AHSS is higher than the conventional micro-alloyed (HSLA) steels, but limited formability remains a problem. The second generation of advanced high strength steels includes, Twin Induced Plasticity (TWIP), Light-weight with Induced Plasticity (L-IP) steels and shear band formation-induced plasticity (SIP) steels. The 2nd generation AHSS steels exhibit superior mechanical properties, but these austenitic grades are highly alloyed resulting in a significant cost increase [Matlock and Speer, 2010]. Despite the growing market for AHSS, the trade-off between strength and formability of the AHSS remains the limitation for its application in the vehicles with stylistically and aerodynamically optimized shapes and safety. In order to fill this gap between first and second generation AHSS a new generation of AHSS with improved strength, formability and low cost was introduced and named as third generation AHSS [Bhattacharya, 2006; Matlock et al., 2012]. The third generation AHSS include: processing to enhance properties of DP steels; modifications to TRIP steel processing; development of high strength steels with ultrafine bainitic microstructures; implementation of new processing routes including Quenching and Partitioning (Q&P) route [Matlock et al., 2012]. Among all of these types of 1st and 2nd generation steels, DP and TRIP steel are considered as a good option as third generation AHSS because of their good combination of strength and ductility without high

amount of austenite stabilizers [Kwon et al., 2010; Matlock and Speer, 2010; Hao, 2011; Matlock et al., 2012].

1.2 Advanced High Strength Steels (AHSS)

The AHSS may be distinguished based upon the strength properties that are defined as yield strength greater than 300 MPa and tensile strength greater than 600 MPa as opposed to the conventional high strength steels, in which ductility decreases with strength increase; modern AHSS steels combine high strength and formability/ductility [Kuziak et al., 2008]. AHSS consist of multi-phase complex microstructure with a ferrite matrix containing martensite and /or bainite, retained austenite [Bhattacharya, 2006; Kuziak et al., 2008]. These steels result in reduction of weight by using high strength thinner gauge sheets in automobile bodies reducing the fuel consumption, and increasing the passenger safety by improved crash worthiness. Mechanical properties of AHSS steels are controlled by many factors, including: phase composition and distribution in the overall microstructure, volume fraction, size and morphology of phase constituents [Kuziak et al., 2008].

1.3 Classification of AHSS

The AHSS can be classified into three categories based on the microstructure and the properties of steels [Matlock and Speer, 2010]. AHSS steels in use today have been classified as ‘first generation’ (primarily ferrite-based steels), ‘second generation’ (austenitic grades with high manganese and sometimes aluminium contents; these steels are closely related to some austenitic stainless steels). Because of the trade-off between poor formability of first generation and high alloying cost of second generation, a new generation was introduced called ‘third generation’ with properties superior to the first generation at cost lesser than the second generation AHSS [Matlock and Speer, 2010]. The classification of AHSS is presented in Fig. 1.1.

1.3.1 First Generation AHSS

The First Generation AHSS include Dual-Phase (DP) steels, Transformation Induced Plasticity (TRIP) steels, Complex Phase (CP) steels and Martensitic (MART) steels. The first generation AHSS concepts were developed in fairly lean compositions and are primarily ferrite-based multi-

phase microstructures. The strength level for first generation of AHSS is far beyond that of the conventional HSLA steels but the limited ductility remains a problem [Matlock et al., 2012].

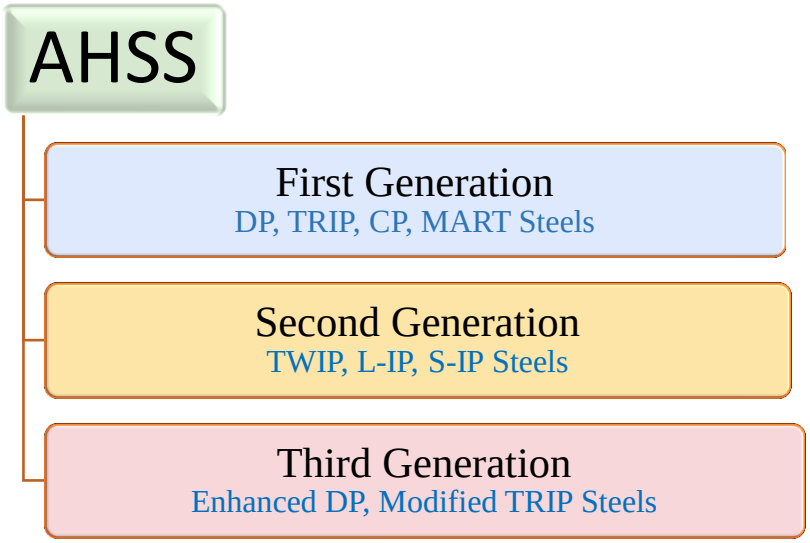

Figure 1.1: Classification of AHSS

1.3.2 Second Generation AHSS

The second generation AHSS include the Twinning-Induced Plasticity (TWIP) steels, Light weight with Induced Plasticity (L-IP) and Shear band formation-Induced Plasticity (SIP). Second generation of AHSS is austenitic steels with high manganese contents and is closely related to conventional austenitic stainless steels [Matlock et al., 2012]. Due to retained austenite in the microstructure, these steel offer excellent combination of strength and formability and overcome the problem of first generation AHSS of low formability. In addition, industrial processing of these alloys, specifically the TWIP steels with high manganese contents, has shown to be extremely challenging and the TWIP grades have also been shown to be prone to delayed cracking [Kwon et al., 2010; Matlock et al., 2012].

1.3.3 Third Generation AHSS

The third generation of AHSS is intended to produce steels with a better combination of strength and ductility than the first generation of AHSS and at a lower cost than the second generation AHSS. The mechanical properties of the third generation of AHSS are intended to fall within the

gap between the first and second generation of AHSS e.g. 1000 MPa tensile strength and 30 % elongation [Hao, 2011]. In order to reduce the cost, lean alloy steel compositions are used in developing this generation of AHSS. Because microstructure determines the behavior and performance of AHSS steels, the design and control of the microstructure becomes essential for the third generation of AHSS. Third generation AHSS are the extension of first generation steels by improving mechanical properties through grain refinement. The strategies pursued for the 'third-generation' AHSS steels include processing to enhance properties of DP steels; modifications to traditional TRIP steel processing; development of high-strength steels with ultrafine bainite microstructures; implementation of new processing routes, including quenching and partitioning (Q&P) and ultra-rapid heating and cooling; and development of high-Mn content TRIP steels [Hao, 2011; Matlock et al., 2012].

1.4 Microstructure and Properties of Common AHSS Grades

AHSS consist of multi-phase complex microstructure with a ferrite matrix and /or martensite, bainite and retained austenite. Different types of AHSS show different properties depending upon their microstructure i.e. DP steel (ferrite, martensite/ bainite), TRIP (ferrite, martensite/ bainite, retained austenite), CP (ferrite/bainite with martensite, austenite, pearlite), MART (lath martensite) etc. [Kuziak et al., 2008; Matlock et al., 2012].

1.4.1 Dual Phase Steels (DP)

Dual-phase (DP) steels mainly consist of a dispersion of hard martensite grains (10–30 %, volume fraction) in a soft ferrite matrix. These steels have impressive mechanical properties such as continuous yielding behavior with superior strength-ductility, better formability and excellent surface finish over other high strength low alloy (HSLA) steels of similar chemistry [Meng et al., 2009]. The strength grade of the developing DP steels covers from 400–1000 MPa. These steels can be welded with all conventional welding methods. Because of their properties, DP steels are currently the most applied AHSS grade [Kuziak et al., 2008; Meng et al., 2009; Hao, 2011].

1.4.2 Transformation Induced Plasticity Steels (TRIP)

Transformation induced plasticity (TRIP) aided steels are of particular interest to the automotive industry as they offer an excellent combination of strength and ductility at affordable costs. The

mechanical properties of TRIP steels are due to the multi-phase microstructure which is composed of ferrite (0.50–0.55), bainite (0.30–0.35), retained austenite (0.07–0.15) and possibly martensite (0.01–0.05) The excellent ductility and strength in TRIP steels is due to the deformation induced transformation of retained austenite to martensite [Kuziak et al., 2008, Hao, 2011].

1.4.3 Complex Phase Steels (CP)

Complex Phase (CP) steels belong to a group of steels with high ultimate tensile strength in the range 400−1000 MPa [Hao, 2011]. The chemical composition and microstructure of these steels is very similar to that of TRIP steels but with no retained austenite in the microstructure. However, additionally these steels contain some quantities of Nb, Ti and or V to cause the precipitation strengthening effect. CP steels with the bainite matrix have superior formability because the difference between hardness of bainite and martensite is relatively small [Kuziak et al., 2008; Hao, 2011; Matlock et al., 2012].

1.4.4 Martensitic Steels (MART)

MART steels provide the highest ultimate strength in final products in the range of 700−1600 MPa [Hao, 2011]. Microstructure of martensitic steels is mainly composed of lath martensite developed by the transformation of austenite during quenching after hot rolling or annealing. These steels are often subjected to post-quench tempering with the aim of improving the ductility and providing good formability even at very high ultimate strength. The concept of chemical composition of martensitic steels is based upon the proper carbon content adoption, since this element increases hardenability and strength. Manganese, chromium, silicon, molybdenum, boron, nickel and vanadium are also used in various combinations to increase hardenability [Kuziak et al., 2008; Hao, 2011; Matlock et al., 2012].

1.4.5 Twinning Induced Plasticity Steels (TWIP)

Twinning Induced Plasticity (TWIP) steels are based on the potential mechanism of obtaining a superior balance of tensile strength and elongation using twinning induced plasticity effect. This superior mechanical performance is obtained by gradual twinning during deformation. The

formation of twins partitions the austenite grains and induces the continuous strain hardening, resulting in improved ductility. The strain hardening behavior is strongly dependent on the stacking fault energy (SFE), which determines the deformation mechanism of the material. Due to lower stacking fault energy of TWIP steels, the twinning behavior is enhanced during deformation and thereby, increases ductility. TWIP steels give superior mechanical performance, but turned out to be commercially unsuccessful due to their low productivity, high cost [Kwon et al., 2010; Matlock et al., 2012].

1.5 Quenching and Partitioning Steels (Q&P)

Quenching and Partitioning is a most innovative heat treatment process to obtain steel specimen with good combination of strength and ductility. In this process specimens are initially heated to either full or partial austenitization temperature, followed by a quenching of the specimen to a temperature (called quenching temperature) in between the martensite start (M_s) and martensite finish (M_f) temperature to form a known fraction of martensite and austenite. This specimen is then soaked at the same or higher temperature (called partitioning temperature) to achieve the diffusion of carbon from the supersaturated martensite to the adjoining austenite. Further, the steel specimen is quenched to room temperature. Due to this partitioning of carbon from martensite to austenite, the austenite gets enriched with carbon and becomes metastable even at room temperature, while the rest unstable austenite transforms to martensite.

This Quenching and Partitioning heat treatment is more effective in obtaining the TRIP effect (transformation of retained austenite to martensite on deformation) in steels. And thus helps to obtain an excellent combination of strength and ductility without use of excessive amount of austenite stabilizers [Santofimia et al., 2008; Santofimia et al., 2011; Wu et al., 2013].

1.6 Strengthening Mechanisms of AHSS

Metallurgists employ various methods to obtain the desired microstructure/ properties in steels. Strengthening and hardening mechanisms are often used in various combinations to meet specific requirements, such as strength, formability etc. Most common methods used for strengthening of AHSS are solid solution strengthening, grain refinement, work hardening, precipitation hardening, and transformation strengthening [Kuziak et al., 2008; Zhang et al., 2012].

1.6.1 Solid Solution Strengthening

The strength of a material is dependent on how easily dislocations in its crystal lattice can be propagated. These dislocations create stress fields within the material depending on their character. When solute atoms are introduced, local stress fields are formed that interact with those of the dislocations, impeding their motion and causing an increase in the strength of the material.When solute and solvent atoms differ in size, local stress fields are created. In substitutional solid solutions, these stress fields are spherically symmetric, meaning they have no shear stress component thus substitutional solute atoms do not interact with the shear stress field characteristic of screw dislocations. And, in interstitial solid solutions, solute atoms cause a tetragonal distortion, generating a shear field that can interact with both edge, screw, and mixed dislocations. All these interactions forms bond between the solute and the dislocation to cause immobilization or pinning of the dislocations. And thus high stress is required to cause the plastic deformation and thus increase in strength takes place.

1.6.2 Grain Refinement

The effect of grain refinement on the strength and toughness of dual phase steels was studied by Calcagnotto et al. (2010) and concluded that the grain refinement affects the properties of dual phase steels and ultrafine grained dual phase steels provide better properties as compared to fine grained and coarse grained dual phase steels.

1.6.3 Work - hardening or Strain- hardening

When a single crystal is continued to be deformed in the plastic range beyond the yield point, the shear stress required to produce further deformation increase continuously. The increase in stress is required to continue the deformation because of previous plastic deformation is called as strain hardening or work hardening. Reason for this is increase in dislocations density with increase in deformation. Pile – up of these dislocations act as a barrier against the further deformation and increase the resistance for further deformation by locking of dislocations on slip planes [Avner, 2007].

1.6.4 Precipitation Hardening

Precipitation hardening, also called age hardening, is a heat treatment technique used to increase the yield strength of materials. In order to apply this treatment, the equilibrium diagram must show partial solid solubility and the solid solubility limit should be decrease with decrease in temperature. It has two stages solution treatment and aging process. In solution treatment, material is heated to a single phase region and then is quenched rapidly to room temperature to result in a super saturated solid solution. In second stage i.e. ageing, controlled decomposition of super saturated solid solution takes place to form finely dispersed precipitates [Avner, 2007].

1.6.5 Transformation Strengthening

In processing of steel, phase transformations often occurs which enable strengthening by creating microstructures with significant amounts of soft phase ferrite and hard phases, such as martensite or bainite . Such transformations occur in operations like hot rolling, continuous annealing where steel can cool from high-temperature austenite and transform to these harder low-temperature phases. This mechanism is mainly utilized in development of advanced high-strength steels and enables dual-phase, transformation-induced plasticity (TRIP), and other AHSS steels as represented by Matlock and Speer, 2010.

1.7 New Trends in Advanced High Strength Steels

Advanced high strength steels such as DP and TRIP steels are now expanding their application since the steels exhibit higher strength and ductility than those of conventional solid solution and precipitation strengthened high strength steels. Efforts have been made enhance the mechanical performance of these steels such as ductility, hole expansion ratio, deep drawability etc. Researchers are focusing on development of extra-AHSS and ultra-AHSS as shown in Fig. 1.2 [Kwon et al., 2010]. Extra-AHSS are designed to utilize nano-scale retained austenite embedded in fine bainite and martensite. Ultra-AHSS are designed to have austenite as the major phase, and the ductility is enhanced primarily by continuous strain hardening generated during forming [Kwon et al., 2010]. Matlock et al. (2012) presented an overview of some of the strategies which can be used to make steels of third generation AHSS. These strategies include development of

high strength steels with ultrafine bainitic microstructures; implementation of new processing routes including quenching and partitioning (Q&P); and development of high Mn content TRIP steels. Also some steels like Enhanced DP, Modified TRIP Steels and Quenching & Partitioning (Q&P) based steels have been discussed by Matlock et al. (2012).

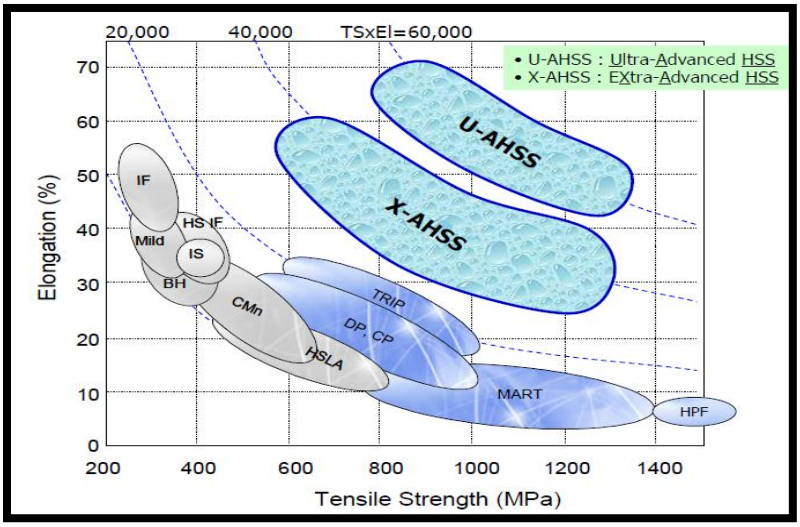

Figure 1.2: Tensile strength and elongation of various steel grades [Kwon et al., 2010]

1.8 Summary of the Chapter

This chapter includes the introduction and need of Advanced High Strength Steels. It discusses the classification of AHSS based on microstructure and resulting properties. The chapter also discusses the most common types of AHSS in use along with their characteristics. The details of strengthening mechanisms related to AHSS have also been explained. Finally, a brief overview of current developments in the area of AHSS has been discussed. The next chapter summarizes the research done by various authors in the field of fabrication of DP, TRIP steels of AHSS and in the field of quenching and partitioning (Q&P) processing route of steels. Also the next chapter illustrates the gaps in the existing literature in the fabrication of DP, TRIP steels along with Q&P route, on the basis of which the objective of the proposed work is defined.

Chapter 2

Literature Review

2.1 General

This chapter will provide literature based on information of AHSS, especially transformation induced plasticity steel and various processes that has been used to improve the properties of third generation transformation induced plasticity steels.

2.2 Review of the Literature

Adamczyk and Grajcar (2006) investigated the effect of heat treatment conditions on the structure and mechanical properties of Dual Phase (DP) type steel. For the experimentation, steel of composition (C:0.09; Mn:1.5; Si:0.26; Ni:0.07; P:0.014; S:0.009; B:0.003; Al:0.029; N:0.012: Fe: balance; all in wt. %) was melted and continuous casting of 100×100 mm slabs was done. After solidification the slabs were hot-rolled and forged in order to obtain the rods with a section of 24×24 mm. The heat treatment of the specimens was realized according to three routes. In the routes I and II, the steel was heated to a temperature of 910 ℃ (α + γ region), held at this temperature for 30 min. In route I, specimen was air cooled to room temp then again heated to 750 ℃ and water quenched. In route II specimen was water quenched from both temperatures viz: 910 ℃ and 750 ℃. The route III consists in austenitizing of steel at a temperature of 910 ℃ and air cooling for 45 s to a temperature of 750 ℃ in order to realize the partial γ to α transformation, followed by water quenching. Route I led to formation of the ferrite structure with an irregular envelope of martensite on grain boundaries. In route II, during heating the steel to an under hardening temperature, the nucleation of austenite mainly occurred on the boundaries of martensite laths formed after primary quenching from a temperature of 910 ℃. The predominated martensite fraction occurred mainly as thin fibers located in surroundings of grain boundaries. Moreover, in surroundings of martensite, especially at a boundary zone of large grains of the alpha phase, small grains of the recrystallized ferrite could be identified. In route III, martensite was located on grain boundaries of the alpha phase. The optimum fraction of martensite averaging 20 % occurred after air cooling of the specimens for 45 s. The used

conditions of heat treatment led in obtaining the DP-type steels of comparable fractions of ferrite and martensite. The optimum fraction of martensite was from 21 % to 24 %, and the grain size of α phase was in the range 7–10 μm. The diversified morphology of martensite had influence on various mechanical properties of the steel and its deformability. The optimum strength and ductile properties were achieved by route II. The yield point of this steel was about 520 MPa, tensile strength about 800 MPa, total elongation 20 %, and uniform elongation about 16 %.

Bhattacharya (2006) reviewed various developments in the area of Advanced High Strength Steels (AHSS) which included Dual Phase steels, Multi Phase steels, Transformation Induced Plasticity (TRIP) steels and Martensitic (MART) steels. The author discussed that AHSS are replacing the conventional steels (used to manufacture structural parts) to increase fuel efficiency and safety performance. Among AHSS, the authors reported that dual phase steels provide an excellent combination of strength and ductility. All the dual phase steels developed have been based on annealing in the two-phase (inter-critical) temperature region and the consequent increase in carbon content in austenite. High carbon contents in austenite after inter-critical annealing results in a significant shift of M_s to a lower temperature. Direct quenching from inter-critical temperature range allows achieving very high strength of steels without expensive alloying. Multiphase steels, also referred to as complex phase steels are steels with a higher level of yield strength at the same comparable tensile strength levels of dual phase steels. The only way to gain yield strength in multiphase structure is to obtain appropriate mixture of pearlite, bainite as well as ferrite straightened by grain refinement and precipitation strengthening.

TRIP steels, based on the Transformation Induced Plasticity effect, offer the highest combination of strength and elongation, which is a measure of high level of energy absorption. In addition, they also show high bake hardening compared to dual phase steels. The relatively slow initial cooling rather rapid cooling down to the temperature of isothermal holding results in further enrichment of the remaining austenite by carbon and enhancing its stability. Further growth in its stability occurs during the austenite to bainite transformation in the presence of strong ferrite forming elements. This significantly retards the carbide formation part of the bainite reaction and helps to keep all carbon in the remaining austenite.

Using water quenching in a continuous annealing line, steels with 100 % martensite are produced. These steels offer very high strength although ductility is lower than other AHSS

steels. The strength of the steel is controlled by the carbon content and a complete austenitizing temperature is used to obtain a fully martensitic structure.

Skalova et al. (2006) studied the effect of thermo-mechanical processing (TMP) consisting of high temperature deformation followed by isothermal holding in the bainite region and cooling to room temperature, on a low alloy TRIP steel. Seven samples with low alloy multiphase steel with same chemical composition of C-0.18, Mn-1.45, Si-1.90, P-0.02, S-0.07, Cr-0.06, Cu-0.05, and Al-0.03 were cut from a forged bar. Samples were processed for seven different TMP methods as shown in Table 2.1, in the TMP simulator SMITWELD TTU 2002.

Optical metallography (OM), transmission electron microscopy (TEM), scanning electron microscopy (SEM) and X-ray diffraction were used to characterize the microstructure of specimens. 3 % nital was used as etchant and Lucia was used as image analyzer to calculate the volume fraction of ferrite phase. Volume fraction of austenite was determined by X-ray diffraction phase analysis for all specimens. Specimens T1–T4 showed a heterogeneous microstructure due to the high austenitization temperature of 950 ℃ and 900 ℃ which resulted in a coarse grained structure.

Table 2.1: Thermo mechanical processing of seven components [Skalova et al., 2006]

Specimen	Austenitization	Compression deformation	Bainitic hold
T1	950 ℃/900 s	710 ℃/16 s, 30 %, water	400 ℃/300 s
T2	950 ℃/450 s	710 ℃/16 s, 30 %, water	400 ℃/300 s
T3	950 ℃/450 s	610 ℃/16 s, 30 %, water	400 ℃/300 s
T4	900 ℃/450 s	660 ℃/16 s, 30 %, water	400 ℃/300 s
T5	850 ℃/450 s	710 ℃/16 s, 30 %, water	400 ℃/300 s
T6	850 ℃/450 s	700 ℃/16 s, 30 %, CO_2	400 ℃/300 s
T7	850 ℃/450 s	700 ℃/16 s, 50 %, CO_2	400 ℃/300 s

For T5–T7, fine and homogeneous grain structure was caused due to low austenitization temperature of 850 ℃. Sample T2 was detected with highest amount of retained austenite (22 %). T5 was also detected with good combination of retained austenite amount (18 %) and ferrite (57 %) along with the some pearlite islands and some transformation of retained austenite to martensite. The desired pearlite-less microstructure was obtained in T6 sample by similar TMP with faster cooling. Retained austenite was obtained as isolated islands in ferrite grains or as a

part of bainitic regions and was homogeneously distributed which caused high ductility. TMP of T7 was similar to T6 along with higher deformation of 50 % and resulted in fine grained ferritic–bainitic microstructure without pearlite. Austenite islands transformed to martensite were found less in T7 than in T6. Also, the increased amount of deformation did not affect the microstructure but only resulted in micro shrinkage in T7 specimen. At the end, the authors concluded that the optimum TMP for the investigated TRIP steel was: austenitization at 850 ℃ followed by 30 % deformation at 700 ℃ and rapid cooling (in CO_2) to the bainite transformation temperature of 400 ℃ i.e. T6.

Kuziak et al. (2008) presented some basic concepts of Advanced High Strength Steels (AHSS) for use in the automobile industry, which included their chemical composition design, microstructure analysis, mechanical properties development during thermomechanical processing, production technology characterization, potential applications and performance in service. The authors reported that AHSS are characterized by improved formability and crash worthiness compared to the conventional steel grades. The category of AHSS covers the following generic types: dual phase (DP), transformation induced plasticity (TRIP), complex phase (CP) and martensitic steels (MART). As opposed to the conventional high strength steels in which ductility decreases with strength, modern AHSS steels combine high strength and formability/ductility. Microstructure of dual phase steels is composed of soft ferrite matrix and 10–40 % of hard martensite or martensite-austenite (M–A) particles which allows achieving the ultimate tensile strength in the range of 500–1200 MPa. The strength of the DP steel is controlled by the amount of martensite and ductility by the size and distribution of this phase. DP steels possess low YS/UTS ratio (around 0.5) and high strain hardening characteristics (high *n* value).

Transformation-induced plasticity (TRIP) steels are based on the principle that the strain or stress induced transformation of retained austenite present in the microstructure in a sufficient amount can substantially harden the steel during deformation. The mechanical properties of TRIP steels are derived from their dispersed multi-phase microstructure which is composed of ferrite (0.50–0.55), bainite (0.30–0.35), retained austenite (0.07–0.15), and possibly martensite (0.01–0.05). To obtain the best mechanical properties in a product, carbon should be distributed to austenite and should enrich this phase as much as possible to preserve the M_s below the room temperature (generally 15−25 ℃ below room temperature). Complex phase (CP) steels belong to a group of steels with very high ultimate tensile strength of 800 MPa or even greater. The chemical

composition of CP steels contains some quantities of Nb, Ti and or V to cause the precipitation strengthening effect. CP steels have no retained austenite in the microstructure, but contain more hard phases like martensite and bainite. Their mechanical properties are characterized by continuous yielding and high uniform elongation. Martensitic (MART) steels provide the highest ultimate strength in final products, up to 1500 MPa. Microstructure of martensitic steels is mainly composed of lath martensite, which is developed by the transformation of austenite during quenching after hot rolling or annealing. AHSS are produced in complex processes involving thermomechanical processing followed controlled cooling. For producing DP steels, the cooling process after rolling starts with slow cooling stage (on the run out table) after rolling in which the desirable amount of ferrite is obtained as a result of the austenite transformation. The ferrite transformation allows the carbon content enrichment in the remaining austenite, which increases its hardenability and reduces M_s Temperature. The optimal combination of strength and ductility of TRIP steels is achieved by grain refinement and obtaining a uniform distribution of fine second phase particles. The cooling stage in the strip rolling process of TRIP steels is more complicated than that for DP strips. After producing 50–60 % of ferrite in the microstructure, accelerated cooling with cooling rate greater than 20 ℃/s to the coiling temperature which lies in the bainitic transformation temperature range, is realized. During coil cooling, bainitic transformation proceeds, further increase the carbon content in remaining austenite to around 1.2 %. A part of this austenite, in the amount of 10–15 %, remains untransformed accounting for the TRIP effect. The concept of CP steels is essentially similar to those of TRIP steels, however less stringent cooling practice is imposed on the hot band during the last stage of processing as no presence of retained austenite is required in their microstructure. Martensitic steels are produced by applying rapid quenching from the austenitic phase to produce the laths martensite microstructure. Finally from the discussion it was concluded that a substantial progress has been achieved during the last same years in the development of AHSS.

Santofimia et al. (2008) studied the effect of partitioning time and temperature on the austenite stability in a multi-phase steel. A specimen with C-0.19, Mn-1.61, Si-0.35, Al-1.10, P-0.09 (in wt. %) of 1.2 mm thickness containing a complex microstructure composed of ferrite, bainite, retained austenite, martensite was taken for experimentation. The specimens were heated at 5 ℃/s to a temperature of 900 ℃, soaked for 10 min and then were cooled at 100 ℃/s to different

temperatures of 125 ℃, 150 ℃ and 175 ℃ respectively. Specimens were held for partitioning at 125 ℃, 150 ℃ and 175 ℃ for 100 s, 10 s, 3 s respectively (as shown in Fig. 2.1).

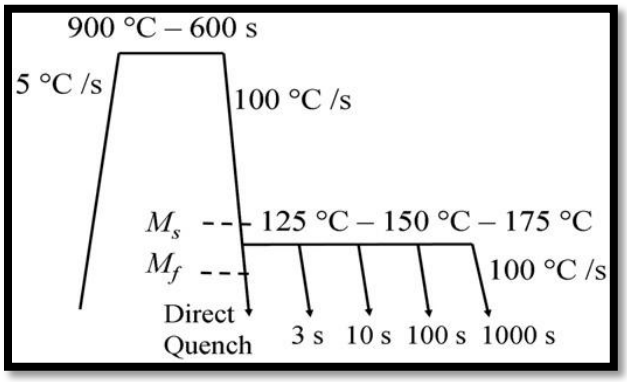

Figure 2.1: Q&P treatments applied to the steel [Santofimia et al., 2008]

Thereafter, they were cooled to room temperature. Light optical microscopy (LOM) with differential interference contrast (DIC), EBSD and image quality (IQ) was used to analyze the microstructures and to distinguish between the BCC ferrite and martensite areas. Results showed that microstructures were composed of ferrite, martensite and retained austenite after the Q&P heat treatment. Small increment in volume fraction and carbon content of retained austenite was observed after partitioning for 100 s at 125 ℃, 10 s at 150 ℃ and 3 s at 175 ℃ respectively. This increment was attributed to faster carbon partitioning from martensite to austenite at higher partitioning temperature. Also, a small decrease of carbon content in retained austenite was observed after 1000 s of partitioning at all the concerned partitioning temperatures. Reason attributed to this was the formation of carbides in austenite. However, the observed carbon reduction in the austenite was not large enough because of the presence of Al which retarded further carbide formation. At the end, the authors concluded that the partitioning time at the chosen temperatures (125 ℃, 150 ℃ and 175 ℃) had a small effect on the microstructure. The carbon enrichment in austenite was mainly responsible for austenite stability in all the specimens. However, a slight carbon enrichment of austenite and increase of its volume fraction was observed with increase in temperatures (125 ℃, 150 ℃ and 175 ℃) at different time periods of 100 s, 10 s, 3 s respectively and was attributed to a faster carbon partitioning from martensite to austenite at higher partitioning temperatures. Authors also reported a reduction in the carbon

content of austenite phase after soaking for 1000 s at partitioning temperatures. The reason attributed to this was carbide precipitation in the microstructure.

Calcagnotto et al. (2010) studied the effect of grain refinement on the strength and toughness of dual phase steels. Large strain warm deformation at different temperatures and subsequent inter-critical annealing had been applied to obtain fine grained (2.4 μm) and ultrafine grained (1.2 μm) ferrite/martensite dual-phase (DP) steels. The mechanical properties of the produced steels were tested under tensile and impact conditions and were compared to a hot deformed coarse grained (12.4 μm) reference material. The chemical composition of the steel used was (in wt. %) 0.17 C, 1.49 Mn, 0.22 Si, 0.033 Al, 0.0033 N, 0.0017 P and 0.0031 S. To obtain the final ferrite/martensite dual-phase microstructure, the specimens were subjected to inter-critical annealing in a salt bath furnace. The temperature was held constant at 730 °C. The samples were annealed for 3 min in the salt bath, before they were quenched in water to obtain a ferrite/martensite DP structure. The martensite volume fraction and grain size were determined using the scanning electron microscope (SEM). The coarse grained (CG) steel had a grain size of 12.4 μm and contained 31.3 % martensite in ferrite matrix. Fine grained (FG) steel had grain size of 2.4 μm and comprised of 30.1 % martensite while the ultrafine grained (UFG) steel had grain size of 1.2 μm with 29.8 % martensite. Cylindrical tensile test specimens with a diameter of 4 mm and a gauge length of 20 mm were machined and tensile tests were conducted at room temperature. Impact tests were also carried out in the temperature range of -40 ℃ to 200 ℃. Results showed that with decrease in the grain size, ultimate tensile strength and yield strength increased remarkably while uniform elongation and total elongation were affected marginally. The ductile to brittle transition temperature was decreased from 127 ℃ to 100 ℃ for fine grained steels and for ultrafine grained steels it was decreased to 90 ℃ which showed the improvement in the impact toughness. The formation of the cracks and cleavage fracture was also suppressed in the fine grained and ultrafine grained steels. Therefore, it was concluded that the grain refinement affects the properties of dual phase steels and ultrafine grained dual phase steels provide better properties as compared to fine grained and coarse grained dual phase steels.

Kwon et al. (2010) discussed the new trends in development of Advanced High Strength Steels and elaborated on the salient characteristics of the next generation AHSS having enhanced performance. The conventional AHSS are high strength steels having tensile strength – elongation (TS-EI) product lower than 25,000 MPa %. The typical steels in this group are DP,

TRIP and martensite-based complex microstructure steels. The microstructure of these steels contains phase transformation products like retained austenite, martensite and bainite. In addition, various thermal cycles are generated to obtain the desired microstructure. These steels have their own advantages and disadvantages as compared to each other (e.g. a primary advantage of DP steels compared to TRIP steels is better weldability. However ductility of TRIP steels is more than DP steels). AHSS with higher hole expansion ratio value have been developed to enhance stretch flangeability and bendability. A few authors are focusing on the development of TRIP steels having TS-EI product greater than 25,000 MPa %. This group of steels are categorized as the so called X-AHSS (e.g. M-TRIP (martensite based TRIP) steel is defined as the TRIP steel with martensitic matrix). M-TRIP steel is produced by Q&P process in which austenite is formed at high temperature either by full austenitization or by inter-critical heat treatment, which is followed by rapid cooling to a temperature between M_s and M_f to control the fraction of martensite and retained austenite. The typical TS-El product value is slightly greater than 25,000 when conventional TRIP steels with lean alloying elements are Q&P processed and the microstructure consists of uniformly distributed annealed martensite matrix and retained austenite. In SB-TRIP (Super Bainite TRIP) steel, nano-sized bainitic microstructure is embedded with retained austenite. This steel has a tensile strength of 1187 MPa and an elongation of 39 %. In order to enhance the ductility of AHSS, it is desired to have austenite as the matrix phase. For improved ductility, it is also important to utilize transformation hardening phenomenon and to control the mechanical stability of austenite phase properly. The typical TS-El product for ultra-AHSS is greater than 50,000 MPa %. These steels have superior strength and ductility combination. TWIP (Twinning Induced Plasticity) is a potential mechanism to obtain the superior balance of tensile strength and elongation, and is extensively utilized to develop steels of the Ultra-AHSS class. The typical value of TS-El product for TWIP steels is about 65,000 MPa %, more than three times greater than those of conventional AHSS. This superior mechanical performance has been obtained by gradual twinning during deformation. The formation of twins partitions austenite grains and induces the continuous strain hardening, resulting in improved ductility.

Matlock and Speer (2010) studied the processing opportunities for new advanced high-strength sheet steels. In this paper author represent the three categories of AHSS and argued that complex microstructure will be required to obtain good combination of strength and ductility. Authors

represent the conventional cold-rolled processing of DP and TRIP steel. After that author represents some new techniques to process DP and TRIP steels. For processing of DP steel a new technique in which a sample of 0.17 C-0.74 Mn steel was processed in 5 steps to produce ultrafine grained DP steel. In first step sample was quenched in ice-brine bath from a temperature of 1000 ℃ after 30 min soaking and result in fully martensite microstructure that was tempered in second step. In third step sample was cold rolled up to 80 %. In fourth step sample was annealed to a temperature 550 ℃ and soaked for 75 min and then water quenched to form an ultra fine aggregate of ferrite and carbide. In fifth step, system rapidly heated at 300 ℃/s to temperature in between Ac_1 and Ac_2, soaked for 5−10 sec. This minimizes the ferrite grain growth and promotes carbide dissolution and austenite formation. An ultrafine structure was developed with a martensite volume fraction of approximately 0.42 having a uniform distribution of 2 um martensite islands on water quenching. For processing TRIP steel author recommended the nitrogen as an austenite stabilizer to provide improved mechanical properties, because of limited nitrogen solubility, 200 ppm N_2 was recommended for conventional steelmaking practice. Because of high nitrogen content lead to high amount of retained austenite stabilization. Author recommended the use of Q&P heat treatment for better result of all kind of AHSS steels. At the end author concluded that steels with good properties will contain significant amounts of a austenite and high strength constituents, including martensite, bainite, ultrafine grained ferrite. The significant opportunities for the production of new AHSS products have been identified, although most require higher heating and/or cooling rates, and advance techniques are required to implement these processing routes.

Nadlene et al. (2011) studied the effect of volume fraction of martensite on the corrosion behavior and the hardness of a dual phase steel. A low carbon steel (C: 0.226; Mn: 0.928; Si: 0.219; Ni: 0.0941; P: 0.0296; S: 0.0359; Cr: 0.126: Fe: balance; all in wt. %) was used for the study. Nine specimens were heated in the furnace at various intercritical temperatures for 25 minutes and quenched in cold water to produce martensite in the microstructure. The first specimen was heated at the lower intercritical temperature (Ac_1) which was 720 ℃ and the temperature was increased 12 ℃ for the following specimens until the upper intercritical temperature (816 ℃) was achieved. After the intercritical annealing process, microstructure of all specimens was observed. The corrosion test was done using the CMS 105^{TM} DC corrosion measurement system. The hardness of the specimens was determined using Vickers Hardness

Testing Machine. Results revealed that the percentage volume fraction of martensite in dual phase steel was influenced by variation in the intercritical annealing temperature. Higher the inter-critical annealing temperature, more the volume fraction of martensite produced in the steel. It was also observed that the interfacial area between the ferrite (anode) and martensite (cathode) increased with increase in martensite fraction. Hence the corrosion rate increased with increase in the volume fraction of the martensite. From the hardness tests it was observed that the hardness of the steel increased with increase in the volume fraction of the martensite. The hardness of martensite was the result of severe lattice distortion produced due to formation of this phase. From the above results, it was concluded that the volume fraction of martensite has great influence on the hardness and corrosion properties of a dual phase steels.

Santofimia et al. (2011) reviewed some important characteristics involved in the Quenching and Partitioning (Q&P) route. The authors described that the initial microstructure of steel strongly affects the microstructural and morphological changes during the Q&P process. Authors reported that existence of high amount of initial martensite promotes the film-like Q&P microstructures, but the presence of high ferrite in the initial microstructure leads to polygonal Q&P morphologies. The film-like microstructure promotes the martensite and austenite interface which leads to the improvement in properties. Authors also reported about the assumptions which must be considered before deciding the optimal quenching and partitioning parameters: (1) carbon must be completely partitioned from martensite to the austenite phase at the end of partitioning process, (2) martensite/austenite interface should remain fixed (austenite fraction should not change during partitioning), and (3) phenomenon such as bainite formation or carbide precipitation must be prohibited. Authors also reported that steels to be employed for Q&P process must have alloying elements to inhibit carbide formation and promote austenite stabilization. Silicon (Si) is recommended as the most promising alloy element to inhibit carbide formation. Nickel (Ni) and manganese (Mn) were reported as effective austenite stabilizers preventing the formation of undesired phases such as epitaxial ferrite, bainite etc. The authors concluded that the mechanism of Q&P process is mainly affected by the initial microstructure of steel, alloying elements and martensite/austenite interface.

Matlock et al. (2012) studied the recent developments in advanced high strength steels (AHSS) and discussed the unique strength and ductility combinations for these steels. The authors argued that the ongoing research in AHSS is focused on increasing strength and/or ductility to higher

levels than exhibited by the first generation AHSS without significantly enriching the alloy compositions, or is aimed at reducing the alloying levels in second generation AHSS grades. These strategies for making third generation AHSS include: processing to enhance properties of DP steels; development of high strength steels with ultrafine bainitic microstructures; implementation of new processing routes including quenching and partitioning (Q&P); and development of high Mn content TRIP steels. An increase in strength of Dual Phase steels can be readily obtained by increasing the martensite volume fraction by altering carbon content and/or intercritical annealing temperature. A strength increase has also been obtained by microstructural refinement resulting from special hot deformation practices, one of which is referred to as Deformation Induced Ferrite Transformation (DIFT). The authors reported about a recent work conducted to create ultrafine bainitic microstructures. The microstructure was obtained after a 15 day heat treatment, a time which may be too long for industrial purposes and thus further work has been done on increasing bainite kinetics, reducing heat treatment to hours rather than days by alloying with Al and/or Co. Quenching & Partitioning (Q&P) has been proposed recently as a new way of producing martensitic steels containing enhanced levels of retained austenite. The process consists of a two-step thermal treatment where the steel is quenched to a predetermined temperature (quench temperature, QT) in the $M_s - M_f$ range to produce a partially martensitic, partially austenitic microstructure. The second, so-called partitioning step, aims at carbon enrichment of the austenite by (partial) carbon depletion of the martensite and carbon transport to the austenite. Thus, carbon stabilized austenite is retained in the microstructure after final quenching to room temperature. The addition of molybdenum retards bainite transformation kinetics and increases the retained austenite volume fraction whereas aluminum substitution for silicon accelerates the bainite reaction and reduces the retained austenite fractions. High retained austenite fractions are believed to result in improved strength and ductility. An alternative process to produce fine grained or ultra-fine grained duplex ferrite-austenite microstructures based on “medium” manganese, low carbon (0.1 wt. %) compositions is manganese enrichment of austenite during inter-critical annealing applied to a cold rolled 0.1-C, 7.1-Mn (wt. %) steel to produce a range of microstructures with varying austenite fraction and stability. Based on equilibrium thermodynamic predictions, samples of the steel are annealed for 168 h at temperatures between 575 ℃ and 675 ℃. The long annealing times are employed to facilitate Mn partitioning. The resulting microstructures includes between 2–43 % retained austenite in a fine

grained ferrite matrix (between 0.9 and 1.5 μm). It is important to note that alloy designs have been based primarily on low carbon steels due to welding considerations.

Ming et al. (2012) studied the combined effect of (deformation induced ferrite transformation) DIFT and Q&P process to get ultrafine-grained ferrite in the matrix of martensite and retained austenite to develop a new kind of advanced high strength steel. Steel of chemical composition (C-0.20, Mn-1.87, Si-1.42, Al-0.040, P-0.012 in wt. % i.e. TRIP 780 slab) was selected for experimentation. Gleeble 3500 thermo-mechanical simulator was utilized to perform experimentation. Specimens were cut in size of 3 mm width and 10 mm length. Specimens were heat treated at a heating rate of 10 ℃/s to 900 ℃, soaked for 5 min followed by cooling at 50 ℃/s to the deformation temperature of 850 ℃. Specimens were then compressed at a strain rate of 1 mm/s to a strain of 0.6. After deformation, specimens were instantly quenched to a temperature of 300 ℃, in between the M_s and M_f temperatures. Partitioning for a few seconds was allowed at this temperature of 300 ℃, and then the specimens were quenched to room temperature. XRD technique was used to investigate the amount of retained austenite. Microstructure of steel was analyzed by optical microscope and a JSM-6460 scanning electron microscope (SEM) after nital etching. XRD results indicated that increased amount of retained austenite can be retained by the Q&P process. In the present work, this amount increased from 3 % to 13 % with increase in partitioning time from 0 s to 120 s. Steel specimens subjected to DIFT process only without partitioning showed the highest ultimate tensile strength (UTS) of 1603 MPa with elongation near about 11 % only. Also the combination of DIFT and Q&P resulted in UTS of 1200 MPa with more than 15 % elongation. The specimen treated by Q&P process only resulted in UTS of about 1281 MPa and elongation about 12 %. At the end, the authors concluded that a good combination of strength and ductility can be achieved by combining DIFT with Q&P process. Also, the percentage elongation of steel could be improved from 12 % to higher values by maintaining UTS of about 1200 MPa. Thus, this new type of combined process (DIFT + Q&P) could be a most useful heat treatment for the new generation of advanced high strength steels (AHSS).

Bohlooli and Nakhaei (2013) studied the effect of ferrite percentage on the mechanical properties of bainite/ferrite dual phase 4340 steels. Steel specimens in the form of 30 mm diameter bars containing C-0.40, Si-0.29, Mn-0.62, P-0.019, S-0.004, Cr-0.73, Ni-1.77, and Mo-0.21 in wt. % were selected for experimentation. Specimens were homogenized at 1000 ℃ for 2

h and finally were cooled to get final microstructure composed of different ferrite concentrations i.e. 37, 46 and 51 %. Optical microscope was used to analyze the microstructure. Ferrite volume fraction was determined by 'Image J' image analyzer software. Vickers indenter with 5 kg load was used to measure the hardness value of specimens. Tensile test specimens were cut from the bars with their longitudinal axes parallel to the rolling direction as per ASTM-A370-B standards. The authors reported that increase in volume fraction of ferrite from 37 to 46 and to 51 % resulted in decrease in yield strength (for change in vol. fraction from 37 to 46 %, decrease in yield strength was about 37 MPa; and for 46 to 51 %, decrease was 87 MPa), ultimate strength (decreased by 45 MPa and 119 MPa respectively), and also decrease in total percentage elongation (decreased by about 2.85 and 3.15 % respectively). Decrease in yield strength with increase in volume fraction of ferrite was attributed to the presence of moving dislocations in ferrite phase which yield at lower stress. Also, increase in volume fraction of ferrite led to decreased bainite volume fraction, increased retained austenite, and thus decreased ultimate tensile strength. Increase of ferrite content increased the hardness and strength of bainite phase (by enriching it with additional carbon). This further overcame the ductility characteristics of ferrite and finally caused decrease in percent elongation of steel with increase of volume fraction of ferrite. Further the authors reported that steel with 37 % ferrite had greater hardness (412 VHN) than the steel with 46 % (362 VHN) and 51 % (321 VHN) ferrite. This reduction was due to increase in presence of soft phase ferrite in microstructure. Further, the authors concluded that increase in ferrite fraction in ferrite-bainite microstructure resulted in decrease in all the properties including yield strength, ultimate tensile strength, hardness and percentage elongation.

Han et al. (2013) studied the effect of cooling rates on the suppression of M_s temperature. Authors reported that different cooling rates lead to the different carbon partitioning from carbon-supersaturated ferrite to metastable austenite during intercritical annealing and thus affect the M_s temperature. Steel with composition 0.17C–0.57Si–2.07Mn (in wt. %) was cold rolled to 1.2 mm from 5 mm thickness. EUAV hot dip process simulator was used to simulate the industrial continuous annealing process. The cold rolled plates were heated to 800 ℃ for 100 s, and then slowly cooled to 660 ℃. After that three different process routes were studied. First was the gas-jet cooled and overaged steel (G-steel); it was cooled to a temperature of 250 ℃ using a gas-jet with cooling rate of 25 ℃/s. Second was the fast spraying water cooled and tempered steel (FT-steel); it was cooled by spraying water (60 ℃/s) to room temperature and then

tempered at 250 ℃. Third was the quenched and tempered steel (Q-steel); it was water quenched (1700 ℃/s) to room temperature and then was reheated to the tempering temperature (250 ℃). Microstructure characterization along with retained austenite measurement was performed by XRD, TEM, and SEM. A dilatometer microstructure evolution experiment using the Baehr DIL805A high-resolution differential dilatometer was designed to analyze the phase transformation process.

Results indicated an increase in yield and tensile strengths of FT-steel by 213 MPa and 172 MPa with increasing cooling rates from 25 ℃/s to 60 ℃/s respectively in comparison with G-steel. This was because of the fast cooling rate of FT-steel which exhibited a microstructure comprising of big packet martensite and ferrite which was almost similar to Q-steel. On the other side, the G-steel relatively exhibited small martensite and ferrite packets. Also XRD analysis reported the austenite volume fraction of 1.9 % and 2.7 % in Q-steel and G-steel respectively. And this was due to the different phase transformations during annealing process. Further the dilatometer test showed that martensitic transformation of G-steel occurred after overaging (121 ℃), and for FT-steel it took place at (346 ℃). The reasons for the suppression of M_s temperature was attributed primarily to ferrite transformation from metastable austenite at a relatively slow cooling rate (i.e. 25 ℃) and secondarily to the increase in carbon concentration of metastable austenite by carbon partitioning from carbon-supersaturated ferrite to metastable austenite during the rapid cooling process. These two conditions did not take place in Q-steel. This was because very fast cooling of sample to room temperature suppresses the carbon diffusion completely and resulted in higher M_s temperature. Authors concluded that the carbon partitioning leads to enrichment of alloy elements in austenite and decrease the M_s temperature considerably. The M_s suppression due to carbon partitioning changed the martensitic microstructure from lath to twinned, resulting in higher strength.

Wu et al. (2013) studied the thermal stability of retained austenite in Q&P steel during tempering at elevated temperature by use of differential scanning calorimetry (DSC). Steel with composition (C-0.20; Si-1.42; Mn-1.87; Al-0.0405; P- 0.012; S-0.0006) was selected for testing. In Q&P process, steel was heated to a temperature of 900 ℃ soaked for 5 min followed by quenching in a salt bath at 320 ℃ for 60 s (i.e. named as Q&P 320-60) and then water quenched to room temperature. Another specimen was quenched into liquid nitrogen from 90 ℃ after soaking for 5 min to produce a fully martensite structure and was named as (liquid nitrogen

quenched) LNQ. Zwick (T1-FR020TN A50) tensile testing machine was used to measure the mechanical properties at a strain rate of 10^{-3} s at room temperature. Nikon (EPIPHOT 300) optical microscope was used for microstructure examination after nital etching. Austenite volume fraction at room temperature was determined by X-ray diffraction by using a (D/max-2550) X-ray diffractometer. Kinetics of austenite decomposition was studied by differential scanning calorimetry (DSC) for which specimens of size 1.3 mm (in height), 3.5 mm (in diameter) were heated from 25 ℃ to 500 ℃ at heating rates of 5, 10, 15, 20 K/min in DSC chamber, and then cooled to 25 ℃ at a rate of 40 K/min. Kissinger method was used to determine activation energy. Q&P based specimen resulted in high amount of retained austenite (10.6 %) than LNQ (1.5 %) specimen. Tensile properties of given two steels are presented in Fig. 2.2. Q&P based steel resulted in a good combination of tensile strength (1311 MPa) and elongation (13.6 %) with large *n* value (0.085) compared to LNQ (0.033). These results indicated that the Q&P steels had more potential to show a better TRIP effect than LNQ. Also, the activation energy of austenite decomposition was determined to be 221.3 KJ/mol with thermal decomposition temperature of retained austenite in range of 400 ℃ to 500 ℃ which was also an indicative of good TRIP effect. At the end the authors concluded that the Q&P steel was superior to LNQ steels with better combination of strength (1311 MPa) and elongation (13.6 %) and with high thermal stability.

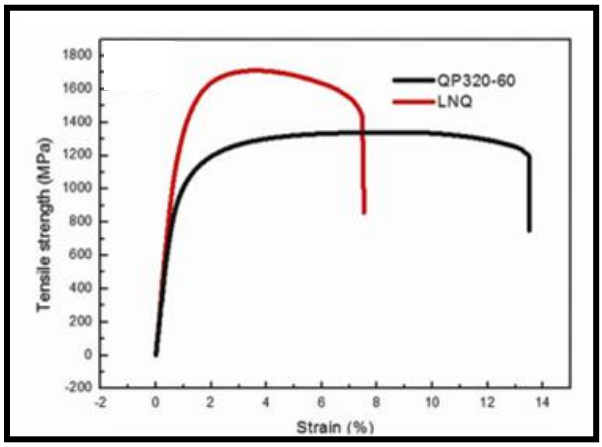

Figure 2.2: Mechanical properties of LNQ and QP 320-60 Steel [Wu et al., 2013]

Meng et al. (2014) performed fast-heating annealing on a cold rolled dual phase steel in order to explore the possibility of fast-heating routine on large scale production. A cold rolled dual phase

steel (Fe – 0.07C, –1.7Mn, – 0.429Si) sheet with 70 pct cold rolled ratio was investigated for the study. Same composition steel produced through continuous annealing was also used for the comparison. From the dilatometer study, the lower and upper critical temperatures were found out to be 1023 K and 1193 K respectively for the heating rate of 500 K/ s. Specimen was heated at 500 K/ s to 1123 K, soaked for 2 s and then cooled down to 323 K. Microstructure evaluation and tensile testing was done for both the steels i.e. fast heated (FH) and continuous annealed (CA). Tensile tests showed that the yield strength for the fast heated sample increased from 277 MPa to 372 MPa and ultimate strength increased from 625 MPa to 666 MPa. The total elongation was also increased from 23.3 % to 26.6 % as compared to the continuous annealed sample. Compared to the continuous annealed sample, the ferrite grains were observed to be refined strikingly in the fast heated sample. The fine and fibrous morphology of the martensite in the FH sample resulted in the improvement of strength. Hence, it was concluded that the simplified fast heating process can be an alternative route for the production of the dual phase steels.

Ramazani et al. (2014) studied the effect of martensite banding on the failure initiation in dual-phase steel. DP600 steel (C - 0.078, Si - 0.025, Mn - 1.58, P - 0.015, S - 0.001, Cr -0.055, Ni - 0.024, Al - 0.032, Cu - 0.010, V - 0.011) in cold-rolled, ferrite-pearlite state with thickness of 1 mm was selected as test sample. To obtain the same percentage of martensite at different temperatures (790 ℃ and 760 ℃) and heating rates (1 ℃/s and 100 ℃/s respectively for the two temperatures), the samples were quickly gas-quenched at a rate of 80 ℃/s to form martensite (35 % vol. fraction) from austenite in both cases. Digimizer software was used to quantify the aspect ratio (length/ height) of martensite islands in DP microstructures. With the first condition (790 ℃;1 ℃ /s), an aspect ratio of close to 1 was obtained and the microstructure was described as an equiaxed microstructure. For the second condition (760 ℃; 100 ℃/s), a banded microstructure with an aspect ratio of 7.2 was obtained. The ferrite grain size was quantified as 5.6 and 6.1 um respectively for equiaxed and banded microstructures through the linear intercept method. Carbon content in ferrite and martensite was calculated as 0.0035 % and 0.216 % for equiaxed microstructure and as 0.0045 % and 0.214 % for banded microstructure, respectively. In order to better localize the area of probable crack formation, the strip was notched. The bending test was performed up to a load of about 130 N and a displacement of the central rod up to 5 mm. The load was held stepwise in order to record the surface images of the samples in the SEM. In order

to identify the crack initiation and the correspondent local strain, three parallel mini tensile tests with digital image correlation (DIC) technique were carried out parallel to the rolling direction. In situ analysis of bending test in SEM combined with electron backscatter diffraction (EBSD) measurements before and after the test showed that crack initiation occurred in martensite islands. Representative volume element (RVE) modeling combined with extended finite element method (XFEM) was applied to simulate martensite cracking on mesoscale. Finally image quality (IQ), the inverse pole figure map and Kernel Average Misorientation map before and after the in-situ test showed that crack initiation occurred in martensite region and thus validated the modeling approach. Figure 2.3 presents the SEM images of the given specimen, this presents that the failure initiation in given DP steel took place in martensite region.

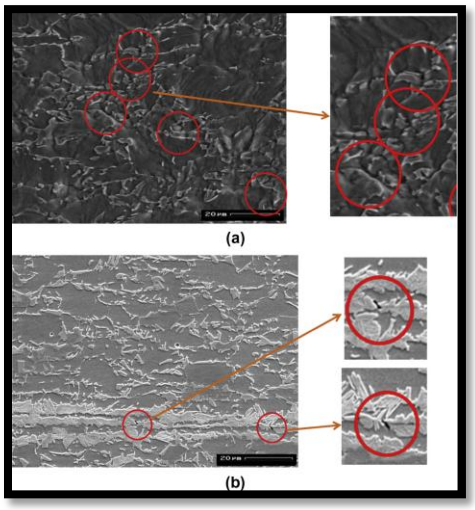

Figure 2.3: Failure initiation positions in DP steel with (a) equiaxed and (b) banded microstructures [Ramazani et al., 2014]

At the end, authors concluded that the martensite cracking was identified to be the main failure initiation mechanism in equiaxed and banded DP steels. Further, in martensite, equiaxed microstructure showed better failure resistance than the banded structure.

2.3 Summary of Given Literature

1. Several authors have worked on the first generation AHSS and have successfully achieved high strengths as compared to the conventional steels. However, achieving good formability still remains a problem. Some authors have worked to overcome this problem and have

substantially improved upon the ductility and strength by forming second generation AHSS. The mechanical properties of second generation, however, depend upon expensive alloy additions which makes them expensive for use. Moreover, alloy additions impair the weldability also in second generation AHSS. Finally, a few authors have reported their work on the third generation AHSS, where first generation steels have been modified through a combination of suitable alloy additions (though leaner than second generation counterparts), and improved processing routes for improved formability, strength and toughness [Bhattacharya, 2006; Kuziak et al., 2008; Matlock and Speer, 2010; Matlock et al., 2012].

2. Some authors have reported that complex microstructures consisting of significant amount of retained austenite and high strength constituents, including martensite, bainite, ultrafine grained ferrite are required to obtain good combination of strength and ductility [Bhattacharya, 2006; Kwon et al., 2010; Matlock and Speer, 2010].
3. Some of the authors have reported that DP and TRIP steels offers the highest combination of strength and elongation, which is a measure of high level of energy absorption and has great potential to act as a third generation AHSS [Kuziak et al., 2008; Matlock and Speer, 2010; Matlock et al., 2012].
4. Some of the authors have made attempts to obtain the microstructure with ultrafine/fine ferrite in order to improve the tensile properties of AHSS steels [Calcagnotto et al., 2010; Ming et al. 2012].

2.4 Gaps in Literature

1. In so far attempts made by researchers refinement of ferrite phase and fraction of martensite was mainly concerned. Very few attempts have been made to investigate the effect of annealing process variables on martensite volume fractions and its subsequent effect on tensile properties.

2. Very limited literature is reported to study the effect of morphology and distribution of the martensite islands on the tensile deformation behavior in a cold rolled dual phase steel.

3. DP steel reported so far contains the lath type martensite and it is also reported that the crack initiations took place in the interlath of martensite which further lead to failure of steel, even after this information no attempts have been made to alter these lath shape martensite into

some more appropriate shape to obtain the better mechanical properties i.e. strength and ductility.

4. Authors have discussed the different approaches for refinement of grain size in the microstructures (i.e. alloying element addition, thermo-mechanical processing etc.) to improve the mechanical properties in DP steels, but no attempt has been in use of thermal cycling (a processing route in general applied for refinement of grain size) for processing of DP steels.

Chapter 3

Design of the Study

3.1 General

This chapter brings forward the detailed design of the proposed research work. It presents the overall objective of the proposed research, methodology, and experimental procedure to be adopted and also specifies the machines, equipment and the software which helped to achieve the desired objective.

3.2 Establishment of the Objective Function

Dual phase steels derive their properties by composite nature of the microstructure, namely; martensite or bainite in a ferrite matrix. Attempts have been made to improve the properties of DP steel by varying the volume fraction of martensite/bainite and refining the grains of ferrite in the DP microstructure. Some authors have investigated the pattern of microstructural deformation and corresponding mechanical behavior of dual phase steels composed of ferrite and martensite. During these investigations of microstructural deformation pattern, authors were mainly concerned about the phase fraction dependent tensile deformation behavior of DP steels. Research has not been conducted to investigate the effect of distribution of different sized martensite grains on the deformation behavior of dual phase steels. The present study is an attempt to look into the effect of morphology and distribution of martensite islands on the tensile deformation behavior of DP steels.

The overall objective of the present work was *to investigate the effect of morphology and distribution of martensite islands on tensile deformation behavior of dual phase steels*.

The key issues to be taken up during the research work were as follows:

- To study the effect of thermo-mechanical processing (TMP) parameters on the microstructural constituents of DP steels, in terms of grain size, phase fraction, and distribution. Four different thermo-mechanical processing routes to be employed for this task.

- To analyse the effect of volume fraction and morphology (shape, size and distribution) of martensite phase on the tensile deformation behavior of dual phase steels.

The overall objective of research work consisted of the following sub-issues:

- To examine the microstructure and mechanical properties of the as-received steel by using optical microscopy/ SEM analysis and tensile testing.
- To predict the martensite fraction required to achieve the desired tensile properties of DP steel under investigation by using micro-mechanical modeling approach.
- To determine the inter-critical annealing parameters like annealing temperatures, soaking time periods and cooling rates etc. (to obtain DP microstructure) by using commercial software viz. Thermo-Calc, DICTRA and JMat-Pro.
- To determine the various annealing processing routes to obtain DP microstructure with different martensite shape, size, fraction and distribution.
- To conduct the annealing experiments in the annealing simulator for the above mentioned heat treatment routes.
- To conduct microstructure characterization of the annealed specimens through optical microscopy, and SEM analysis. Also, to determine the area fractions and distributions of ferrite and martensite phases using 'analySIS FIVE Digital Imaging Solutions' software.
- To carry out the tensile testing of samples treated under various conditions and to analyse the microstructural dependent tensile deformation behavior of dual phase steels.
- To identify the factors resulting in good tensile strength-percentage elongation combinations to further improve the heat treatment routes for processing of DP steels.

3.3 Experimental procedure

The detail of experimental procedure followed in the present research work is described as follows:

3.3.1 Starting Material

The starting material was a 67 % cold rolled steel sheet of chemical composition as shown in Table 3.1. The as-received steel comprised of ferrite and pearlite in its microstructure. Specimens of the as-received steel were prepared for microstructural examination using standard

metallographic techniques like mounting, grinding, rough polishing, final polishing, etching etc. Nital etchant (solution of 3 % HNO_3 in ethanol) was used to analyse the phase details present in the steel through optical microscopy.

Table 3.1: Chemical composition of the starting steel

Element	C	Mn	Si	S	P	Al	N	Fe
% wt.	0.074	1.83	0.43	0.002	0.012	0.026	0.0032	Balance

3.3.2 Prediction of Material Properties Using Micro-Mechanical Modelling

Micro-mechanical modeling is a technique to predict a material's behavior based on its microstructural characteristics, without extensive experimental investigations. In the present work, micro-mechanical modeling technique was employed to estimate the tensile strength of steel under investigation containing DP structure with different martensite fractions.

In one of the approaches of micro-mechanical modeling put forward by Allabasi (2004), tensile curve of each phase (here, fully ferritic and fully martensitic separately) present in the steel with DP microstructure is determined individually. In order to predict the tensile curve of individual phases, the steel is subjected to heat treatment to develop a fully ferritic or fully martensitic structure, and subsequently, the tensile curve for individual phases is obtained by actual tensile testing [Allabasi, 2004; Singh, 2014]. In another approach of micro-mechanical modeling, flow stress of an individual phase is predicted through a dislocation based strain hardening methodology [Sodjit et al., 2012; Toudeshky et al., 2014]. This approach was used in the present work. According to this approach, the effective stress-strain curve for individual phases can be described using Eq. 3.1 [Toudeshky et al., 2014].

$$\sigma = \sigma_o + \Delta\sigma + \alpha M \mu \sqrt{b}\, \frac{\sqrt{1-\exp(-Mk\varepsilon)}}{kL} \tag{3.1}$$

where, σ is the flow stress at a true strain of ε. σ_o is the initial flow stress and represents the effect of alloying elements in solid solution and is given as Eq. 3.2 [Toudeshky et al., 2014].

σ_o (in MPa) = 77 + 750 (%P) + 60 (%Si) + 80 (%Cu) + 45 (%Ni) + 60 (%Cr) + 80 (%Mn) + 11 (%Mo) + 5000 (%N) (3.2)

$\Delta\sigma$ provides material strengthening by carbon content in solution. For ferrite, it is given by Eq. 3.3 [Toudeshky et al., 2014].

$\Delta\sigma$ (in MPa) = 5000 * (%Css^{f}) (3.3)

For martensite, it is given by Eq. 3.4 [Toudeshky et al., 2014].

$\Delta\sigma$ (in MPa) = 3065 * (%Css^{m}) – 161 (3.4)

where, '%Css^{f}' and '%Css^{m}' denote the percent weight carbon content in ferrite and martensite phases respectively. In the present work, the value of %Css^{f} and %Css^{m} were taken as 0.005 % and 0.15 % respectively [Ramzani et al., 2013].

The term, $[\alpha M\mu\sqrt{b}\frac{\sqrt{1-\exp(-Mk\varepsilon)}}{kL}]$ signifies the effects of dislocation strengthening as well as work softening due to recovery, where α is a material constant having a value of 0.33, M is the Taylor factor with value of 3, μ is the shear modulus of material (taken 80000 MPa for the given steel), b is the Burger's vector and was taken as 2.5×10^{-10} m, k is the recovery rate. The value of k, in case of ferrite was taken as $10^{-5}/d_{\alpha}$ (d_{α} refers to the average ferritic grain size). For martensite, k was taken as 41 [Toudeshky et al., 2014]. L is the dislocation mean free path. For ferrite, it is equal to the ferritic grain size d_{α}, while for martensite, it is taken as 3.8×10^{-8} m [Toudeshky et al., 2014]. The value of d_{α} was assumed to vary in the range 3–8 μm in the present work [Sodjit et al., 2012; Ramzani et al., 2013; Toudeshky et al., 2014].

Using the values of various parameters in Eq. 3.1, the true stress-strain curve for individual phases was obtained.

Further, Eq. 3.5 and Eq. 3.6 were used to determine the parameters n_f, n_m, K_f, K_m for each phase (i.e. ferrite and martensite) by fitting linear curves between *ln (true stress)* and *ln (true strain)* obtained individually for ferrite and martensite respectively, as reported by Allabasi (2004).

$\sigma_{f=} K_f\ (\varepsilon_o\ +\ \varepsilon_f)n_f$ (3.5)

$\sigma_{m=} K_m\ (\varepsilon_o\ +\ \varepsilon_m)n_m$ (3.6)

Here, n_f and n_m are the strain hardening exponents for ferrite and martensite phases respectively; K_f and K_m are the Hollomon strength coefficients for ferrite and martensite respectively; ε_o is taken as taken as 0.002. ε_f and ε_m are the uniform true strains for ferrite and martensite respectively. These values of n_f, n_m, K_f, K_m and ε_o are further used in the rule of mixture [Eq.

3.7, as reported by Alabbasi, 2004] to get the composite true stress behavior of the DP steel at different volume fractions of martensite phase in the microstructure.

$$\sigma_c = V_m K_m (\varepsilon_o + \varepsilon_m)n_m + (1- V_m) K_f (\varepsilon_o + \varepsilon_f)n_f \quad (3.7)$$

where, σ_c is true stress (composite stress) for the given material (i.e. DP steel processed through a particular route and containing a particular martensite volume fraction), V_f and V_m are the volume fractions of ferrite and martensite respectively in the given steel.

Composition used in the present work belongs to the DP 590 steel i.e. UTS of 590 MPa [Sung et al., 2010; Li et al., 2013; Meng et al., 2014]. In the present work, micro-mechanical modeling was employed to predict the minimum martensite volume fraction needed in the given steel to provide strength value in excess of 590 MPa (UTS ≥ 590 MPa).

3.3.3 Study of Phase Transformations Using Commercial Software

The next step was to determine the annealing process parameters to obtain the desired DP microstructures (as predicted by the previous step). Thus, in this phase of research, annealing parameters including inter-critical temperature range (lower and upper critical temperature of the steel under investigation), soaking time periods at the heat treatment temperature, cooling rates etc. to be followed for the steel during its annealing were determined by commercial software viz. JMat-Pro, Thermo-Calc and DICTRA. These software were used to construct the CCT diagrams, equilibrium phase diagrams, and phase fraction diagrams etc. of the steel under various conditions.

3.3.4 Annealing Simulation and Microstructural Analysis

Annealing simulations were now conducted with process parameters as predicted in the last section. Annealing experiments were conducted on tensile specimens cut into standard dog-bone shape with gauge length of 35 mm as per the ASTM standard E-8M. Annealing experiments were performed in the annealing simulator for various processing routes (by following different soaking temperatures, soaking time periods and cooling rates). The alternate cooling routes were obtained in the simulator through a mixture of hydrogen and nitrogen gases, by varying the proportion of gases in the mixture or by varying the injection pressure.

To reveal the microstructure clearly, two types of etching techniques (i.e. nital etching, and picral+ $Na_2O_3S_5$ respectively) were employed. Nital (3 % HNO_3 in ethanol), a non- color etching

revealed the ferrite as white and martensite as black. The second etching technique was a color etching technique and was used in some selected cases. In this color etching technique, specimens were pre-etched with picral etchant (i.e. 4 % picric acid in ethanol) for 60 s and thereafter etched in a solution of 10 % $Na_2O_3S_5$ in distilled water for 15 s. Color etching revealed ferrite as light brown and martensite as dark brown. Evaluation of the morphology i.e. Shape, size and distribution etc. of phases in various steel samples was done with the help of image analyzer software 'analySIS FIVE'.

3.3.5 Analysis of Microstructure Dependent Tensile Deformation Behaviour

Microstructure deformation pattern is most effective to explain the mechanical behavior of materials. In order to evaluate the deformation behavior of microstructures and their effect on tensile properties, microstructural examination of tensile tested specimens was conducted on the tensile specimen at two places i.e. one at the fracture tip, and the other at a location away from the fracture tip. Stress level at the fracture tip was considered to be the higher than the stress level at the location away from the tip. Parameters that affect the tensile deformation behavior such a size, shape and distribution of martensite phase were evaluated.

3.4 Commercial Software

Thermo-Calc, DICTRA and JMat-Pro were used in the present study to predict the intercritical temperatures, soaking periods and cooling rates desired to obtain different DP microstructures. Further 'analySIS FIVE software' was used to study the distribution and fractions of martensite and ferrite phases. The details regarding use of these software packages in the present research are as follows:

A) Thermo-Calc

Thermo-Calc software (Thermo-Calc 3.0; developed by *Thermo-Calc Software AB*, Stockholm, Sweden) was used to determine the inter-critical temperatures and phase fraction diagrams. For this purpose, equilibrium phase diagram and phase fraction diagrams were plotted for the given alloy chemistry. Equilibrium phase diagram provided information about the inter-critical temperatures (Ac_1 and Ac_3), while phase fraction diagram provided information about the volume fraction of various phases.

B) DICTRA

Diffusion **C**ontrolled **TRA**nsformations (DICTRA) software (DICTRA: version 27; developed by *Thermo-Calc Software AB*, Stockholm, Sweden) is a general software package for simulation of single and multicomponent systems. Any number of components may be treated (provided that necessary thermodynamic and kinetic data are available). DICTRA is particularly suitable for treating problems involving one-phase problems, moving boundary problems, diffusion in multi-phase systems etc. DICTRA is based on numerical solutions of multi-component diffusion equations in various regions of a material. DICTRA software was used in the present work to predict the time required for complete pearlite dissolution during isothermal holding at different annealing temperatures respectively.

C) JMat-Pro

JMat-Pro software (JMat-Pro 6.1; developed by *Sente Software Limited*, Guildford, United Kingdom) was used to construct the CCT diagrams at different annealing temperatures. For each annealing temperature, a distinct CCT diagram was prepared. CCT diagram helped to predict the cooling rate required for complete austenite to martensite transformation, as required in dual phase microstructure.

D) analySIS FIVE Digital Imaging Solutions

The 'analySIS FIVE Digital Imaging Solutions' software (analySIS Five 5.05.07; developed by *Olympus Soft Imaging Solutions*, Notting Hill, Australia) is a leading software for image analysis and processing. It can analyze area and pixel value statistics of user-defined selections and intensity threshold objects. This software can display, edit, analyze, process, save, and print 8-bit color and gray scale, 16-bit integer and 32-bit floating point images. It can create density histograms and line profile plots and distribution plots for various phases. For the present study, analySIS FIVE was used to measure the fraction and size distribution of martensite phase from the optical micrographs for the various steel samples.

3.5 Annealing Simulator

Annealing simulator is specialized equipment for annealing of steel samples in a controlled environment. In this simulator, the samples to be annealed can be heated in a controlled

environment and can be cooled under controlled cooling rates. The simulator has been designed and developed jointly by CSIR-NML and Tata Steels, Jamshedpur (as in Fig. 3.1). The description of the annealing simulator is as follows:

a) **Heating system:** The simulator is based on a unique high speed heating method which makes it capable of typically running the thermal tests at rates 7–10 times faster than the conventional furnace equipped devices. Also, the simulator can maintain and hold the specimens at steady-state equilibrium temperatures. The thermocouples fitted in the chamber provide signals for accurate feedback control of specimen temperatures.
b) **Cooling system:** Cooling of the specimens is achieved by purging a gas mixture of hydrogen and nitrogen at very high pressures. Different cooling rates can be achieved by either changing the percentage of hydrogen gas in the gas mixture or the purging pressure or both.
c) **PLC based digital control system:** The heart of the system is the PLC based digital control system. It provides all the signals necessary to control the annealing simulator variables simultaneously through a digital closed-loop system. The system can be operated in several modes (totally manual control, combination of computer and manual control etc.) to provide maximum versatility in the annealing simulations.

Process simulation of annealing simulator

Simulation of metallurgical processes requires controlled process environment, high temperatures and controlled heating and cooling rates over a wide range. Annealing simulator enables controlled process environment and controlled heating and cooling rates.

Heating mode: Heating mode is by radiation. A maximum operating temperature of 1050 ℃ is achievable at controlled heating rates.

Process environment: Gas mixing system can produce a H_2-N_2 gas mixture of 5–30 % H_2 for maintaining the inert atmosphere, which is desired for bright annealing of steels. Pure H_2 or N_2 gas medium can also be used in the system.

Cooling medium: Controlled cooling rates (>100 ℃/s) of specimens can be achieved by using high pressure gas jet. Multiple options for cooling medium are available; such as hydrogen, nitrogen, or mixture of these, atomized water etc.

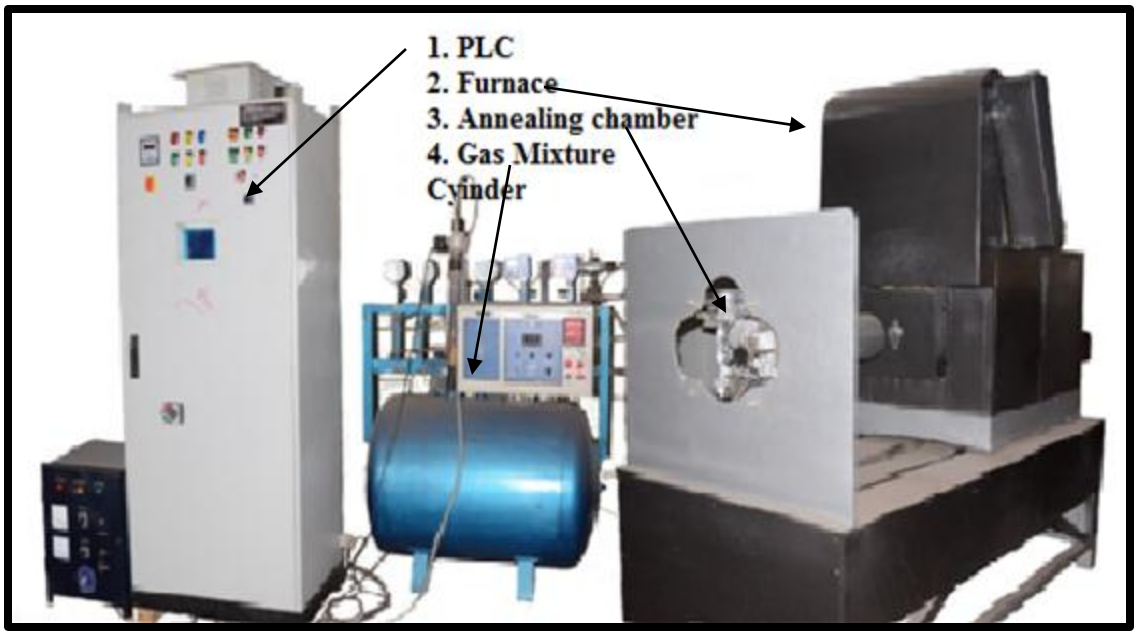

Figure 3.1: Annealing simulator (Courtesy: NML, Jamshedpur)

3.6 Sample Preparation to Evaluate Microstructures

Mechanical properties are strongly influenced by the microstructure, so microstructural evaluation is important. This section describes the machines and equipment employed to prepare the sample for metallographic examination. In order to prepare samples for metallographic examination, some basic steps such as mounting, planar grinding, rough polishing, final polishing, etching and microscopic analysis are needed to be followed. These steps along with equipment employed are described as follows:

A) Precision Cutter

The precision cutter (Make: Micracut 125, *Metkon Instrumens Inc*., Bursa, Turkey) was used to cut small specimens for microstructural evaluation of annealed steel from its tensile specimens. The specimens were mounted on an aluminium vice. The specimens were placed in a position relative to the cutting wheel using a micrometer screw. The material was cut by lowering the specimen over the cutter using a dead weight mechanism. Figure 3.2 shows the precision cutter utilized in the present work.

Figure 3.2: Precision cutter (Courtesy: NML, Jamshedpur)

B) Mounting

The use of mounting of samples is to facilitate their easy handling. Mounting is done either with copper or with bakelite. Copper was used for mounting when specimen was to be used for SEM analysis. Specimens were hot mounted at a temperature of 160 ℃ by following the procedure of powder metallurgy. The edges of the mounted samples were rounded to minimize the damage to grinding/polishing discs. The mounting press (Make: BAINMOUNT METCO, *Chennai Metco Pvt. Ltd.*, Chennai, India) was used in the proposed work and is shown in Fig. 3.3.

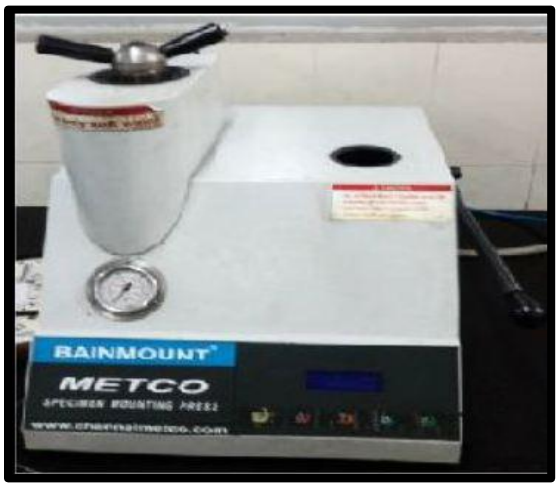

Figure 3.3: Mounting press (Courtesy: NML, Jamshedpur)

C) Grinding

The surfaces to be examined by microscope were polished with abrasive papers of successive finer grades such as 80, 120, 220, 320, 400, 600, 800, 1000, 1200, 1500 and 2000 mesh abrasive paper. The sample was rubbed on SiC paper to avoid the scratch, then switched on the next paper with finer grade and the direction of rubbing was switched perpendicular to previous scratches. Similarly the process was repeated from the coarse grade paper (80 grit size) up to fine grade paper (2000 grit size). The over-heating of samples was avoided so that no modification in the microstructure occurred. The pressure needed to be adjusted, as high pressure could lead to introduction of deep scratches and low pressure could result in long time consumption. Some of the SiC papers used in the present work are shown in Fig. 3.4.

Figure 3.4: Abrasive papers (Courtesy: NML, Jamshedpur)

D) Polishing

The next step was polishing on a horizontal rotating wheel. Polishing wheels were covered with a soft cloth (velvet, canvas, suede or selvet etc.) which need to be soaked with a polishing medium (alumina or colloidal) along with some water. The polishing cloth was washed thoroughly with water before start of polishing to remove any chances of introduction of contaminants which may cause deep scratches on surfaces. The specimen was held on the rotating disc in order to obtain a scratch free surface with mirror like finish. Polishing machine (Make: BAINPOL METCO, Model No: PMV018, *Chennai Metco Pvt. Ltd.,* Chennai, India) was used in the proposed work. Polishing machines have been shown in Fig. 3.5.

Figure 3.5: Polishing machine (Courtesy: NML, Jamshedpur)

E) Etching

Etching is done in order to reveal the microstructure of the metal/alloy system through selective chemical attack. The sample must be thoroughly cleaned before etching. Etchant must be selected and prepared accurately. Etchant may be applied using a cotton bud wiped over the surface for a few times (necessary precautions must be taken while etching, as very small difference occurs between etching and over-etching). To reveal the microstructure clearly, two type of etching techniques (i.e. Nital etching and Picral+ $Na_2O_3S_5$) were employed. Nital (3 % HNO_3 in ethanol), a non-colour etching revealed the ferrite as white and martensite as dark grey/black. Second etching technique employed was a colour etching technique. In this colour etching technique, specimens were pre-etched with picral etchant (i.e. 4 % picric acid in ethanol) for 60 s; after that specimen were etched in the solution of 10 % $Na_2O_3S_5$ in distilled water for 15 s. Colour etching revealed the ferrite as light brown and martensite as dark brown.

F) Leveling

The surface to be examined optically should be perfectly flat and leveled. If not, then the viewing area would be out of focus i.e. if the center is focused the sides would go out of focus or vice versa. By using a specimen leveling press (shown in Fig. 3.6) this problem can be avoided, as it presses the mounted specimen into clay on a microscope slide, making it leveled. A small piece of paper or cloth covers the surface of the specimen to avoid scratching.

Figure 3.6: Leveling machine (Courtesy: NML, Jamshedpur)

3.7 Equipment for Microstructure Evaluation

This section describes the equipment used for microscopic analysis such as optical microscopy (OM), scanning electron microscopy (SEM) etc. These equipment are as follows:

A) Optical Microscope

Optical microscope is used for the purpose of magnifying small samples with the help of visible light and a system of lenses. Metallic materials are usually opaque and therefore investigations of plane cross-sections by incident light prevail in metallography. Due to the difference in the refractive indices there appear different color shades. Starting from the sample preparation, to etching of the specimen, and setting up of microscope, all steps should be carefully optimized in order to get maximum information from a microscopic study. The optical microscope (Make: Leica DM2500 M; *Lieca Microsystems*, Wetzlar, Germany) used in the study is shown in Fig. 3.7.

B) Scanning Electron Microscope (SEM)

A scanning electron microscope (SEM) is a type of electron microscope that images a sample by scanning it with a high-energy beam of electrons. The electrons interact with the atoms that make up the sample and produce signals that contain information about the sample's surface topography, composition, and other properties such as electrical conductivity etc.

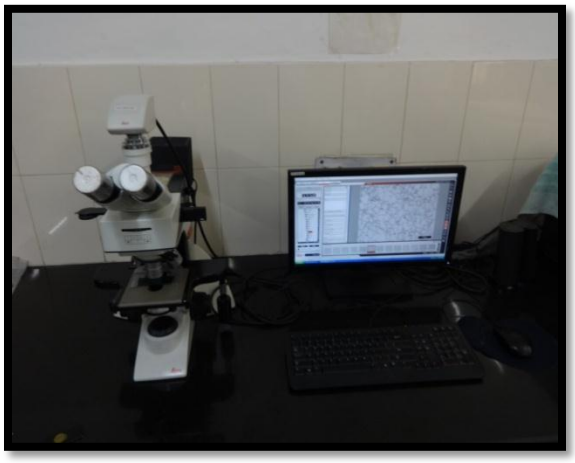

Figure 3.7: Optical microscope (Courtesy: NML, Jamshedpur)

SEM can produce very high-resolution images of the sample's surface, revealing details less than 1 nm in size. Due to the very narrow electron beam, SEM micrographs have a large depth of field yielding a characteristic three-dimensional appearance useful for understanding the surface structure of a sample. Figure 3.8 shows the scanning electron microscope (Make: Nova Nano SEM 430; *Field Emission Inc.,* Hillsboro, USA) which was used in the present study.

Figure 3.8: Scanning electron microscope (Courtesy: NML, Jamshedpur)

3.8 Equipment for Evaluation of Mechanical Properties

This section describes the machine/ equipment used to evaluate the mechanical properties of the material before and after the annealing simulation/ heat treatment performed on the specimens. This equipment is as follows:

A) Tensile Testing Machine

The tensile testing machine (Make: Instron 8501 System, *Instron Engineering Corporation*, Norwood, USA) with a loading capacity of 100 kN was used for stress-strain analysis in the present work. The machine provides data in form of values of stress corresponding to respective strains. The data when plotted can be used to calculate the yield strength, ultimate tensile strength and total elongation. Figure 3.9 shows the tensile testing machine (Make: Instron 8501 System, *Instron Engineering Corporation*, Norwood, USA) used in the present work. An extensometer (gauge length of 25 mm) was used to measure the elongation. A flat dog-bone shaped specimen with gauge length of 35 mm as per the ASTM standard E-8M was used to test the specimens.

Figure 3.9: Tensile testing machine (Courtesy: NML, Jamshedpur)

B) Hardness Testing Machine

Vickers hardness tester is a key piece of equipment that is vital to metallographic research. In Vickers micro-hardness test procedure, indentation is made with a range of loads using a diamond indenter which is then measured and converted to a hardness value. For this purpose, test samples are carefully and properly prepared by grinding and polishing. Two types of indenters are generally used for Vickers test family; a square base pyramid shaped diamond indenter for Vickers hardness testing and a narrow rhombus shaped indenter for Knoop hardness testing. The Vickers hardness test method requires a pyramidal diamond with square base having

an angle of 136° between the opposite faces. Upon completion of indentation, the two diagonals are measured and the average value is considered.

Figure 3.10: Vickers Micro-hardness tester (Courtesy: NML, Jamshedpur)

Vickers Hardness Number (VHN) is obtained by dividing the applied load in kilogram-force by surface area of indentation. Figure 3.10 shows the hardness tester used in the present work (Make: Leica Q550MW VMHT Auto, *Leica Microsystems*, Wetzlar, Germany)**.** In the present study, the micro-hardness tester was operated at a low load of 10 g-force for a dwell time of 15 s and with an indenter speed of 30 μm/s.

3.9 Summary of the Chapter

This chapter brings forward the design of the present study. In this chapter, the objective function and key issues to be considered have been discussed. An overview of the experimental procedure to be followed has been provided. Also, machines and equipment used for sample preparation for metallography, microstructural analysis and mechanical properties evaluation have been discussed.

Chapter 4

Results and Discussion

4.1. General

This chapter brings forward the results pertaining to predictions made by empirical formulae in terms of martensite volume fraction required to obtain the desired strength in DP steel. The details obtained from commercial software viz. Thermo-Calc, DICTRA and JMat-Pro in terms of annealing temperatures, soaking periods and cooling rates required to obtain the desired microstructure in steel are also discussed. The simulations carried out for different time-temperature conditions, and results thereof, are also presented in this chapter. Further, the microstructures and corresponding tensile behaviors obtained from different simulations are discussed in this chapter.

4.2. Characteristics of Starting Material

The low carbon (67 % cold rolled) steel sheet comprising of ferrite and pearlite in its microstructure was selected as the starting material for the present study. Figure 4.1a–b presents the optical and SEM micrographs of the as-received material. 'analySIS FIVE' software determined the volume fractions of ferrite and pearlite as 84 % and 16 % respectively. Average grain size of 8 μm was calculated by using the linear intercept method. Cold deformation resulted in highly deformed ferrite and pearlite microstructure. Pearlite lamellae were destructed and were non-uniformly distributed. This type of microstructure leads to non-uniform dissolution of pearlite phase during the course of austenite formation. The starting cold rolled material resulted in yield strength (YS; 0.2 % offset) of 895 MPa, ultimate tensile stress (UTS) of 948 MPa and percentage elongation of 4.3 % (see Fig. 4.1c). This high YS and UTS with low ductility were attributed to the highly deformed microstructure. High cold deformation increased the dislocation density, refined the grain size and hence increased the YS and UTS at the expense of ductility [Shakhova, et al., 2012; Ahmad et al., 2013].

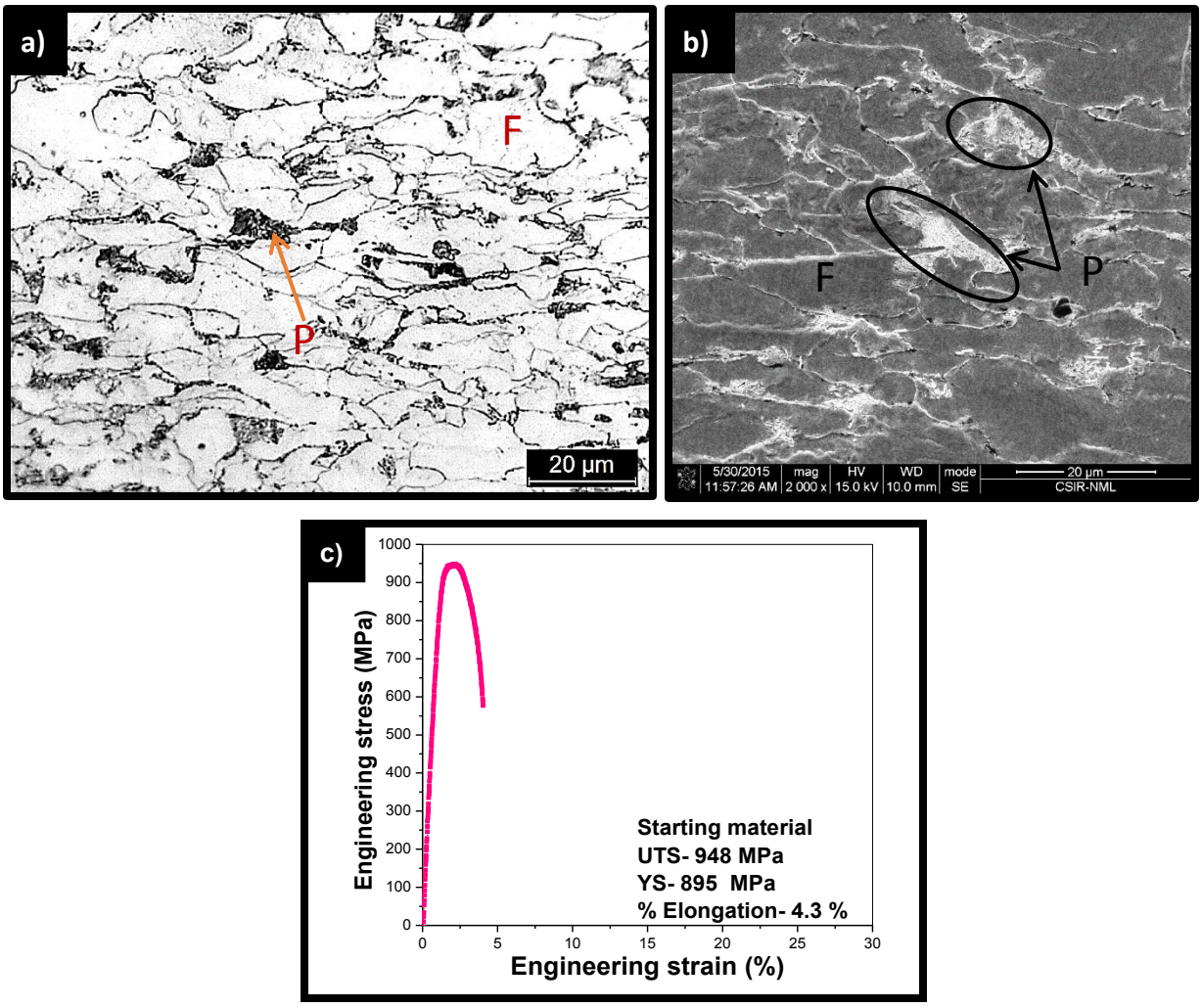

Figure 4.1: Characteristics of the as-received steel sheet (a) optical micrograph, (b) SEM micrograph, and (c) stress-strain curve. F = Ferrite and P = Pearlite

4.3. Micromechanical Modelling for Flow Curve Prediction of DP Steel

Micromechanical modeling approach (as described in section 3.3.2) was employed to estimate the tensile properties of given steel, assuming DP structures with different martensite volume fractions. Composition used in the present work belongs to the DP 590 steel i.e. UTS of 590 MPa [Sung et al., 2010; Kim et al., 2011; Li et al., 2013; Meng et al., 2014]. The micromechanical modeling approach was employed to predict the martensite fraction required in the DP microstructure (to be developed in the present work) that could provide an ultimate tensile strength in excess of 590 MPa (UTS $\geq$ 590 MPa) [Alabbasi, 2004; Singh, 2014].

In the use of micromechanical modeling, first of all, the flow curve for each phase (present in the microstructure) was to be obtained individually. In order to predict the flow curve of individual

phases in the steel, the dislocation based strain hardening approach as given by Sodjit et al. (2012) and Toudeshky et al. (2014). According to this approach, the true stress-strain diagram for single phase (i.e. ferrite and martensite separately) was described by using Eq. 3.1. The value of σ_o calculated by using Eq. 3.2 was 266 MPa. Further the values of $\Delta\sigma$ for ferrite and martensite calculated from Eq. 3.3 and Eq. 3.4 were equal to 25 MPa and 298 MPa respectively. Figure 4.2a–b presents the flow curves for ferrite and martensite respectively obtained after using Eq. 3.1 (for ferrite and martensite individually).

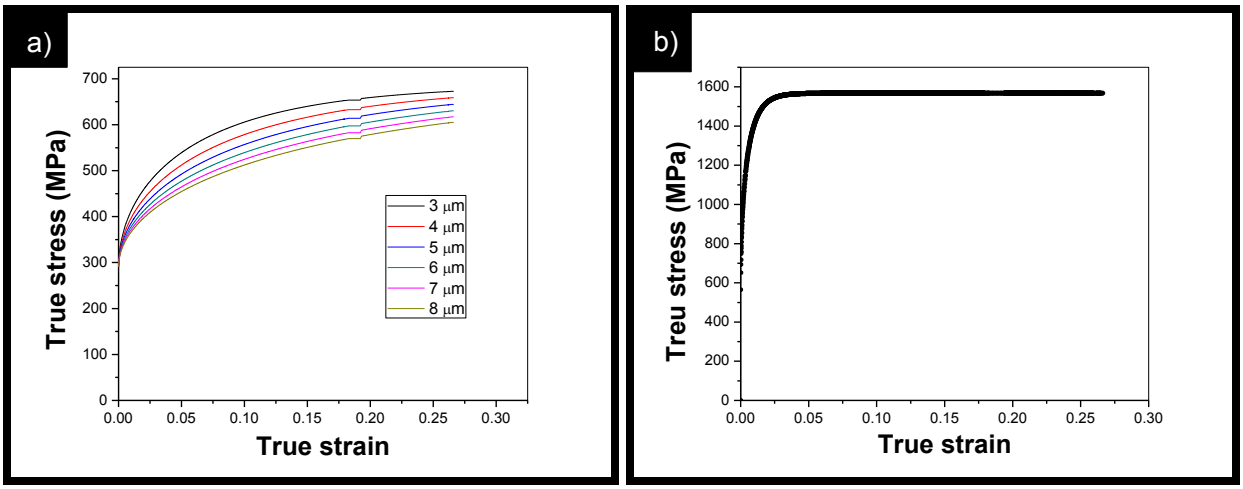

Figure 4.2: Predicted mechanical behaviour of each phase (a) ferrite; with different grain sizes, and (b) martensite

Further, Eq. 3.5 and Eq. 3.6 were used to determine n_f, n_m, K_m, K_f (constants used in the rule of mixture to predict the DP flow curve behavior) for each phase (i.e. ferrite and martensite) by fitting linear curves between *ln (true stress)* and *ln (true strain)* individually for ferrite (with different grain sizes) and martensite [Alabbasi, 2004; Singh, 2014] as shown in Fig. 4.3. Figure 4.3a presents the linear curve fitting between $\ln(\sigma_f)$ and $\ln(\varepsilon_o + \varepsilon_f)$ for ferrite grain size of 5 μm; the intercept of the linear curve gave the value of K_f and slope gave the value of n_f (see Table 4.1). Similar procedure was followed to calculate the values of n_f and K_f for different ferrite grain sizes and results obtained are presented in Table 4.1 (also see Appendix-I). Linear curve fitting between $\ln(\sigma_m)$ and $\ln(\varepsilon_o + \varepsilon_m)$ as shown in Fig. 4.3b, provided the values of n_m and K_m as 0.075 and 1503 MPa respectively.

Further, these values were used in the rule of mixture (Eq. 3.7) to get the composite true stress behavior of the DP steel at different volume fractions of martensite. Literature also

provides that the optimum martensite fraction in DP steels for good combination of strength and ductility is in the range of 10–40 % [Kuziak et al., 2008; Meng et al., 2009; Wang et al., 2011]. In the present work, calculations were restricted to DP steel containing martensite volume fraction (MVF) in this range (10–40 %). Specifically, experimental work has been reported by Kim et al. (1987) and Zhengming et al. (1989) stating that for DP steels, the optimum martensite fraction is 20–25 %.

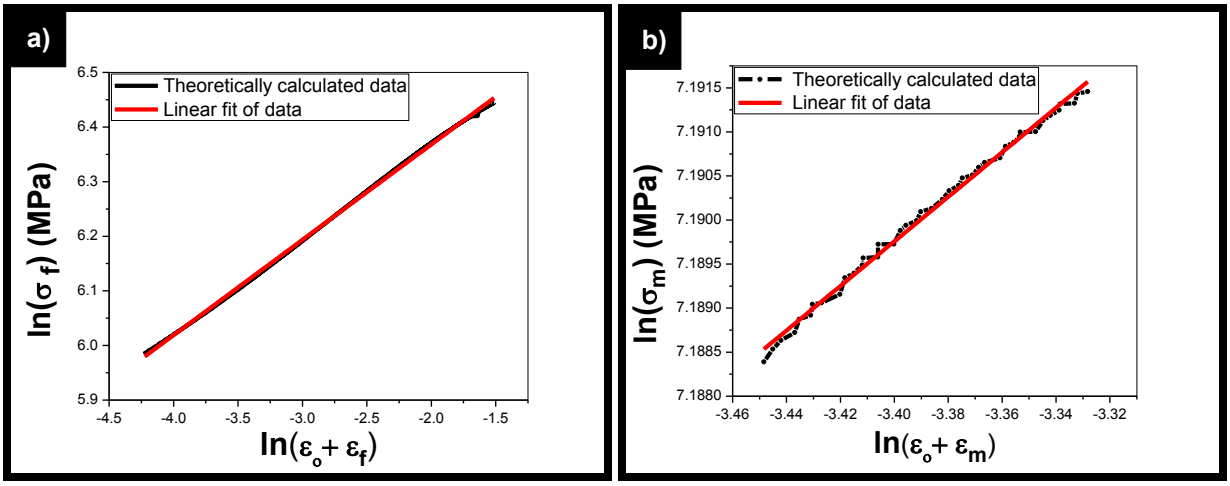

Figure 4.3: Strain hardening exponent for (a) ferrite with 5 µm grain size, and (b) martensite

Table 4.1: Values of n_f and K_f

Average ferrite grain size (µm)	n_f	K_f
3	0.18	837
4	0.19	825
5	0.20	813
6	0.21	794
7	0.22	770
8	0.23	755

For the given steel, when containing DP microstructure (with average grain size of ferrite as 5 µm; and different martensite fractions), the micromechanical modeling provided predictions as presented in Fig. 4.4. Similarly, the flow curves were obtained for DP steel with different martensite fractions (10–40 %) at different ferrite grain sizes (i.e. 3–8 µm), as presented in Appendix-II.

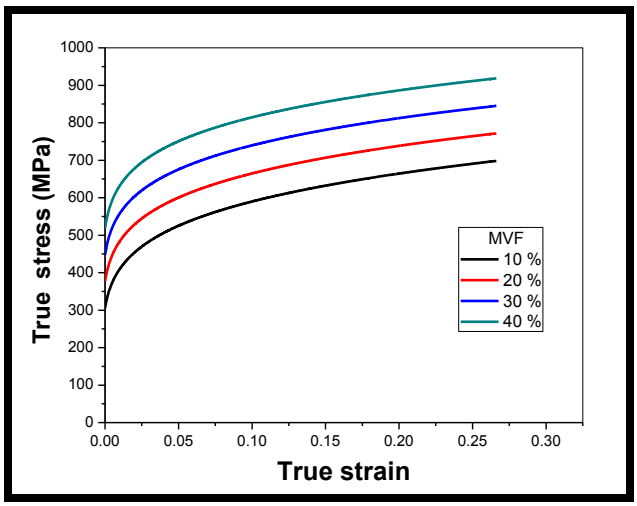

Figure 4.4: Predicted true stress-strain curves for DP steel with different martensite fractions

The true stress and strain values were then converted to engineering stress and strain values for different volume fractions of martensite (10–40 %) with different grain sizes of ferrite (i.e. 3–8 μm). The values of UTS (for a given MVF in the steel), thus obtained, were plotted and are shown in Fig. 4.5. It can be observed from Fig. 4.5 that in order to obtain the ultimate tensile strength in excess of 590 MPa in the steel composition under investigation, the minimum martensite volume fraction required is 25 % (while maintaining the average grain size of ferrite in the range of 3–8 μm).

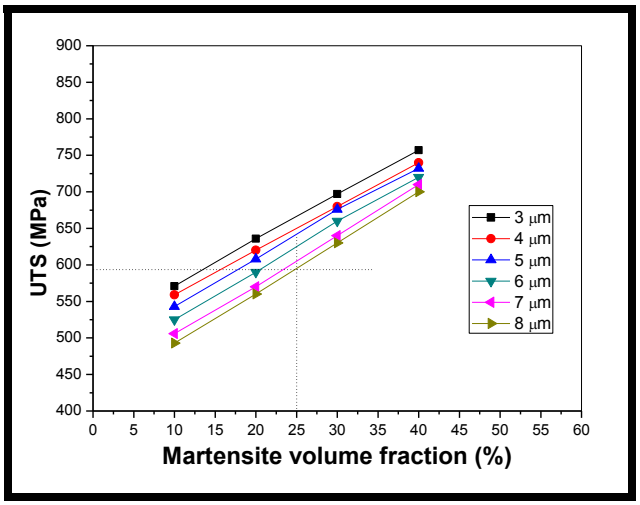

Figure 4.5: Variation of UTS for the steel with DP microstructure containing different volume fractions of martensite

4.4. Process Parameters Predictions Using Commercial Software

In this phase of research, predictions with regards to process parameters i.e. upper and lower critical temperatures, soaking time periods, phase fractions and cooling rates etc. were determined using commercial software viz. Thermo-Calc 3.0, DICTRA, and JMat-Pro 6.1. The objective of this section of research work was to select the appropriate conditions (i.e. annealing temperature, soaking time periods, etc.) for experimentation to develop DP microstructure in steel having a martensite volume fraction of about 25 %.

4.4.1. Predictions of Phase Fractions Using Thermo-Calc

Thermo-Calc software was used to generate the equilibrium phase diagram and the phase fraction diagram for the as-received steel. Figure 4.6 presents the result window of Thermo-Calc software showing the equilibrium diagram (see Fig. 4.6a) and the phase fraction diagram (see Fig. 4.6b). The lower (Ac_1) and upper (Ac_3) critical temperatures predicted by equilibrium phase diagram were 680 ℃ and 839 ℃ respectively.

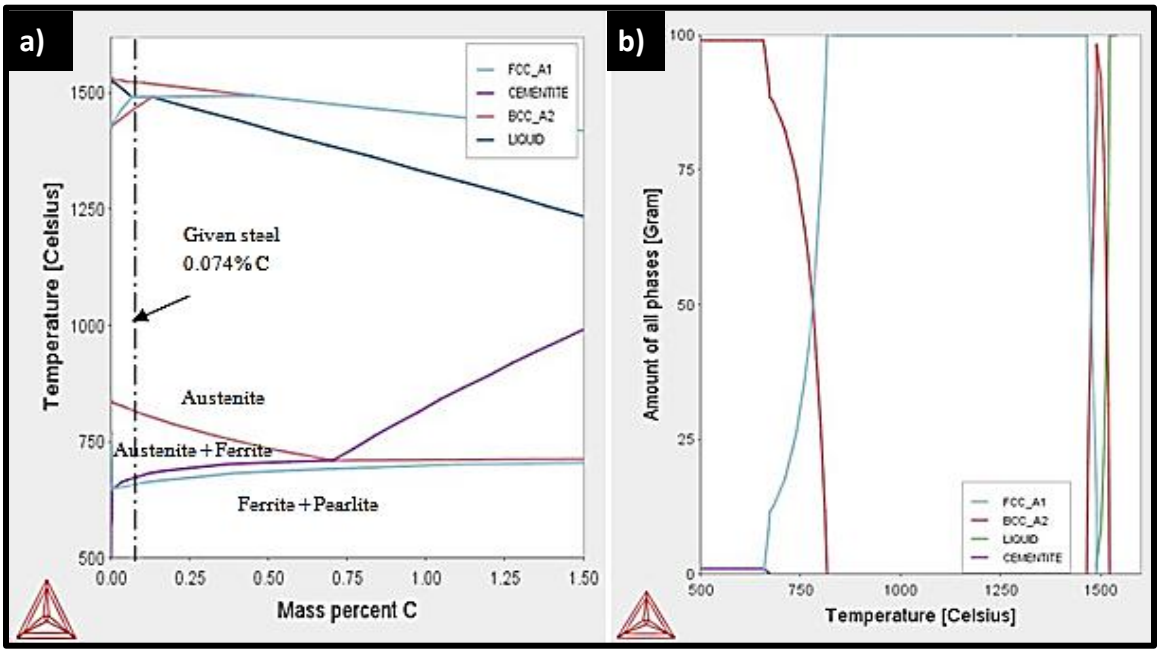

Figure 4.6: Result window of Thermo-Calc showing (a) equilibrium phase diagram, and (b) property diagram under equilibrium conditions

The results of Fig. 4.6b related to austenite fractions at different annealing temperatures were summarized separately and presented in Fig. 4.7. So, Fig. 4.7 presents the variation of austenite fractions formed with respect to different annealing temperatures, under equilibrium conditions. Increasing trend in austenite fraction with increase in annealing temperature can be observed from Fig. 4.7. From Fig. 4.7 it was observed that for formation of austenite (and hence martensite) with a volume fraction of 25 % in the steel, the minimum annealing temperature required was 750 ℃. However, this predicted temperature (750 ℃) obtained from Thermo-Calc software was valid if conditions were of equilibrium. Since, the conditions for practical/ industrial situations are not one of equilibrium, it was expected that the actual amount of austenite (and hence martensite) obtained in the steel at 750 ℃ will be lesser than the desired 25 % MVF (as predicted by micro-mechanical modeling for achieving UTS ≥ 590 MPa). For the aforesaid reason, the starting annealing temperature for experiments was needed to be higher than 750 ℃.

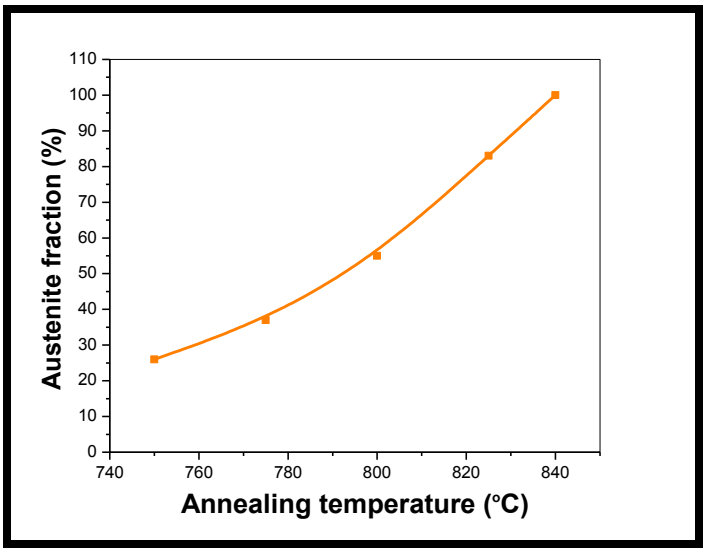

Figure 4.7: Thermo-Calc predictions for variation in austenite fraction with annealing temperature

4.4.2. Predictions Using DICTRA

DICTRA software was used in the present work to predict the holding time periods required for the condition “just completion of pearlite dissolution into austenite” at a given annealing temperature. DICTRA simulation results for various time-temperature combinations are shown in Fig. 4.8.

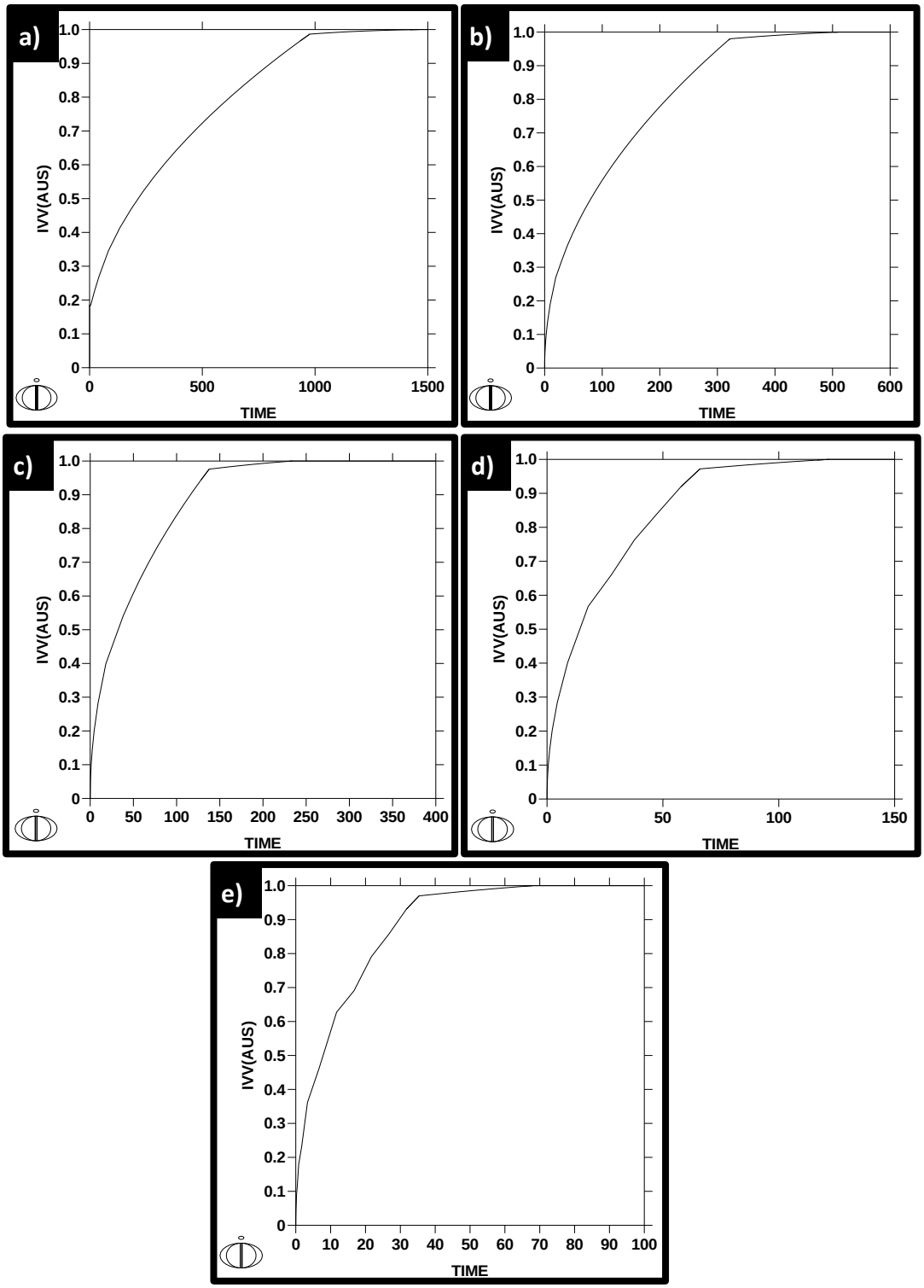

Figure 4.8: Results window of DICTRA simulations for holding periods required at annealing temperatures of (a) 750 ℃, (b) 775 ℃, (c) 800 ℃, (d) 825 ℃, and (d) 840 ℃

The simulation results were summarized and are presented in Fig. 4.9. The results showed that as the isothermal annealing temperature increases, the time taken for dissolution of pearlite into austenite reduces. It was observed from the DICTRA simulation results that annealing temperature of 750 ℃ demanded an extremely large holding period of 1000 s (not suitable for industrial applications). For the aforesaid reason, the starting annealing temperature for experiments was needed to be higher than 750 ℃.

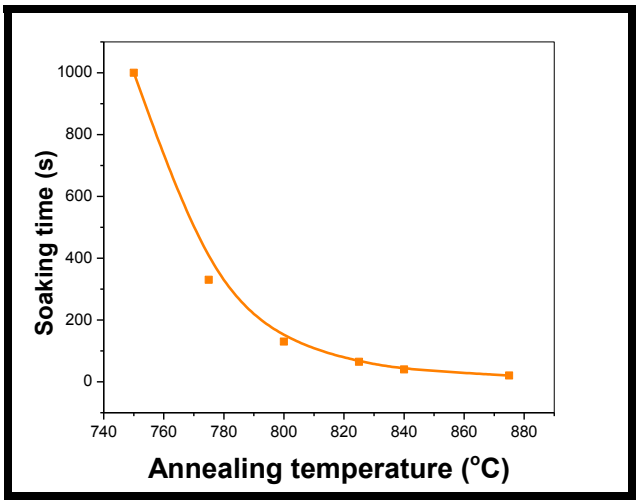

Figure 4.9: DICTRA predictions regarding soaking time as a function of annealing temperature

In the light of the above discussions (both, Thermo-Calc and DICTRA results), it was decided to use 775 ℃ as the starting temperature for experimentation work. This temperature appeared to overcome both the limitations of the earlier predicted temperature of 750 ℃. With 775 ℃ as the annealing temperature, an austenite (and hence martensite) fraction of more than 25 % could be obtained in the steel under experimental conditions and that too with a much lower predicted holding of 330 s.

4.4.3. Predictions Using JMat-Pro

The starting annealing temperature for experiments was decided as 775 ℃ as discussed in the last section. Further, it was decided that experiments be conducted in the whole intercritical range, and thus four different annealing temperatures of 775, 800, 825, and 840 ℃ (just above the theoretically predicted UCT). JMat-Pro 6.1 software was now used to construct CCT diagrams for the steel at the selected annealing temperatures. For every annealing temperature, a distinct

CCT diagram was constructed to determine the cooling rate required for complete transformation of austenite to martensite. Figure 4.10 presents the CCT diagrams obtained from JMat-Pro for different annealing temperatures. Figure 4.10a demonstrates the cooling rate required for the complete transformation of austenite to martensite during annealing at 775 ℃. Results provided by CCT diagrams with regards to cooling rates required (for austenite to martensite transformations) for different annealing temperatures are summarized in Fig. 4.11. Further, it can be observed form Fig. 4.11 that as the annealing temperature increases, the cooling rate required for complete austenite to martensite transformations also increases.

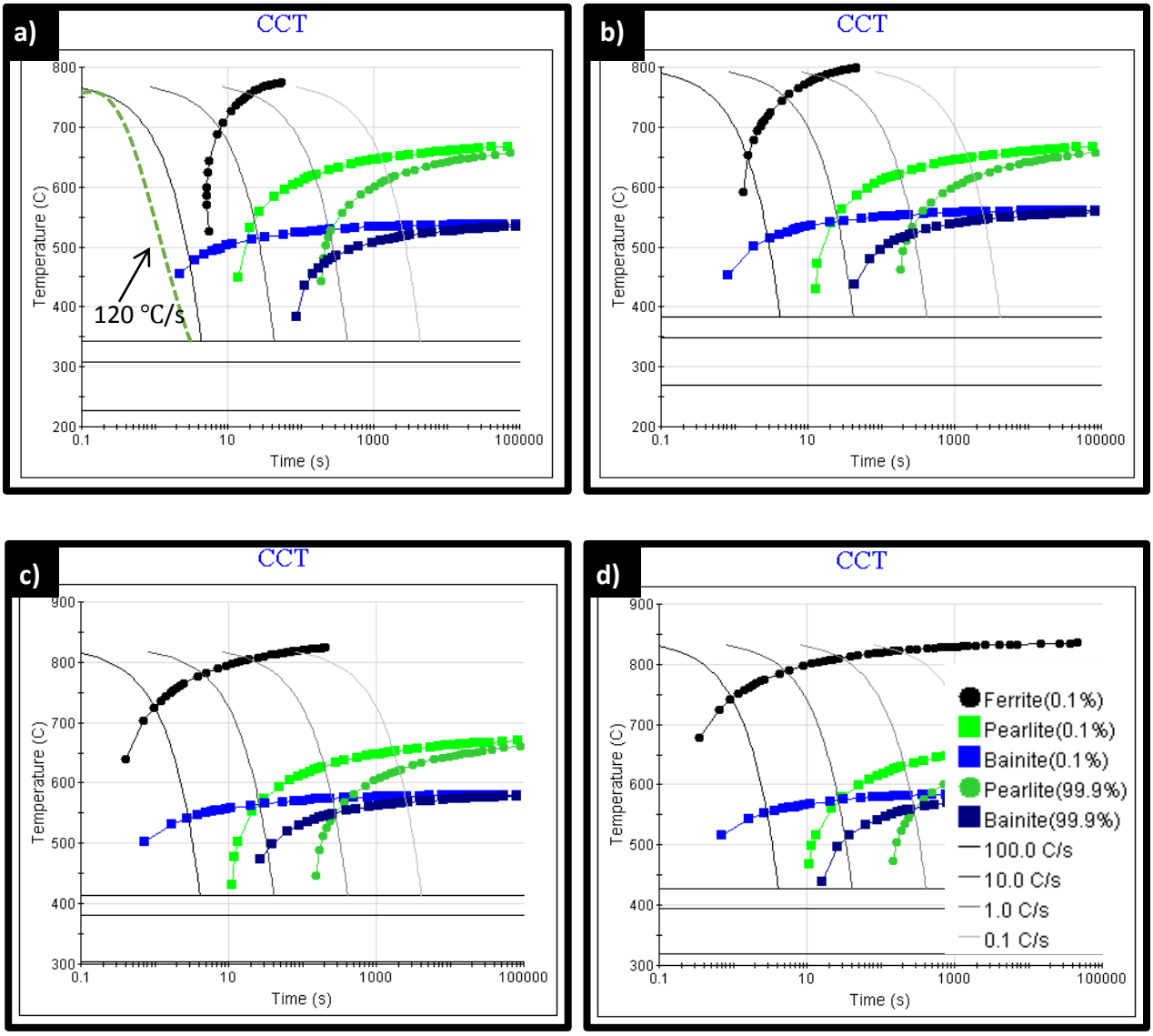

Figure 4.10: Results window JMat-Pro showing CCT diagrams for the steel at annealing temperatures of (a) 775 ℃, (b) 800 ℃, (c) 825 ℃, and (d) 840 ℃

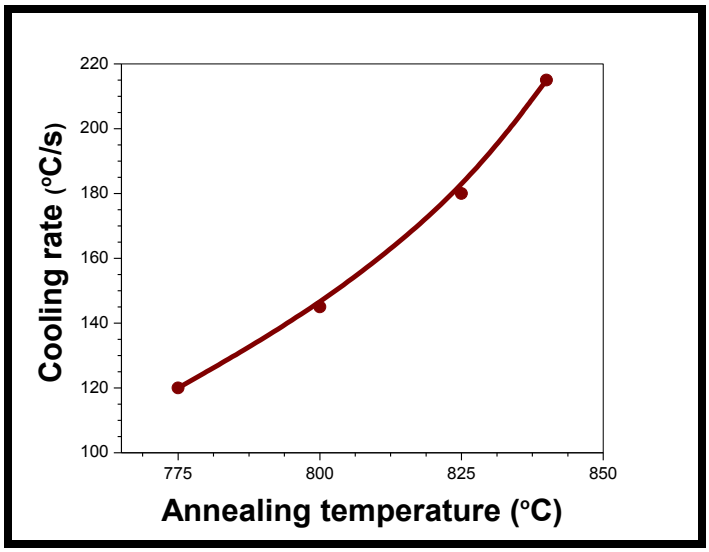

Figure 4.11: Cooling rate as a function of annealing temperature predicted from JMat-Pro

4.5. Annealing Experiments and Microstructural Analysis

After predicting the process parameters, the next step was to perform the heat treatment experiments in the annealing simulator. In this step, tensile samples (dog bone shaped samples of 35 mm gauge length as per ASTM standard E-8M) were heated in a controlled environment and were cooled under controlled cooling rates. Annealing experiments were performed in the annealing simulator by following different processing routes i.e. different soaking time periods, annealing temperatures and different cooling rates (as decided in the above discussed sections) to obtain different microstructures.

4.5.1. Intercritical Annealing Simulation at 775 ℃

This section describes the heat treatment of specimen subjected to inter-critical annealing at a temperature of 775 ℃. Specimen was heated at a heating rate of 10 ℃/s from room temperature to 775 ℃ and was soaked there for 330 s (time, as predicted by DICTRA for complete pearlite dissolution). After soaking for the desired period, the specimen was cooled with the cooling rate of 120 ℃/s (cooling rate, as predicted by JMat-Pro) to the room temperature. The complete annealing simulation thermal profile followed for simulation at 775 ℃ is presented in Fig. 4.12. Figure 4.13a–b presents the optical micrographs showing the corresponding microstructures.

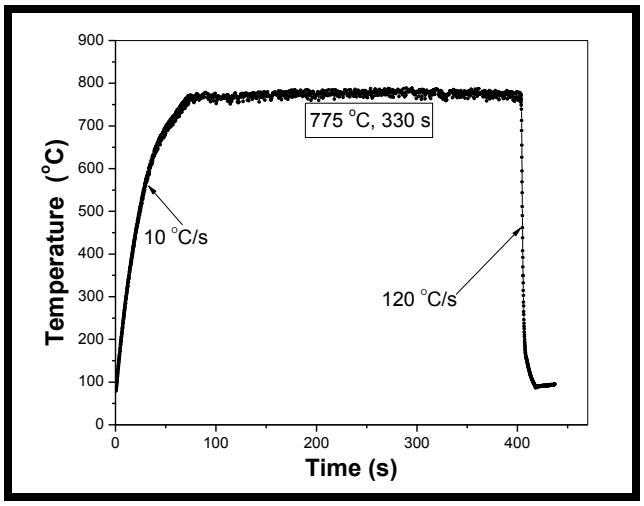

Figure 4.12: Annealing simulation thermal profile at annealing temperature of 775 ℃

Microstructural Analysis

The optical microscopy of the specimen austenitized at 775 ℃ for 330 seconds followed by rapid cooling at the rate of 120 ℃/s resulted in ferrite and martensite dual phase microstructure as presented in the Fig. 4.13a. For better identification of phases in the microstructure, color etchant was also used (as described in section 3.3.4). Color metallography also revealed the dual phase microstructure consisting ferrite (light brown) and martensite (dark brown) [Zakerinia et al., 2009] as shown in Fig. 4.13b. In order to confirm the results of optical microscopy, microhardness values of constituent phases were determined (see Appendix-III). Microhardness values were compared with previous work on similar steels [Armaki et al., 2014] and confirmed the presence of ferrite and martensite phases in the microstructure of processed steel. This showed that during the heating and soaking steps for annealing temperature of 775 ℃, complete pearlite dissolution took place for transformation to austenite phase. Phase fraction analysis by using 'analySIS FIVE software' determined the martensite volume fraction at about 28 %. Since this amount (28 %) was more than the initial pearlite fraction (16 %), it meant that austenite formation had occurred because of transformation of pro-eutectoid ferrite also in addition to the dissolution of pearlite. The increase in austenite fraction during experiments (as compared to Thermo-Calc predictions) was because of the holding time selected from DICTRA results. DICTRA predictions are ideally not for cold worked steels. Since, cold rolled structures have high dislocation densities and increased nucleation rates for phase transformations as compared to normal steel, these deformed states in steels always result in higher phase fractions for a given

time-temperature condition. For this reason, the holding time predicted for dissolution of only pearlite led to conversion of some pro-eutectoid ferrite also along with pearlite for the formation of austenite, and hence its increased amount in the microstructure.

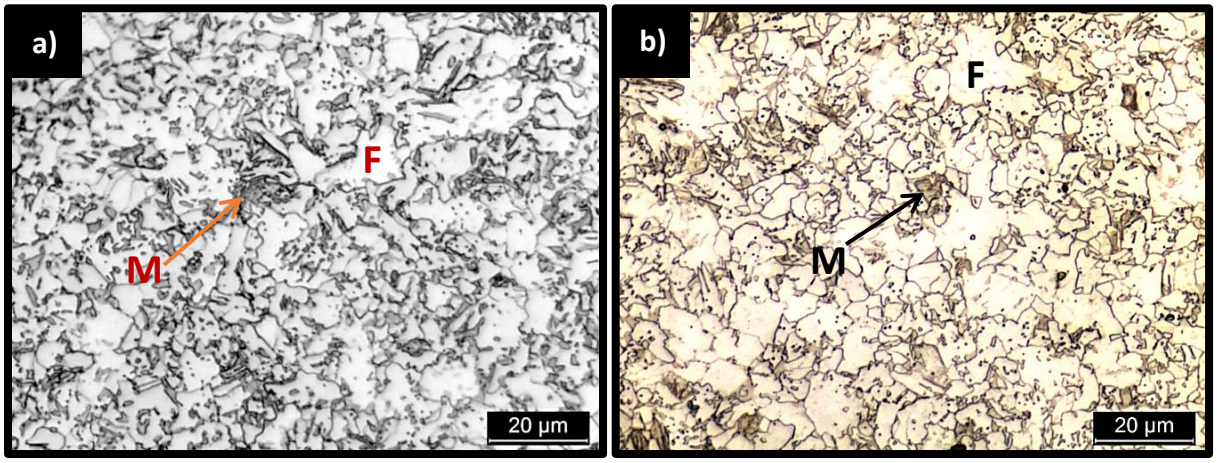

Figure 4.13: Optical micrographs of specimens annealed at 775 ℃ etched with (a) nital, and (b) picral+$Na_2O_3S_5$. F= Ferrite and M= Martensite

Further, during subsequent cooling, the ferrite phase remained unchanged, however austenite (28 %) transformed to martensite. Further, the average grain sizes of ferrite and martensite phases (measured by using 'analySIS FIVE') recorded after this treatment was about 6.7 µm and 3.2 µm respectively. For the annealing temperature of 775 ℃ , Thermo-Calc had predicted the volume fraction of austenite as 37 %. But, as the conditions during experimentation were not of equilibrium, lesser austenite (~28 % in terms of martensite) was actually observed in the annealed sample. Further, this decrease in austenite fraction meant that austenite actually formed in steel during experiment was of higher carbon content (as compared to austenite if it was 37 % in volume fraction as predicted by Thermo-Calc). This increased amount of carbon in the actually formed austenite stabilized it. As a result this austenite, in order to transform to martensite would require a relatively lower cooling rate than what was predicted by JMat-Pro. For, the aforesaid reason cooling rates lower than what were predicted by software for a given annealing temperature were employed for the remaining experiments. JMat-Pro had predicted the cooling rates (for transforming austenite to martensite) for annealing temperatures of 800, 825, and 840 ℃ as 165, 195, 215 ℃/s respectively. However, for these annealing temperatures a lower constant cooling rate of 150 ℃/s was used for experimentation work.

4.5.2. Intercritical Annealing Simulation at 800 ℃

This section describes the heat treatment of tensile specimen subjected to inter-critical annealing at a temperature of 800 ℃. Specimen was heated with the heating rate of 10 ℃/s from room temperature to 800 ℃ and soaked there for 130 s (time, as predicted by DICTRA for complete pearlite dissolution). After the soaking, specimen was cooled with a cooling rate of 150 ℃/s (lesser than 165 ℃/s as predicted by JMat-Pro) to the room temperature. The complete annealing simulation thermal profile followed for simulation at 800 ℃ is presented in Fig. 4.14. Figure 4.15a–b presents the optical micrographs showing the corresponding microstructures.

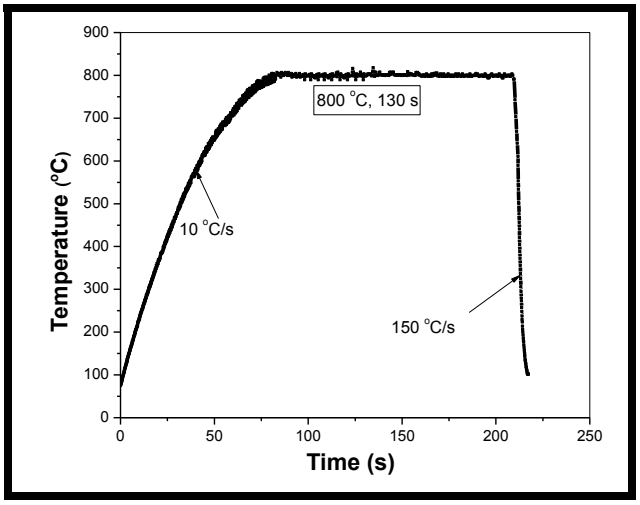

Figure 4.14: Annealing simulation thermal profile at annealing temperature of 800 ℃

Microstructural analysis

Specimen annealed at 800 ℃ resulted in a dual phase microstructure comprising of ferrite and martensite as presented in the Fig. 4.15a. For better identification of phases in microstructure, color etchant was also used (as described in section 3.3.4). Color metallography also revealed the dual phase microstructure consisting of ferrite (light brown) and martensite (dark brown) as shown in Fig. 4.15b. Phase fraction analysis using 'analySIS FIVE' determined martensite volume fraction to be about 31 %. This showed that during the heating and holding steps of annealing at 800 ℃, pearlite available in initial microstructure transformed to austenite. As, the martensite fraction (~31 %) after simulation was more than the pearlite fraction (~16 %) before simulation, this evidenced that during heating and holding process some existing ferrite was also transformed into austenite (as already explained in section 4.5.1). During subsequent cooling, the

ferrite phase remained unchanged, however austenite transformed to the martensite. Transformation of austenite to martensite at a cooling rate even lower than predicted by JMat-Pro was for reason already explained in section 4.5.1. Average ferrite and martensite grain sizes obtained under this annealing condition were about 6.4 µm and 3.5 µm respectively.

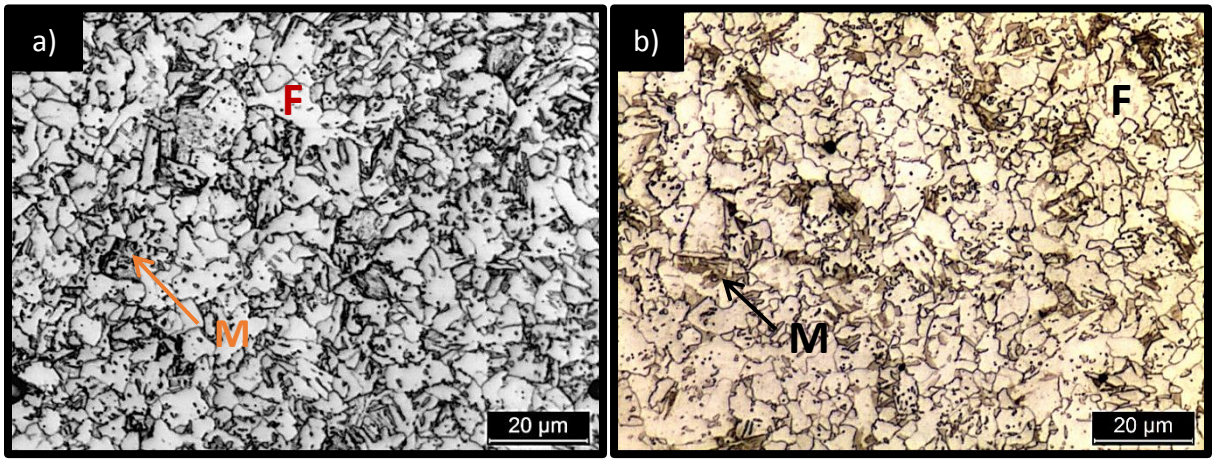

Figure 4.15: Optical micrographs of specimens annealed at 800 ℃ etched with (a) nital, and (b) picral+$Na_2O_3S_5$. F= Ferrite and M= Martensite

4.5.3. Intercritical Annealing Simulation at 825 ℃

This section describes the heat treatment of tensile specimen subjected to inter-critical isothermal annealing at a temperature of 825 ℃. Specimen was heated with the heating rate of 10 ℃/s from room temperature to 825 ℃ and soaked there for 65 seconds (time, as predicted by DICTRA for complete pearlite dissolution). After soaking for the desired period, specimen was cooled at 150 ℃/s to room temperature. The complete annealing simulation thermal profile followed for simulation at 825 ℃ is presented in Fig. 4.16. Figure 4.17a–b presents the optical micrographs showing the corresponding microstructures.

Microstructural analysis

The specimen annealed at 825 ℃ for 65 seconds resulted in the microstructure composed of ferrite and martensite (see Fig. 4.17a and for colour etching Fig. 4.17b). The 'analySIS FIVE' software determined martensite volume fraction to be about 35 %. This showed that during the heating and holding steps of annealing at 825 ℃, pearlite available in the initial microstructure transformed to austenite. Also, some existing ferrite transformed into fine grained austenite.

During subsequent cooling the ferrite phase remained unchanged, however austenite transformed to fine grained martensite.

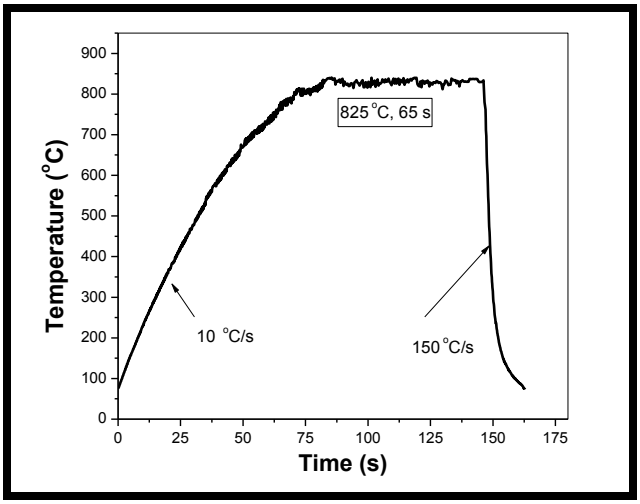

Figure 4.16: Annealing simulation thermal profile at annealing temperature of 825 ℃

At this annealing temperature, refinement in ferrite grain size was observed, as compared to the previous annealing temperatures. Also, the martensite obtained was in the form of globular/oblong type martensite along with the lath type. Martensite laths obtained after annealing at this temperature were larger than the ones obtained during previously discussed two experiments (at 775 and 800 ℃ respectively) and was attributed to the increased martensite fraction at higher annealing temperature of 825 ℃. Average ferrite and martensite grain sizes recorded after this experimental condition was about 4.8 µm and 5 µm respectively.

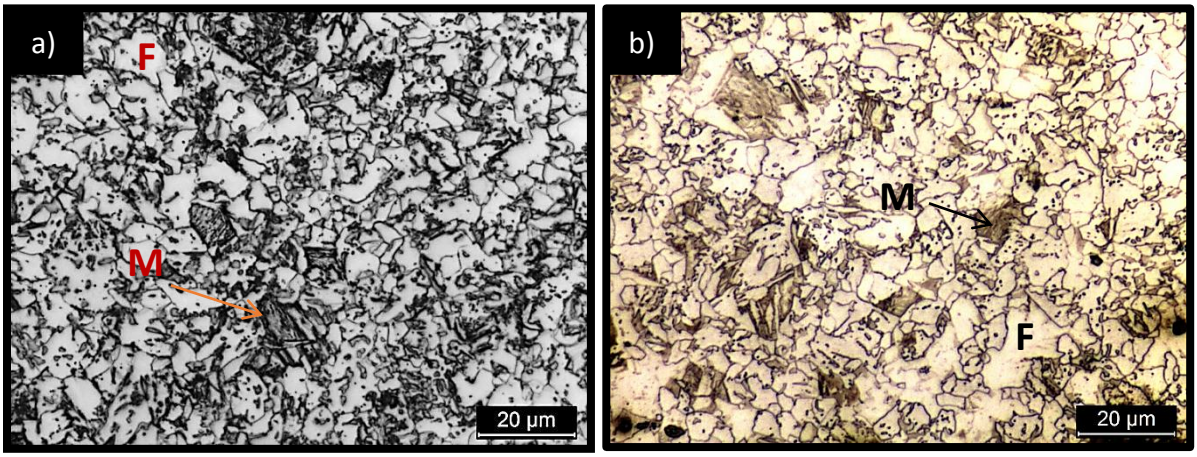

Figure 4.17: Optical micrographs of specimens annealed at 825 ℃ etched with (a) nital, and (b) picral+$Na_2O_3S_5$. F= Ferrite and M= Martensite

4.5.4. Annealing Simulation at 840 ℃

This section describes the heat treatment of tensile specimen subjected to isothermal annealing at a temperature just above the intercritical annealing temperature i.e. at temperature 840 ℃. Specimen was heated with the heating rate of 10 ℃/ s from room temperature to 840 ℃ and soaked there for 40 seconds (time, as predicted by DICTRA for complete pearlite dissolution). After soaking for the desired period, specimen was cooled with the cooling rate of 150 ℃/s to the room temperature. The complete annealing simulation thermal profile followed for simulation at 825 ℃ is presented in Fig. 4.18. Figure 4.19a–b presents the optical micrographs showing the corresponding microstructures.

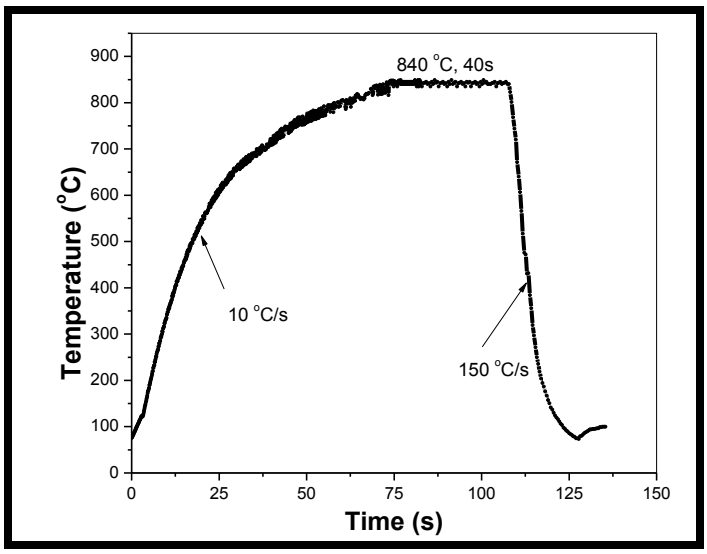

Figure 4.18: Annealing simulation thermal profile at annealing temperature of 840 ℃

Microstructural analysis

The specimen annealed at 840 ℃ resulted in a dual phase microstructure comprising of ferrite and martensite (see Fig. 4.19a–b). The 'analySIS FIVE' software determined the martensite volume fraction of 31 %. This showed that during the heating and holding steps of annealing at 840 ℃, pearlite available in initial microstructure transformed to austenite. Also, some existing ferrite transformed into fine grained austenite. During subsequent cooling at 150 ℃/s , the ferrite phase remain unchanged, however austenite transformed to ferrite and martensite. Martensite obtained after this heat treatment was even finer (finest with average grain size of 2.7 μm) than obtained from the previous heat treatment routes.

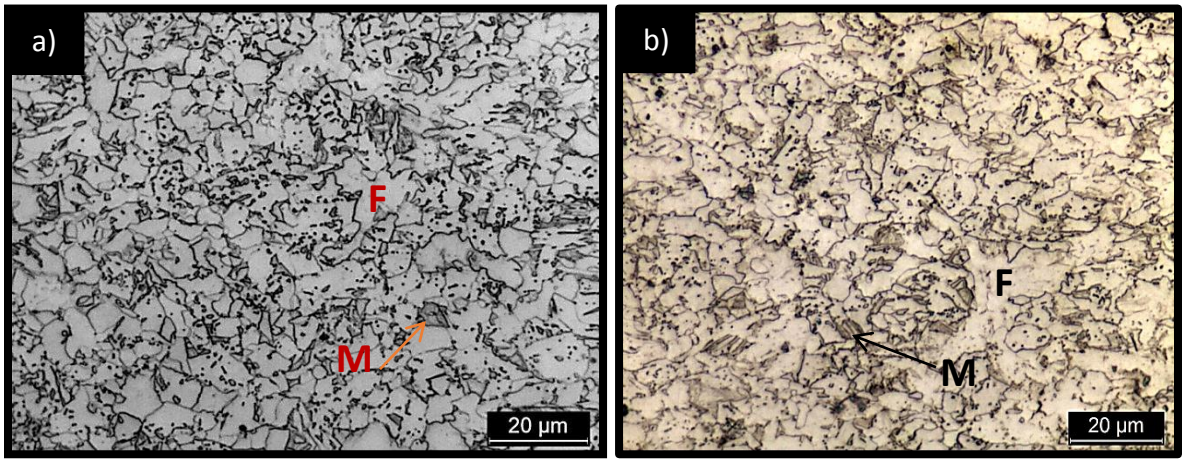

Figure 4.19: Optical micrographs of specimens annealed at 840 ℃ etched with (a) nital, and (b) picral+$Na_2O_3S_5$. F= Ferrite and M= Martensite

This was attributed to the increased annealing temperature (i.e. slightly above Ac_3 temperature) which resulted in increased austenite nucleation during heating; subsequent, fast cooling immediately after short holding time (40 s), prevented the grain growth and thus resulted in fine martensite grains. Average ferrite and martensite grain sizes recorded after this experimental condition was about 5 µm and 2.7 µm respectively. Table 4.2 summarizes the input conditions and results obtained for processing of the given steel at various annealing temperatures.

Table 4.2: Details of DP microstructures obtained in the given steel under different processing conditions

Processing conditions			**Details of DP microstructure obtained in the given steel**			
Annealing temperature (℃)	**Holding time (s)**	**Cooling rate (℃/s)**	**Volume fraction of constituent phases (%)**		**Average grain size of constituent phases (µm)**	
			Martensite	**Ferrite**	**Martensite**	**Ferrite**
775	330	120	28	72	3.2	6.7
800	130	150	31	69	3.5	6.4
825	65	150	35	65	5	4.8
840	40	150	31	69	2.7	5

Effect of Annealing Process on Phase Fraction, Size, Shape and its Distribution

The main focus of the present study was to find the critical microstructure parameters for achieving a good combination of strength and ductility in the given steel. It is well established by various researchers that for DP steels, in addition to the volume fraction of constituent phases

(i.e. ferrite and martensite phases), the size and distribution of martensite phase also plays a major role in determining the properties of DP steel [Armaki et al., 2014; Toudeshky et al., 2014]. Figure 4.20 shows the size and its distribution for the martensite phase present in the given steel processed under different conditions. In Fig. 4.20, the size is presented by the area of martensite grain size.

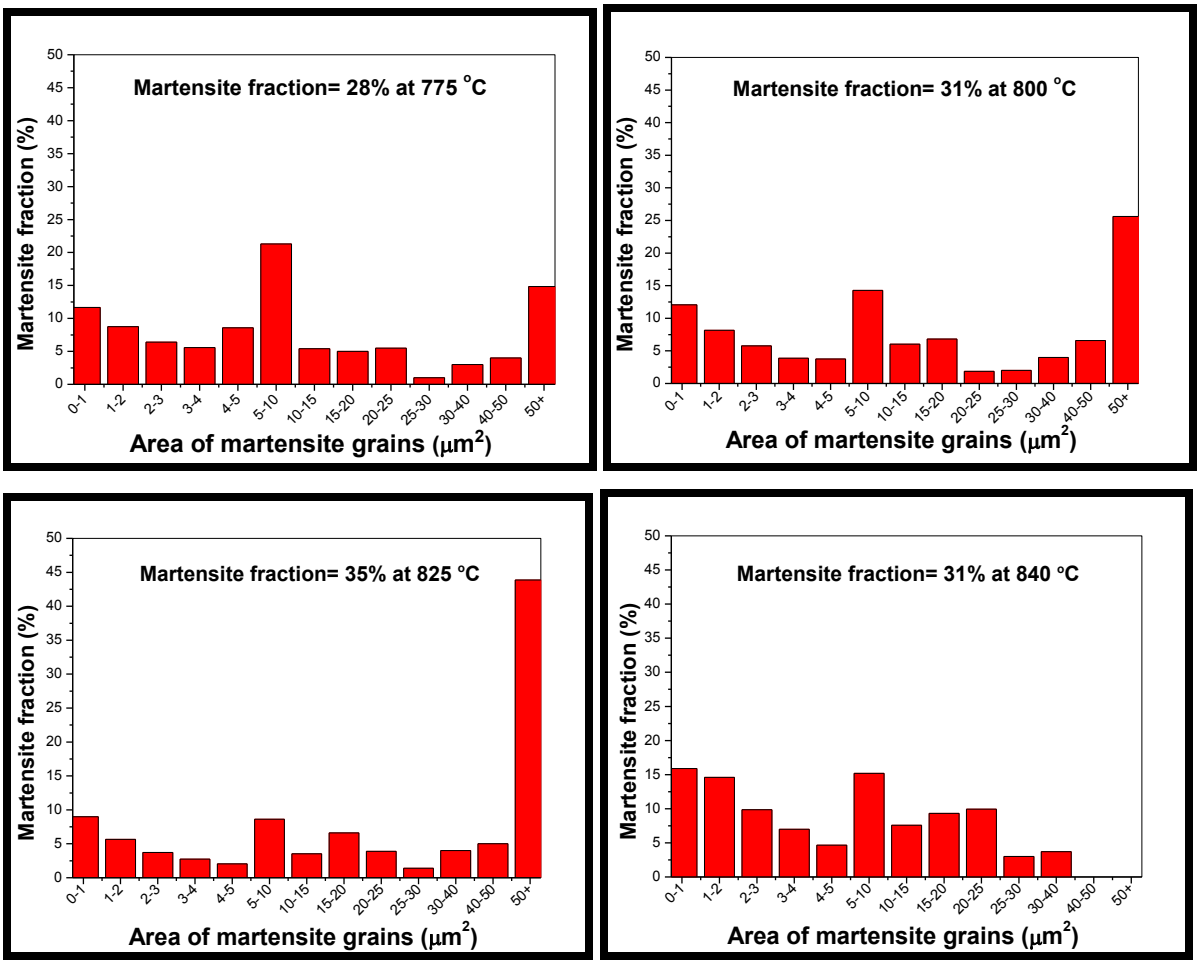

Figure 4.20: Size and distribution of martensite phase in steel under different processing conditions

It can be observed from Fig. 4.20 that for change in annealing temperature from 775 ℃ to 800 ℃, an increase in average grain size of martensite grains was observed (increased from 3.2 to 3.5 μm). Sample annealed at 775 ℃ contained more martensite fraction in the range of 5–10 μm^2 (finer grains) and lesser martensite fraction in the range of 50+ μm^2 (coarser grains) than sample annealed at 800 ℃. At 825 ℃, a substantial increase in martensite volume fraction (35 %) was

observed with relatively large grains (average martensite grain size of 5.0 μm; maximum fraction of grains were of area in the range of more than 50 μm^2). However, for annealing of steel beyond this inter-critical temperature of 825 ℃ (i.e. annealing at 840 ℃), the martensite volume fraction decreased (became 31 % from 35 % at 825 ℃), but resulted in relatively finer martensite grains (average martensite grain size of 2.7 μm; martensite grains were restricted to area in the range of less than 40 μm^2). Thus, as compared to all previous annealing temperatures, the temperature of 840 ℃ resulted in most effective refining of martensite grains. From the results, it was concluded that with increase in annealing temperature in the inter-critical range, the MVF increases and martensite grain size increases till a particular annealing temperature value. However, till this maximum inter-critical temperature, during the annealing process, austenite transforms only into martensite phase. For annealing in the inter-critical range, but beyond this maximum temperature, refinement of martensite grains occurs because of phase transformation, other than austenite to martensite. For annealing at 840 ℃, it was noted that during cooling, austenite transformed initially to ferrite and then to martensite. This austenite to ferrite transformation decreased the martensite fraction (more martensite would have otherwise formed in the absence of austenite to ferrite transformation) and also reduced the martensite grain size (ferrite grains grew in regions where otherwise martensite grains were to form).

In this section, the effect of different processing routes on the martensite volume fraction, its size and accompanying distribution etc. was discussed. The next section further elaborates on the effect of these resulting microstructures on the tensile deformation behavior of the processed steel.

4.6. Tensile Deformation Behavior

Microstructure deformation pattern is most effective in predicting the mechanical behavior of materials [Toudeshky et al., 2014]. This section describes the deformation behavior of various microstructures obtained through different processing routes, and thus, the resulting tensile properties obtained. To study the deformation behavior of microstructures and their effect on tensile properties, microstructural examination of tensile tested specimens (annealed at 775, 800, 825 and 840 ℃ respectively) was conducted on specimens at two different locations (i) at the fracture tip, and (ii) away from the fracture tip (see Fig. 4.21). The stress level at the fracture tip was considered to be higher than the stress level at the location away from the tip, in the

fractured tensile specimen. Microstructural examination at these distinct locations helped to understand the deformation behavior of the investigated steel, at different stress levels i.e. at high stress level near to fracture tip and at low stress level away from fracture tip. In other words, in the fractured specimen, the location, 'fracture tip' represented the microstructure corresponding to UTS of material; however, the location, 'away from the fracture tip' represented the microstructure of material corresponding to stress levels developed in the material lesser than the UTS value.

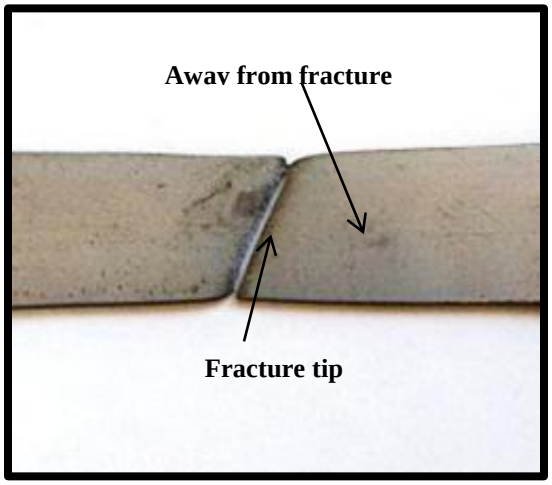

Figure 4.21: Tensile tested specimen describing the locations selected for analysis of deformation behavior

4.6.1. Deformation Response of Specimen Annealed at 775 ℃

Figure 4.22a–b presents the microstructures at 'fracture tip' and 'away from fracture tip' locations respectively for the (fractured) tensile tested specimen annealed at 775 ℃. It was observed from the two micrographs that the microstructures present in the fractured specimen at the two distinct locations (at the fracture tip, and away from it respectively) were markedly different. It was noted that the microstructure of specimen at the fracture tip was relatively more deformed than was for the location away from the tip (i.e. martensite and ferrite grains present in microstructure of specimen at location of fracture tip were more deformed than their counterparts for location away from the fracture tip). Also, it was noted that for this annealing temperature, for a given location, ferrite grains appeared more deformed as compared to martensite grains (i.e. alignment of ferrite grains in the tensile deformation direction was more than the martensite grains). It is well known that stress level at location away from the fracture tip is less than the

stress level at the fracture tip. In other words, the location away from the fracture tip in the fractured specimen represents conditions of low applied stress on the material. Since, the micrograph of specimen for location away from the fracture tip showed ferrite grains to be more deformed as compared to martensite grains, it showed that deformation of ferrite started in steels prior to the deformation of martensite phase. Thus, the initial yielding/ yield strength of the dual-phase steel is correlated with the start of plastic deformation of ferrite. In the present case, it resulted in yield strength of 285 MPa (see Fig. 4.23).

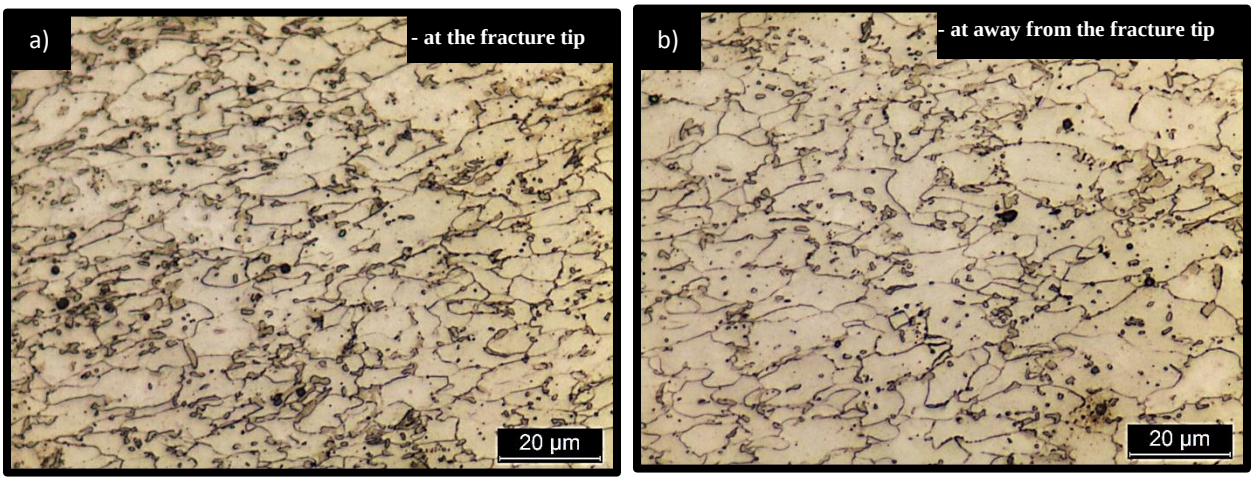

Figure 4.22: Optical micrographs of fractured specimen annealed at 775 ℃ for locations: (a) at the fracture tip, and (b) away from the fracture tip

Further, Fig. 4.22b evidenced the small deformation of martensite grains even at low stress levels (i.e. location away from the fracture tip; so low stress level). This showed that the onset of plastic flow and hardening of martensite phase commences well before the ultimate tensile strength is reached in the dual-phase steel (i.e. strain hardens the steel) and thus, helps in achieving a low YS to UTS ratio, as also reported by Armaki et al. (2014).

Further, it was also observed that the martensite grains at/ near the grain boundary regions were aligned more in the direction of tensile deformation, whereas the fine martensite grains inside the ferrite grains were not deformed to that extent (see Fig. 4.22a–b). Figure 4.23 presents the tensile properties of specimen annealed at 775 ℃.

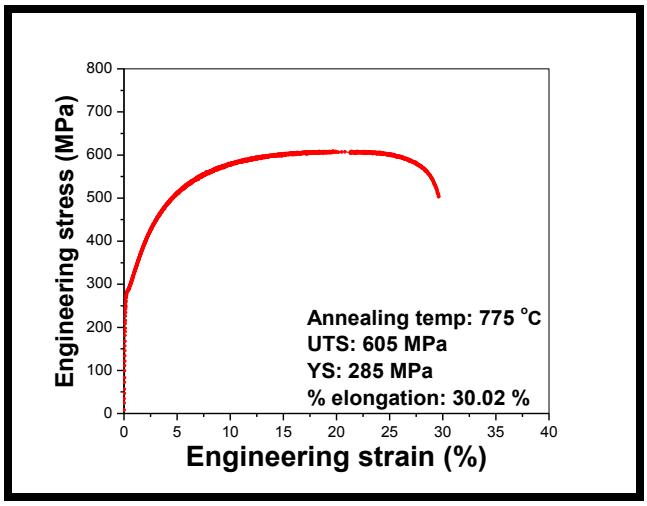

Figure 4.23: Tensile curve of specimen annealed at 775 ℃

4.6.2. Deformation Response of Specimen Annealed at 800 ℃

Figure 4.24a–b presents the microstructures at 'fracture tip' and 'away from fracture tip' locations respectively for the (fractured) tensile tested specimen annealed at 800 ℃. Deformation behavior of the specimen annealed at 800 ℃ was similar to that of the specimen annealed at 775 ℃. This means (i) more deformation in ferrite than martensite was observed (see Fig. 4.24a–b), (ii) relatively coarse martensite grains deformed more than the fine martensite grains, and (iii) the martensite grains at/ near the grain boundary regions were aligned more in the direction of tensile deformation, whereas the fine martensite grains inside the ferrite grains were less deformed (see Fig. 4.24a–b).

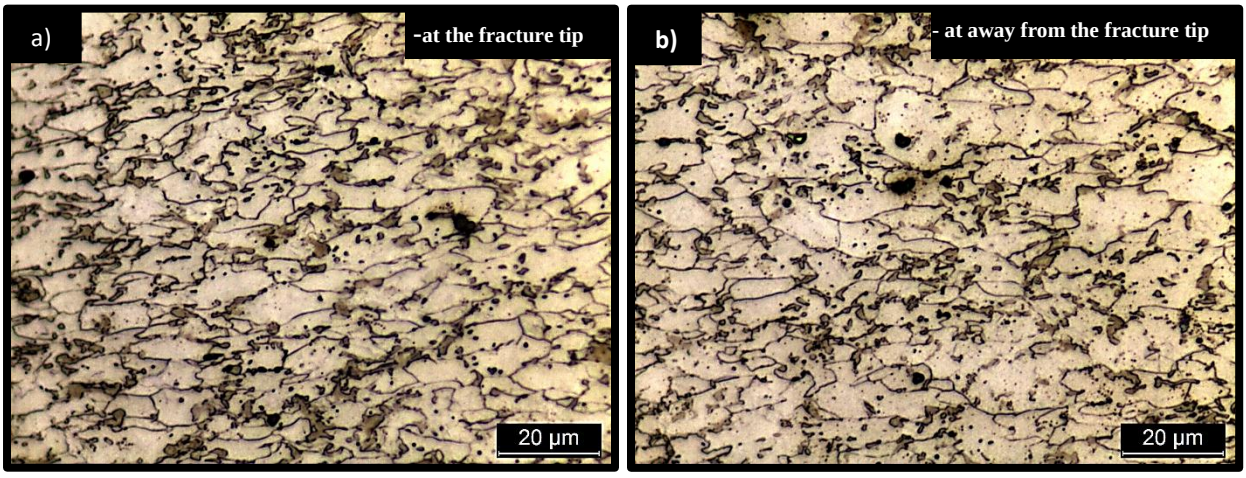

Figure 4.24: Optical micrographs of fractured specimen annealed at 800 ℃ for locations: (a) at the fracture tip, and (b) away from the fracture tip

The tensile properties obtained in the specimen at 800 ℃ were comparable to the properties of specimen annealed at 775 ℃ because of their almost similar microstructure i.e. martensite phase fraction, size and its distribution, and morphology of phases. A little improvement observed in the Even the martensite contents in sample annealed at 800 ℃ was slightly more than the sample annealed at 775 ℃, but the tensile properties were almost similar as can be observed from Fig. 4.23 and 4.25. Similar tensile properties were attributed to the similar ferrite-martensite fraction, size distribution and deformation characteristics after these two annealing conditions.

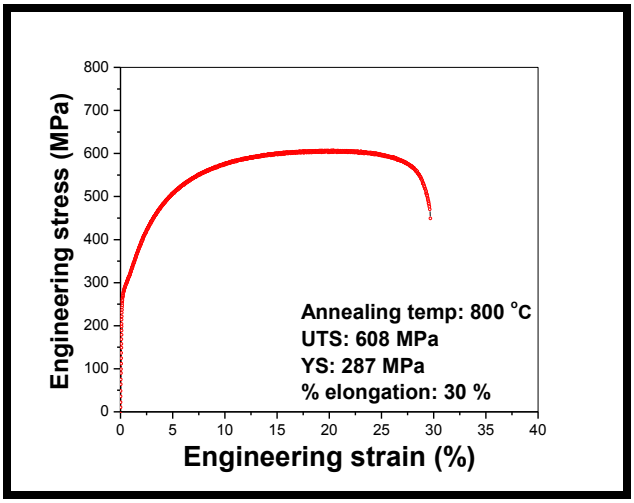

Figure 4.25: Tensile curve of specimen annealed at 800 ℃

4.6.3. Deformation Response of Specimen Annealed at 825 ℃

Figure 4.26a–b presents the microstructures at 'fracture tip' and 'away from fracture tip' locations respectively for the (fractured) tensile tested specimen annealed at 825 ℃. Again, it was observed from the two micrographs that the microstructures present in the fractured specimen at the two distinct locations (at the fracture tip, and away from it respectively) were markedly different. It was noted that the microstructure of specimen at the fracture tip was highly deformed than was for the location away from the tip (i.e. martensite and ferrite grains present in microstructure of specimen at location of fracture tip were far more deformed than their counterparts for location away from the fracture tip). However, it was noted that as compared to specimens annealed at 775 ℃/ 800 ℃, the deformation in microstructure at location away from fracture was significantly lesser for the specimen annealed at 825 ℃ (see Fig. 4.22b and Fig.

4.26b; the microstructure at 825 ℃ shows very little alignment of grains along the tensile direction as compared to microstructures obtained at 775 ℃/ 800 ℃).

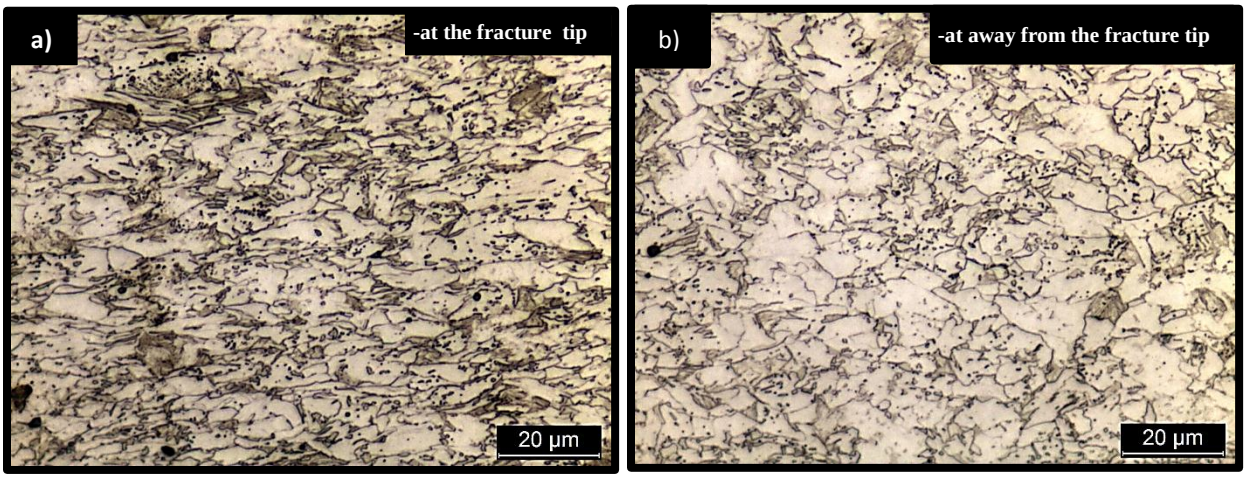

Figure 4.26: Optical micrographs of fractured specimen annealed at 825 ℃ for locations: (a) at the fracture tip, and (b) away from the fracture tip

This significantly less deformation at low stress level (represented by location away from fracture tip) resulted in a high value of yield stress (375 MPa, see Fig. 4.27) required for initial yielding in the specimen annealed at 825 ℃.

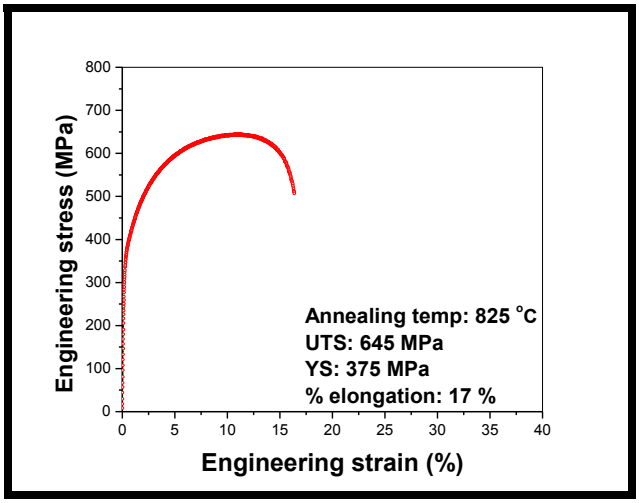

Figure 4.27: Tensile curve of specimen annealed at 825 ℃

Further, for the location at the fracture tip, for the specimen annealed at 825 ℃, severe deformation of microstructure as compared to location 'away from the fracture tip' was observed

(see Fig. 4.26a–b). This difference in the extent of deformation of microstructure at the two locations showed large stress localization at the tip. Stress localization at the fracture tip was attributed to the presence of high contents of martensite and refinement of ferrite grains (as compared to annealing temperatures of 775 and 800 ℃). The increased martensite content around ferrite strengthened the ferrite against deformation, and thus increased the yield strength (see Fig.4.26b). Also, the increased martensite fraction raised the UTS of steel but at the expense of decrease in ductility (see Fig. 4.27). Further, it was also observed that the martensite grains at/ near the grain boundary regions were aligned more in the direction of tensile deformation, whereas the fine martensite grains inside the ferrite grains were not deformed to that extent (see Fig. 4.26a–b).

4.6.4. Deformation Response of Specimen Annealed at 840 ℃

Figure 4.28a–b presents the microstructures at 'fracture tip' and 'away from fracture tip' locations respectively for the (fractured) tensile tested specimen annealed at 840 ℃. Again, it was observed from the two micrographs that the microstructures present in the fractured specimen at the two distinct locations (at the fracture tip, and away from it respectively) were markedly different. It was noted that the microstructure of specimen at the fracture tip was highly deformed than was for the location away from the tip (i.e. martensite and ferrite grains present in microstructure of specimen at location of fracture tip were far more deformed than their counterparts for location away from the fracture tip).

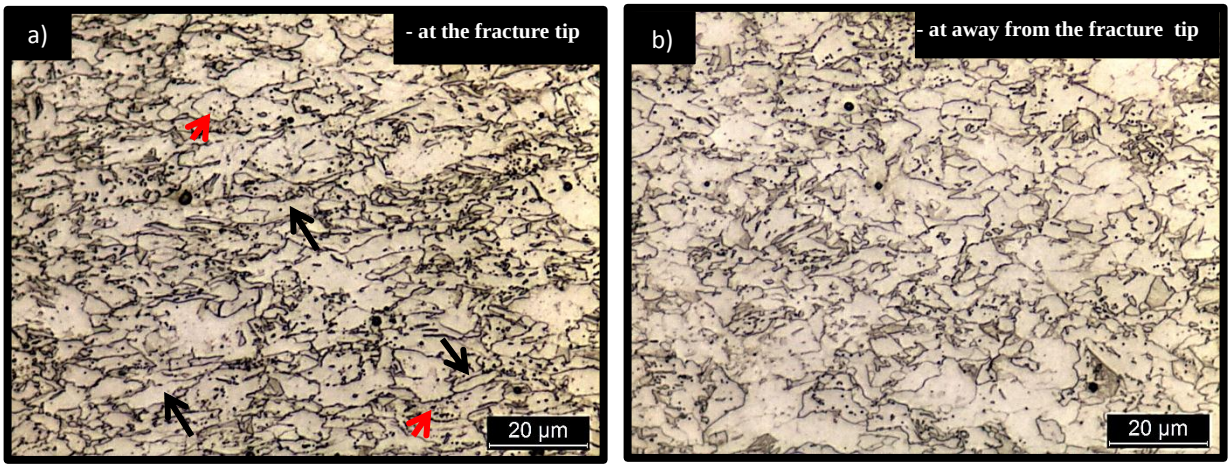

Figure 4.28: Optical micrographs of fractured specimen annealed at 840 ℃ for locations: (a) at the fracture tip, and (b) away from the fracture tip

However, it was noted that as compared to specimens annealed at 775 ℃/ 800 ℃, the deformation in microstructure at location away from fracture was significantly lesser for the specimen annealed at 840 ℃, an observation similar to what was noted for 825 ℃ specimen also (see Fig. 4.22b and Fig. 4.28b; the microstructure at 840 ℃ shows very little alignment of grains along the tensile direction as compared to microstructures obtained at 775 ℃/ 800 ℃). This significantly less deformation at low stress level (represented by location away from fracture tip) resulted in a high value of yield stress (422 MPa) required for initial yielding in the specimen annealed at 840 ℃. This annealing temperature also resulted in the maximum UTS (677 MPa) with ductility of 16 % (comparable to what was obtained for 825 ℃). Annealing of the steel at 840 ℃ resulted in a dual phase microstructure with extremely fine grains of martensite (MVF = 31 %). These fine grains of martensite were distributed around and also within the fine ferrite grains. The increased martensite content around ferrite strengthened the ferrite against deformation, and thus increased the yield strength (see Fig. 4.29). It was observed from Fig. 4.28a that ferrite grains in which fine martensite grains were embedded did not show considerable deformation. On the contrary, ferrite grains within which martensite grains were absent, deformed considerably in the tensile direction, thus meaning that embedded martensite grains assisted in improvement of strength (see markings in Fig. 4.28a; black arrows represent the elongated grains, while red arrows represent the non-elongated grains). These fine martensite clusters embedded in ferrite grains were more in the amount in the specimen annealed at 840 ℃, resulting in higher UTS (677 MPa) and YS (422 MPa).

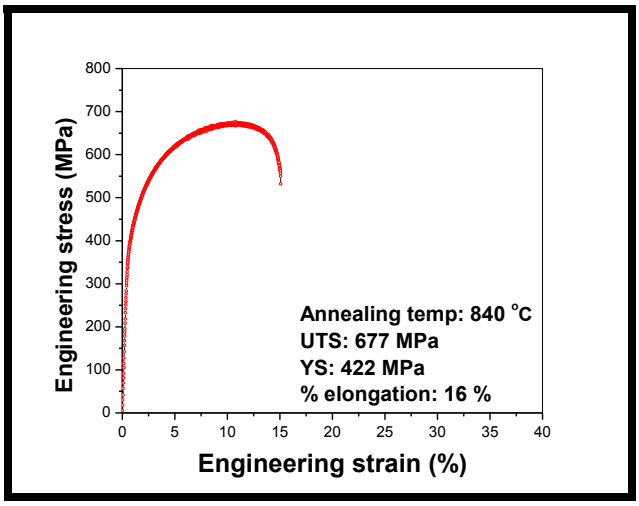

Figure 4.29: Tensile curve of specimen annealed at 840 ℃

Further, the specimen annealed at 840 ℃ resulted in almost similar ductility (16 %) as compared to the specimen annealed at 825 ℃ (ductility 17 %). This similar ductility, even at increased amount of UTS was attributed to the decrease of martensite content from 35 % (at 825 ℃) to 31 % (at 840 ℃).

From the discussion of results in this section it was noted that the initial yielding of dual-phase steel is correlated with the start of plastic deformation of ferrite. It was also observed that the plastic flow and hardening of martensite commenced well before the ultimate tensile strength is reached in the dual-phase steel. Further, it was observed that the resistance to deformation offered by fine grained martensite was more than what was offered by coarse grained martensite. Also, it was observed that the resistance to deformation offered by fine grains of martensite distributed around and also within the fine ferrite grains helped to improve the UTS.

The next section will describe the approach employed for obtaining (i) further refinement of martensite grains, and also (ii) clusters of fine martensite grains in ferrite grains.

4.7. Thermal Cycling

Thermal cycling is a kind of heat treatment that helps to refine the grains present in the microstructure. Thermal cycling process prevents the grain growth kinetics and increases the recrystallization kinetics by imposing strain heterogeneity between the recrystallized and deformed regions. Nucleation occurs in high strain energy regions during the first few thermal cycles. It creates increased strain heterogeneity between the recrystallized and residual deformed regions. On subsequent thermal cycles, nucleation takes place in the residual deformed regions, as these are the more potential sites owing to their high stored strain energy in preference to the recrystallized regions.

In the present work, thermal cycling was utilized to further understand the effect of martensite fraction and morphology on the resulting tensile properties. Thermal cycling of the steel was conducted at 840 ℃ to further refine the martensite grains, and also to increase their presence within ferrite grains [Kumar et al., 2014]. For the steel annealed by conventional annealing at 840 ℃, the microstructure was characterized by presence of large volume fraction of martensite phase (31 %) along with fine martensite grains embedded within the ferrite grains. Thermal cycling was planned in a manner so as to develop another microstructure in the steel at the same annealing temperature with slightly lesser martensite fraction but with more amount of fine

martensite embedded within the ferrite matrix (to study the effect of increase in the amount of embedding of fine martensite grains within ferrite grains, at the expense of decrease in martensite fraction, on the properties of steel). To meet the said objective, it was decided to soak the steel during this treatment at the heat treatment temperature for a period lesser than used during conventional annealing (to reduce the martensite fraction in the steel).

4.7.1. Thermal Cycling at 840 ℃

This section describes the thermal cycling process provided to the steel at 840 ℃. In this thermal cycling route, four thermal cycles [Kumar et al., 2014] were given at 840 ℃. The first three cycles were given at 840 ℃ without any holding and the fourth cycle was given at the same temperature with a holding of 30 s (slightly lesser than the holding given at this temperature during conventional annealing; see Kumar et al., 2014). Specimen was heated at a heating rate of 10 ℃/s and was cooled at a cooling rate of 150 ℃/s during every cycle. Figure 4.30 presents the complete thermal profile followed during the thermal cycling process.

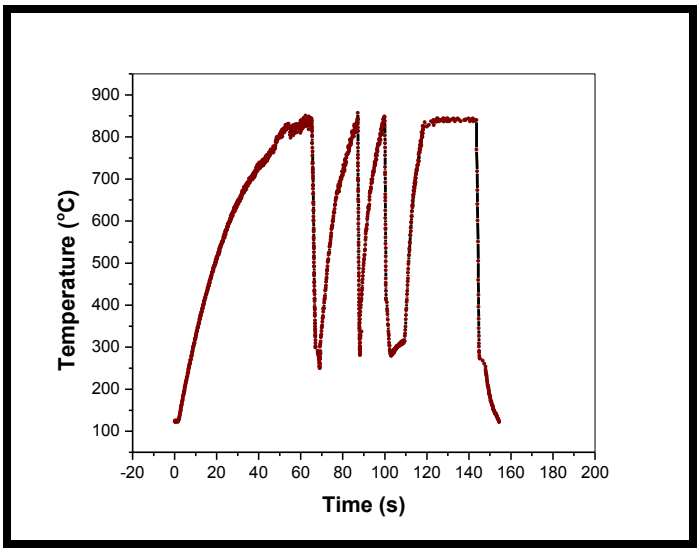

Figure 4.30: Annealing simulation thermal profile for thermal cycling at 840 ℃

Microstructure obtained after the thermal cycling process comprised of ferrite and fine martensite grains. As required, the martensite fraction was reduced (MVF ~ 17 %) and amount of fine martensite grains within the ferrite grains increased (compared to microstructure after conventional annealing at 840 ℃; see Fig. 4.19 and Fig. 4.31). There was another characteristic

difference with regards to martensite phase obtained through conventional annealing at all previous temperatures and the thermal cycled specimen. Whereas all conventionally annealed specimens contained a large fraction of lath type martensite, the thermally cycled specimen contained most of the martensite as very fine grained and embedded within the ferrite grains (and the lath shaped in very less quantity; this martensite showing nearly a globular type of morphology).

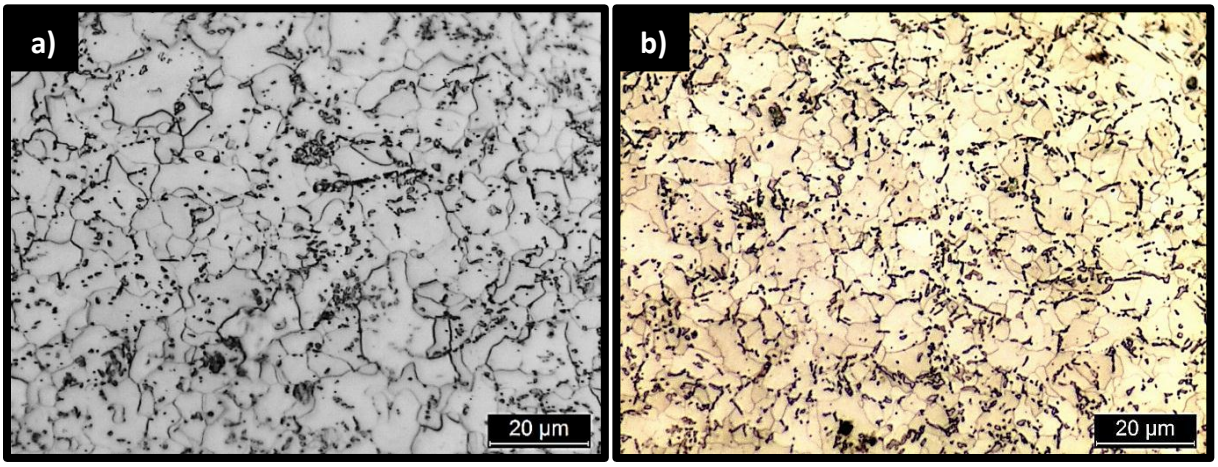

Figure 4.31: Optical micrographs of specimen subjected to thermal cycling at 840 ℃ and etched with (a) nital, and (b) picral+$Na_2O_3S_5$

Figure 4.32 shows the effect of thermal cycling on the size and distribution of martensite phase present in the microstructure. A significant increase was observed in the fraction of martensite in the fine size range.

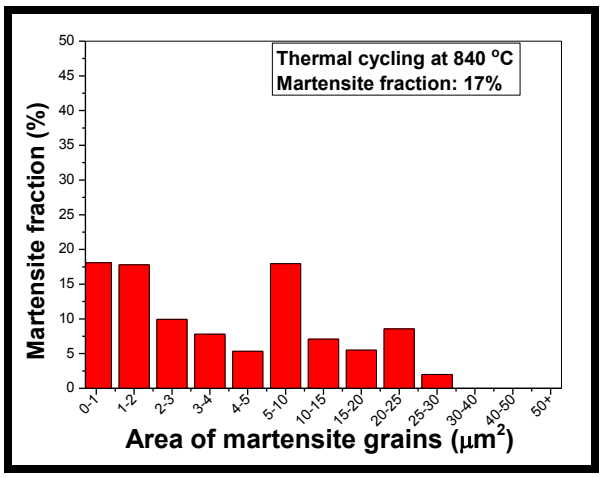

Figure 4.32: Size and distribution of martensite in steel subjected to thermal cycling at 840 ℃

Micrographs clearly showed the embedded fine martensite grains (average grain size ~ 1.65 µm) within the ferrite grains (average grain size ~ 7.2 µm). This composite i.e. martensite embedded in a ferrite microstructure helped in adapting the ductility from ferrite and strength from the fine martensite grains embedded within the ferrite grains. Thus, both the properties i.e. high UTS of 640 MPa and high ductility 30 % were obtained (see Fig. 4.33).

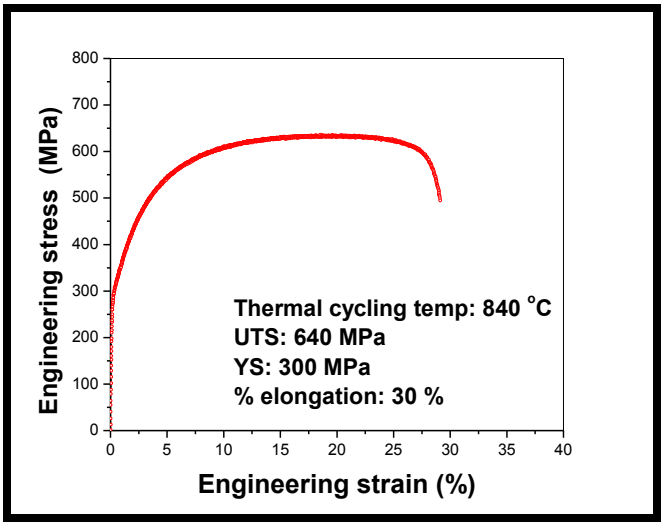

Figure 4.33: Tensile curve of specimen thermal cycled at 840 ℃

4.8. Tensile Property Comparison

From the analysis of microstructures, it was found that the martensite fraction, shape, size and its distribution can be varied by a proper selection of annealing process for given steel. A comparison of martensite fraction and tensile properties obtained in the investigated steel under different processing conditions is presented in Fig. 4.34. A continuous decrease in ductility with increase in UTS was observed in the conventionally annealed (CA) specimens processed at 775, 800, 825 and 840 ℃ respectively. Increase in strength at the expense of loss in ductility in the CA processed specimens was attributed to increase in martensite fraction and also its role in decreasing the ferrite grain size. However, for CA at 840 ℃, despite decrease in MVF (as compared to a lower temperature of 825 ℃), the UTS still increased because processing at this annealing temperature resulted in further refinement of martensite grains and also increased the fraction of martensite embedded within the ferrite grains. In the thermally cycled (TC) specimen, though the martensite fraction was very less than the CA specimens (MVF ~ 17 % in TC sample

as compared to CA samples having MVF in the range of 28–35 %), higher UTS as well as ductility were observed.

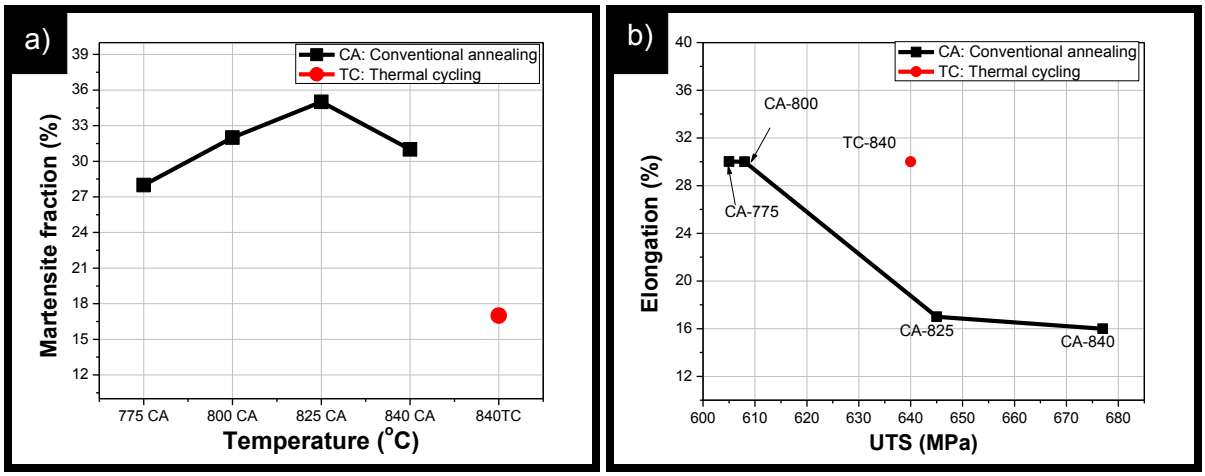

Figure 4.34: Comparison of (a) martensite fraction, and (b) tensile properties obtained in the investigated steel under different processing conditions

This was attributed to the presence of still finer martensite, and too mainly embedded within the ferrite grains. This characteristic microstructure provided the composite effect of ferrite and martensite and helped to retain high ductility even at high UTS.

Chapter 5

Conclusions

5.1. General

Dual phase (DP) steel is an automotive high strength steel with combination of majorly two phases. These steels derive their excellent combination of mechanical properties via second phase, viz., martensite and/or bainite in a ferrite matrix. Because of the composite nature of the microstructure, this class of steels offers very attractive mechanical properties when compared to similar strength steels which are based on micro-alloyed chemistry. Most of the characteristics related to tensile behavior of DP steels are strongly dependent on size and spatial distribution of the second hard phase. The present work was an attempt to investigate the effect of morphology and distribution of martensite islands on the tensile deformation behavior in a cold rolled dual phase steel.

5.2. Results and Conclusions

The main results and conclusions from the present experimental work are as follows:

Starting material

- The starting cold rolled material was composed of deformed ferrite and destructed pearlite colonies distributed non-uniformly in the ferrite matrix.
- High cold deformation resulted in high yield strength (0.2 % offset yield strength) of 895 MPa, high ultimate tensile stress of 948 MPa with very poor percentage elongation of 4.3 %.

Micromechanical modeling for flow curve prediction of DP steel

- Micromechanical modeling predictions provided that for the DP590 steel containing ferrite grains in the size range of 3−8 μm, the minimum martensite fraction for achieving the desired strength (i.e. ~ 590 MPa) was about 25 % (MVF ~ 25 %). The actual processing of steel through subsequent experimentation validated the predicted results.

Phase transformation studies using commercial software

- Thermo-Calc software predictions showed an increase in austenite fraction with increase in annealing temperature during heating.
- Thermo-Calc software predicted a minimum annealing temperature of 750 ℃ to obtain a martensite fraction of 26 % (near to desired MVF of 25 %) under equilibrium conditions. As the actual experimental conditions were not of equilibrium, a higher temperature was needed for actual experimentations. Further, DICTRA software predicted a reasonably long uneconomical holding time of 1000 s for complete pearlite dissolution for annealing at 750 ℃. In order to reduce the holding time, a temperature higher than 750 ℃ was needed. For these two reasons, the starting annealing temperature for the steel was selected as 775 ℃.
- DICTRA software results predicted a decrease in soaking time period required for complete pearlite dissolution with increase in annealing temperature.
- In order to obtain the desired MVF nearer to 25 % at a reasonably lesser holding time period during annealing, starting annealing temperature of 775 ℃ with holding time of 330 s (predicted by DICTRA) was selected.
- JMat-Pro software predicted an increase in cooling rate required for complete austenite to martensite transformation with increase in annealing temperature.

Annealing experiments and microstructural analysis

- A continuous increase in martensite volume fraction (from 28 to 35 %) and average martensite grain size (from 3.2 to 5 μm) was observed with increase in annealing temperature in the inter-critical annealing range of 775–825 ℃.
- On the contrary, annealing at 840 ℃ resulted in minimum size of martensite (average grain size of 2.7 μm). This was attributed to the increased austenite nucleation during heating and also to the transformation of austenite to ferrite (along with martensite) during cooling.
- A continuous decrease in ferrite grain size (from 6.7 to 4.8 μm) with increase in martensite fraction (from 28 to 35 %) was observed.

Tensile deformation behavior

- Initial yielding of dual-phase steel was correlated with the start of plastic deformation of ferrite phase in the DP microstructure.
- The plastic flow and hardening of martensite phase commenced well before the ultimate tensile strength reached in the dual-phase steel.
- A continuous decrease in ductility (30.02 % to 17 %) with increase in UTS (605 MPa to 645 MPa) was observed in the conventionally annealed (CA) specimens processed at 775, 800, 825 ℃ respectively. This change was attributed to the increase in martensite fraction and also its role in decreasing the ferrite grain size.
- For the conventionally annealed steels at 840 ℃, despite the decrease in MVF (31 % as compared to MVF of 35 % at a lower temperature of 825 ℃), the UTS increased (from 645 MPa at 825 ℃ to 677 MPa at 840 ℃) without significant loss of ductility (17 % at 825 ℃ and 16 % at 840 ℃). This was attributed to further refinement of martensite grains and also to increase in the fraction of martensite embedded within the ferrite grains which helped to improve the UTS without significant loss of ductility.

Thermal cycling

- Thermal cycling (at 840 ℃) resulted in the lowest martensite volume fraction of 17 % with absence of lath type morphology and an increased amount of nearly globular martensite in the microstructure.
- Thermal cycled specimen contained most of the martensite as very fine grained and embedded within the ferrite grains. This microstructure resulted in the best combination strength-ductility with UTS and percent elongation of 640 MPa and 30 % respectively.

5.3. Major Conclusions and Recommendations

- Thermo-Calc, DICTRA, and JMat-Pro predictions can be used to determine the annealing process parameters (annealing temperature, isothermal hold time periods, and cooling rates) for producing desired microstructures in an industrially cold rolled DP590 grade steel.

- Micromechanical modelling approach can be used for DP steels (here, DP590 grade) to determine the martensite volume fraction required for achieving the desired minimum strength in the DP steel (here, MVF ~ 25% was predicted for the desired UTS ~ 590 MPa).
- Volume fraction, size, and the shape of martensite phase present in the dual phase steel have a pronounced effect on the tensile deformation behavior of the steel (conventional annealing at 840 ℃ achieved the maximum YS and UTS of 422 MPa and 677 MPa respectively, and ductility of 16 % because of its microstructure).
- Thermal cycling process can be used to tailor the martensite. Formation of in-grain globular shaped martensite was observed after thermal cycling which provided the composite effect of ferrite and martensite and helped to retain high ductility 30 % even at high UTS of 640 MPa. Tensile properties of the microstructure with in-grain martensite produced UTS and good ductility. Globular or fine size of martensite was observed to induce plasticity in the material. Further, this was also found to be effective in increasing the strength of the material.

5.4. Scope of Future Work

In the present work, the effect of processing parameters viz. annealing temperature, holding time etc. on the martensite morphology and resulting tensile properties was discussed. However, the effect of different heating rates was not discussed. The effect of morphology of martensite on the properties was studied with the help of optical microscopy and SEM only. Advanced tools like EBSD, TEM need to be used for further clarifications. Further studies can also include tailoring of the microstructure by thermal cycling to obtain fine ferrite and fine martensite simultaneously in order to provide further improvements in tensile properties of DP steels.

References

- Adamczyk, J.; Grajcar, A. (2006) Effect of heat treatment conditions on the structure and mechanical properties of DP-type steel. *Journal of Achievements in Materials and Manufacturing Engineering*, 17: 305–308.
- Ahmad, E.; Karim, F.; Saeed, K.; Manzoor, T.; Zahid, G.H. (2013) Effect of cold rolling and annealing on the grain refinement of low alloy steel. *Materials Science and Engineering*, 60: 1–8.
- Alabbasi, F. (2004) Micromechanical modeling of dual phase steels [dissertation]. Canada: McGill University; 2004.
- Armaki, H.G.; Maab, R.; Bhatt, S.P.; Sriram, S.; Greer, J.R.; Kumar K.S. (2014) Deformation response of ferrite and martensite in a dual-phase steel. *Acta Materialia*, 62: 197–211.
- Avner, S.H. (2007) Introduction to Physical Metallurgy. Tata McGraw Hill Education Private Limited, New Delhi.
- Bhattacharya, D. (2006) Developments in advanced high strength steels. *Proceedings of Advanced High Strength Steel Workshop*, Arlington, Virginia, *USA*.
- Bohlooli, H.; Nakhaei, M. (2013) Comparison of mechanical properties of bainite/ferrite dual phase 4340 steels with different percents of ferrite. *World of Sciences Journal*, 2307–3071(3): 161–169.
- Calcagnotto, M.; Ponge, D.; Rabbe, D. (2010) Effect of grain refinement to 1 μm on strength and toughness of dual-phase steels. *Materials Science and Engineering A*, 527: 7832–7840.
- Han, Q.; Kang, Y.; Zhao, X.; Stanford, N.; Cai, M. (2013) Suppression of M_s temperature by carbon partitioning from carbon-supersaturated ferrite to metastable austenite during intercritical annealing. *Materials and Design*, 51: 409–414.
- Hao, Q.U. (2011) Advanced high strength steel through paraequilibrium carbon partitioning and austenite stabilization [dissertation]. United States: Case Western Reserve University; 2011.
- Kim, I.S.; Reichel, U.; Dahl, W. (1987) Effect of bainite on the mechanical properties of dual-phase steels. *Steel Research*, 58: 186–190.

- Kim, J.H.; Sung, J.H.; Piao, K.; Wagoner, R.H. (2011) The shear fracture of dual-phase steel. *International Journal of Plasticity*, 27: 1658–1676.
- Kumar, B.R.; Gujral, A. (2014) Plastic deformation modes in mono- and bimodal-type ultrafine-grained austenitic stainless steel. *Metallography, Microstructure, and Analysis*, 3(5): 397–407.
- Kuziak, R.; Kawalla, R.; Waengler, S. (2008) Advanced high strength steels for automotive industry. *Archives of Civil and Mechanical Engineering*, 8: 103–117.
- Kwon, O.; Lee, K.; Kim, G.; Chin, K.G. (2010) New trends in advanced high strength steel developments for automotive applications. *Materials Science Forum*, 638–642: 136–141.
- Matlock, D.K.; Speer, J.G.; Moor, E.D.; Gibbs, P.J. (2012) Recent developments in advanced high strength sheet steels for automotive applications: an overview. *JESTECH*, 15(1): 1–12.
- Matlock, D.K.; Speer, J.G. (2010) Processing opportunities for new advanced high-strength sheet steels. *Materials and Manufacturing Processes*, 25(1): 7–13.
- Meng, Q.; Li, J.; Wang, J.; Zhang, Z.; Zhang, L. (2009) Effect of water quenching process on microstructure and tensile properties of alloy cold rolled dual-phase steel. *Material and Design*, 30: 2379–2385.
- Meng, Q.; Li, J.; Zheng, H. (2014) High-efficiency fast-heating annealing of a cold-rolled dual-phase steel. *Materials and Design*, 58: 194–197.
- MingMing, C.; RiMing,W.; HePing, L.; Li, W.; Jie, S.; Han, D.; XueJun, J. (2012) An ultrahigh strength steel produced through deformation induced ferrite transformation and Q&P process. *Science China Technological Sciences*, 55(7): 1827–1832.
- Nadlene, R.; Esah, H.; Norliana, S.; Mohd, M.A. (2011) Study on the effect of volume fraction of dual phase steel to corrosion behaviour and hardness. *World Academy of Science, Engineering and Technology*, 5: 483–486.
- Ramazani, A.; Schwedt, A.; Aretz, A.; Prahl, U.; Bleck, W. (2013) Characterization and modelling of failure initiation in DP steel. *Computational Materials Science*, 75: 35–44.
- Ramazani, A.; Ebrahimi, Z.; Prahl, U. (2014) Study the effect of martensite banding on the failure initiation in dual-phase steel. *Computational Materials Science*, 87: 241–247.
- Santofimia, M.J.; Zhao, L.; Petrov, R.; Sietsma, J. (2008) Characterization of the microstructure obtained by the quenching and partitioning process in a low-carbon steel. *Materials Characterization*, 59: 1758–1764.

- Santofimia, M.J.; Zhao, L.; Sietsma, J. (2011) Overview of mechanisms involved during the quenching and partitioning process in steels. *Metallurgical and Materials Transactions A*, 42(12): 3620–3626.
- Shakhova, Y.E.; Yanushkevich, Z.C.; Belyakov, A.N. (2012) Effect of cold rolling on the structure and mechanical properties of austenitic corrosion resistant 10Kh18N8D3BR steel. *Russian Metallurgy*, 9: 772–778.
- Singh, S. (2014) Inter-critical annealing of lean composition steel under controlled cooling to produce multiphase microstructure [dissertation]. India: Thapar University; 2014.
- Skalova, L.; Divisova, R.; Jandova, D. (2006) Thermo-mechanical processing of low-alloy TRIP-steel. *Journal of Materials Processing Technology*, 175: 387–392.
- Sodjit, S.; Uthaisangsuk, V. (2012) A micromechanical flow curve model for dual phase steels. *Journal of Metals, Materials and Minerals*, 22(1): 87−97.
- Sung, J.H.; Kim, J.H.; Wagoner, R.H. (2010) A plastic constitutive equation incorporating strain strain-rate, and temperature. *International Journal of Plasticity*, 26: 1746–1771.
- Toudeshky, H.H.; Anbarlooie, B.; Kadkhodapour, J.; Shadalooyi, J. (2014) Microstructural deformation pattern and mechanical behavior analyses of DP600 dual phase steel. *Materials Science & Engineering A*, 600: 108–121.
- Wang, J.; Li, G.; Xiao, A. (2011) A Bainite-Ferrite Multi-Phase Steel Strengthened by Ti-Microalloying. *Materials Transactions*, 52(11): 2027–2031.
- Wu, R.M.; Wang, L.; Jin, X.J. (2013) Thermal stability of austenite and properties of quenching & partitioning (Q&P) treated AHSS. *Physics Procedia*, 50: 8–12.
- Zakerinia, H.; Kermanpur, A.; Najafizadeh, A. (2009) Color metallography; a suitable method for characterization of martensite and bainite in multiphase steels. *International Journal of ISSI*, 6(1): 14−18.
- Zhang, H.; Johansson, B.; Ahuja, R.; Vitos, L. (2012) First-principles study of solid-solution hardening in steel alloys. *Computational Materials Science*, 55: 269–272.
- Zhengming, S.; Zhongguang, W.; Suhua, A. (1989) Effects of morphology on the tensile and fatigue behaviour of a dual phase steel. *Steel Research*, 60: 215–220.

Appendix-I

Values of n_f and K_f for different ferrite grain sizes

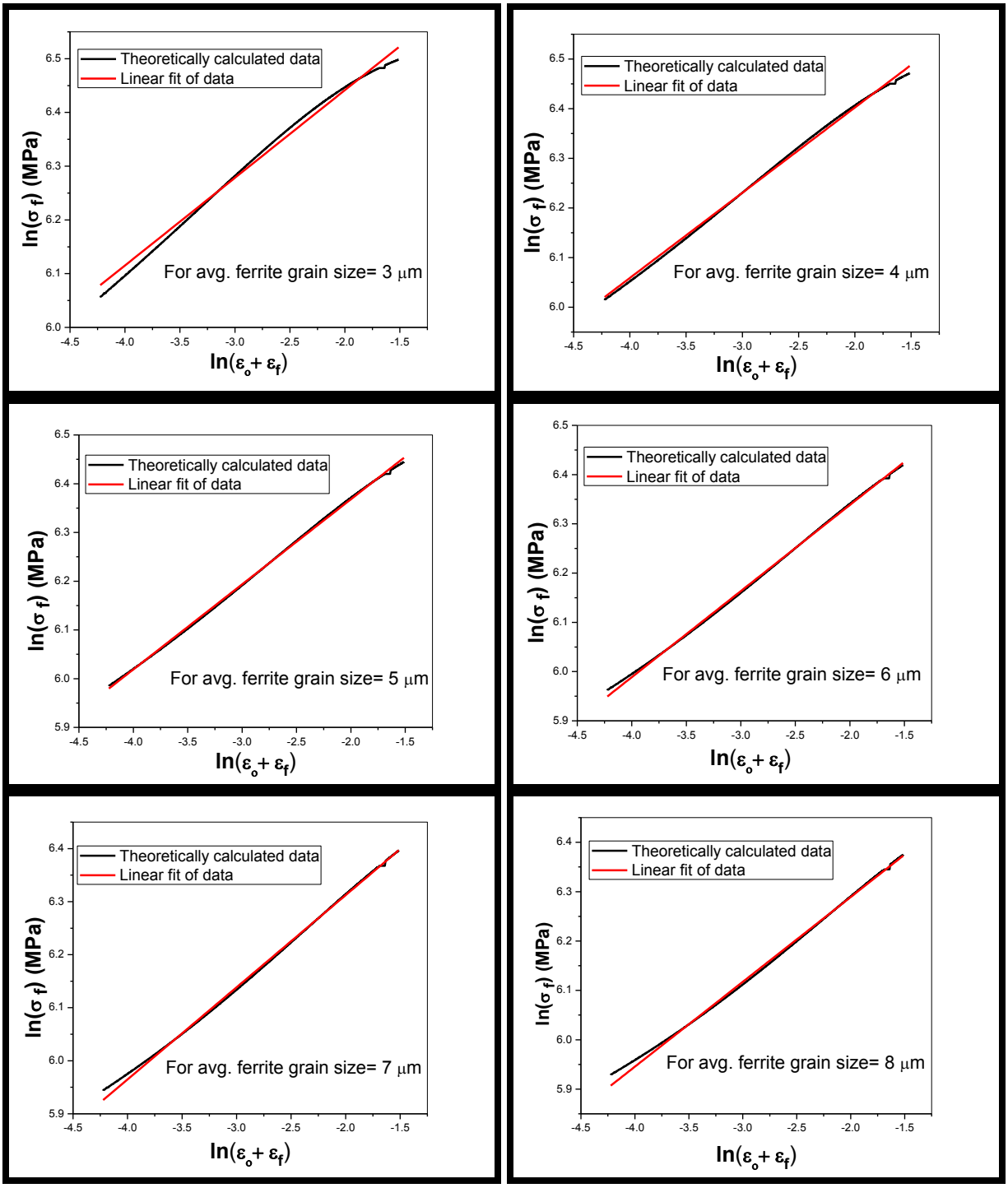

Appendix-II

Predicted true stress-strain curve for various martensite fraction in DP with different ferrite grain size

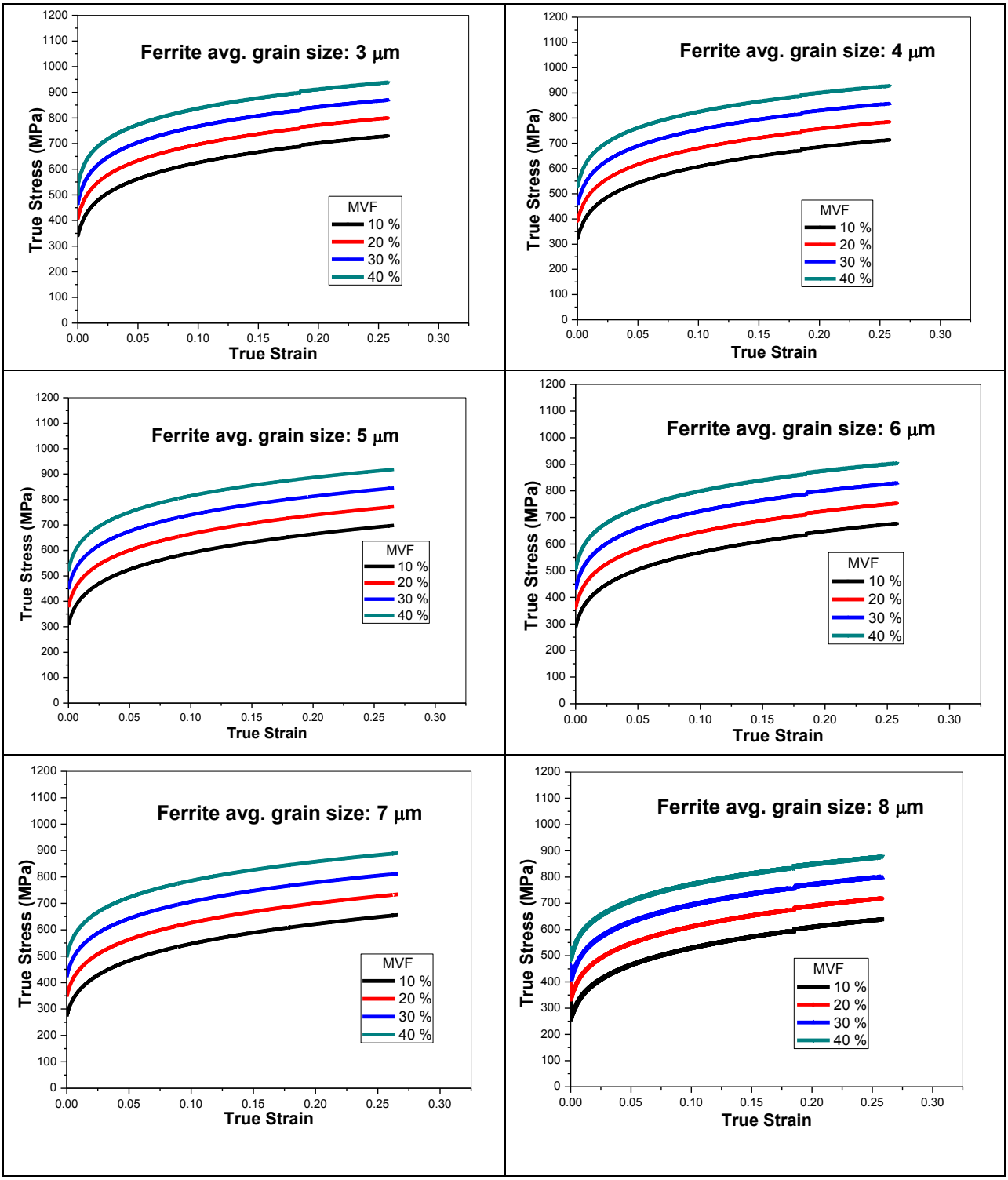

Appendix-III

Microhardness data under various annealing conditions

Annealing Temp. (℃)	Time (s)	Average Microhardness value of ferrite (Hv)	Average Microhardness value of martensite (Hv)
775	330	239	363
800	130	234	344
825	65	229	326
840	40	216	318